Hydrodynamic linear stability of the two-dimensional bluff-body wake through modal analysis and initial-value problem formulation

POLITECNICO DI TORINO

SCUOLA DI DOTTORATO
Dottorato in Fluidodinamica – XX ciclo

Tesi di Dottorato

Hydrodynamic linear stability of the two-dimensional bluff-body wake through modal analysis and initial-value problem formulation

Stefania Scarsoglio

Tutore
Prof. Daniela Tordella

Marzo 2008

Contents

Chapter 1

Introduction

The hydrodynamic stability of fluid flow is an important subject in different fields, such as aerodynamics, mechanics, astrophysics, oceanography, atmospheric sciences, and biology. Stability can be defined as the ability of a dynamical system to be immune to small disturbances (Betchov and Criminale, 1967). In general, a system excited with infinitesimal perturbations is considered stable if the initial state of equilibrium, in the short or long term, is reached again. On the contrary, a system is unstable if, subject to small oscillations, it departs from any state of equilibrium. The central issue of the stability analysis is to understand the underlying reasons for the breakdown of laminar flow and its subsequent transition to turbulence. Although many improvements have been made over a hundred years, this remains an open question and a definitive means for prediction is still to be found.

The fundamental property of linearity has been often applied in literature to the stability analysis of flows. Disturbances superposed on the laminar flow are assumed to be small so that perturbation higher order terms are negligible, and this implies a simplification of the governing equations. Moreover, from a physical point of view, the assumption of small disturbances is supported by the fact that these infinitesimal oscillations are always present in a dynamical system and cannot be eliminated. Anyhow, as the disturbance velocity grow, non-linear effects become important and the linear equations no longer accurately predict the perturbation evolution. Although the linear theory has a limited region of validity, it turns out to be useful to observe physical growth mechanisms and dominant disturbance types. The linearized equations are important in identifying the onset and a possible development of the instability, but not in considering its following evolution. Indeed, when a perturbation sets in, after a possible initial transient growth, it shows an exponential behaviour. However, the subsequent temporal evolution is modified

by the non-linear dynamics. This interaction makes the perturbations assume a behaviour which is no longer exponential.
The present work is developed within the linear theory framework and the laminar flow here considered for the stability analysis is the two-dimensional wake past an infinite circular cylinder. In general, the bluff-body wake is an important prototype of free shear flow for the study as well as for the applications in environmental and biological fluid dynamics.

First important contributions to the hydrodynamic stability are due to Helmholtz (1868), Kelvin (1887a,b) and Rayleigh (1880, 1887, 1892, 1895, 1913, 1915). Independently, Orr (1907a,b) and Sommerfeld (1908) framed the basis of the normal mode theory. Although the stability has been widely recognized as an initial-value problem, for several years the attention was mainly focused on the final fate of disturbances imposed. It was considered sufficient to know whether or not a flow is asymptotically stable or unstable. In this context, normal mode analysis turns out to be a powerful and synthetic means to predict the perturbation asymptotic behaviour.

Significant results for the two-dimensional wake stability are given, among others, by Mattingly & Criminale (1972), Triantafyllou et al. (1986), Hultgren & Aggarwal (1987), Huerre & Monkewitz (1990). In these works, and often in literature, stability analysis has been carried out according to criteria based on the study of the dispersion relation in the surrounding of saddle points. Betchov & Criminale (1966) first reported occurrence of singular points in the dispersion relation. Although they were unable to explain how the flow could be influenced by singularities in the eigenvalue relationship, they suggested that these particular points had some special significance in the stability analysis. Afterwards, it was clear and largely accepted that, as the saddle point occurs where group velocity vanishes, there is a local increase of perturbation energy and this could lead to an absolutely unstable configuration if the temporal growth rate is positive (see also Huerre & Monkewitz, 1990).
An important feature characterizing most of recent results in literature is the assumption of local parallelism of the base flow (see Mattingly & Criminale 1972, Triantafyllou et al. 1986, Hultgren & Aggarwal 1987, Huerre & Monkewitz 1990, Monkewitz & Nguyen 1987). In the case of the bluff-body wake, at every longitudinal station downstream the body, the wake profile is approximated by means of a parallel flow with the same velocity profile. This is a restrictive assumption, as the transversal dynamics of the system is largely neglected. Moreover, when using this approach, absolute instability pockets are found in the near wake (see for instance

Monkewitz, 1988; Young & Zebib, 1989), where the streamlines are not parallel and the near-parallel flow assumption is no longer valid.

The recognition of the two-dimensional wake as a slowly evolving flow in the longitudinal direction suggests that non-parallel aspects can be inserted into the stability analysis through a multiple scales approach. Two scales are usually considered: a long scale for the mean flow variations, and a short scale where the perturbations vary. This method, known as WKBJ (Wentzel-Kramers-Brillouin-Jeffreys) asymptotic analysis (see Bender & Orszag, 1978), identifies a small parameter that characterizes the non-parallel aspects, and which is usually defined as the inverse of the Reynolds number. The introduction of multiple spatial and temporal scales (Schmid & Henningson, 2001) allows non-parallel effects to be directly inserted into the stability analysis (see Bouthier, 1973; Belan & Tordella, 2006; Tordella, Scarsoglio & Belan, 2006; Tordella, Scarsoglio & Belan, 2008). In the context of locally absolutely unstable flows and according to the slow evolution of spatially developing flows, the concept of global instability has been introduced and often adopted (see among others Huerre & Monkewitz 1990, Chomaz 2005). A global mode can be defined as an extended wavepacket over a distance of the same order of magnitude of the scale characterizing the streamwise non-uniformity of the base flow. In other words, if local absolute instability pockets show up in a sufficiently large wake region (of the order of the base flow scale), the instability can be defined as global (see results by Chomaz et al., 1988; Monkewitz et al., 1993; Pier, 2002).

Only lately the transient growth has become of great interest and its importance for the complete temporal evolution of the perturbed system has been widely accepted. Recent shear flows studies have shown that instability can be due to transient growth of disturbances (see Butler & Farrell 1992; Criminale & Drazin 1990; Criminale, Long & Zhu 1991) long before the growing exponential mode occurs. In principle, this kind of behaviour could cause perturbation amplitude that violates the assumption of linearity and promote rapid transition, phenomenon known as bypass transition.

There can be early time growth even if the asymptotic perturbation amplitude is damped and this fact has been confirmed in different ways. First, for three-dimensional perturbations, as the Squire and Orr-Sommerfeld operators are not self-adjoint, the eigenfunctions are mutually non-orthogonal and this can cause algebraic growth in the early time (Sommerfeld, 1949). Second, for three-dimensional perturbations, resonance between Orr-Sommerfeld equation set of solutions and those of the Squire equation can occur. Resonance has been demonstrated to be possible for channel flow (Gustavsson & Hultgren 1980; Gustavsson 1981; Benney & Gustavsson

1981) but does not occur for the boundary layer. Resonance in the free shear flows is yet to be determined. In the end, the use of the Laplace transform to solve an arbitrary initial-value problem (Gustavsson 1979) showed that branch cuts as well as poles must exist when the inversion back to the real space is to be made. This implies the existence of a continuous spectrum and the transient behaviour associated to it.

Many contributions, often directed to find the optimal initial conditions that maximize the energy growth at a finite time, have been made for early-period dynamics for fully bounded flows (e.g. Criminale et al. 1991; Criminale et al. 1997; Gustavsson 1991; Bergstrom 1993; Schmid & Henningson 1994, Schmid 2007) and partially bounded flows (Lasseigne et al. 1999; Hultgren & Gustavsson 1981; Criminale & Drazin 2000). About free shear flows, the attention was first focused to obtain closed-form solutions to the initial-value inviscid problem (Bun & Criminale 1994; Criminale, Jackson & Lasseigne 1995) by considering piecewise linear parallel basic flow profiles. This analysis was then extended to obtain explicit unsteady solutions through multiple scales analysis for continuous parallel basic flow profiles (Blossey, Criminale & Fisher 2007). Recently, the initial-value problem first proposed by Criminale & Drazin (1990) has been applied to a growing wake (parameterized through the longitudinal coordinate and the Reynolds number), to study the temporal dynamics of small three-dimensional perturbations applied to a spatially developing flow (Scarsoglio, Tordella & Criminale 2007; Tordella, Scarsoglio & Belan, 2008).

In the present study, the interest was first focused on the asymptotic fate of disturbances through a multiple scales normal mode analysis. Then, the stability analysis is considered as an initial-value problem to capture both the early transient as well as the asymptotic behaviour of any disturbance initially imposed. The common aspect to both these analyses is the base flow description. The two-dimensional bluff-body wake is approximated through two-dimensional non-parallel asymptotic Navier-Stokes expansions (Tordella & Belan, 2003). This linking aspect will allow results coming from the two approaches to be compared.

The fundamental aspect of the normal mode approach is the assumption of an exponential time dependence, which allows the transformation of the linear initial-value problem into a corresponding eigenvalue problem. This hypothesis yields the temporal asymptotic behaviour, once the most unstable mode is established, but is lacking information on the transient growth. On the contrary, the initial-value problem formulation for the stability analysis proposed by Criminale & Drazin (1990) does not provide any *a priori* evolution in time, and the governing equations are expressed

in terms of partial differential equations. In like fashion, the temporal evolution of disturbances initially imposed can be observed at any time. As a very preliminary comment, the normal mode analysis turns out to be a powerful and synthetic approach to observe whether or not a flow is asymptotically stable or unstable. Anyhow, as there are no results concerning the completeness of the discrete spectrum in unbounded flows, the continuum should be examined in order to consider the most arbitrary initial conditions. In the initial-value problem formulation both the early transient growth (associated to the continuous spectrum) as well as the asymptotic behaviour are directly taken into account, and distinction between discrete and continuous spectra is no more needed. However, the latter approach is less concise than the modal analysis, as different parameters have to be considered.

In chapter 2 the physical problem is presented in details. First, a general qualitative description of the wake behind a finite body is given. In particular, attention is paid to the base flow evolution at different Reynolds number values, since this is a fundamental parameter to study the two-dimensional wake. Then, properties and hypotheses made to approximate the base flow profile are introduced. The physical domain is divided into two regions. An inner flow region, behind the body and including the wake, and an outer flow region, behind the body but outside the wake, can be identified. For both the regions analytical asymptotic expansions according to the Navier-Stokes model are adopted. The matching criteria and the general structure of the expansions are described, and the detailed expressions of the inner and the outer flows are then given. The base flow is approximated through the inner expansions, according to the boundary layer approach. Velocity profiles at differing downstream stations and for Reynolds number values in the range between 20 and 100 are shown.

In chapter 3 the linear stability analysis is presented and carried on through the classical modal treatment. The essentials of the normal mode theory for 2D disturbances are introduced for viscous incompressible steady parallel flows. After the perturbed system is linearized with respect to small oscillations, a partial differential equation is obtained to describe the spatio-temporal evolution of the disturbance. The normal mode hypothesis is adopted so that an asymptotic exponential behaviour in time is prescribed for any disturbance, once the most unstable mode is established. Subsequently, the Orr-Sommerfeld equation is derived by introducing the stability characteristics of the eigenvalue problem. The physical meaning of the saddle points of the dispersion relation is discussed, and the configurations of convective and absolute instability are then presented. Some general aspects and significant results on three-dimensional perturbations are considered. A brief

overview on the concepts of discrete and continuous spectra is made.

Chapter 4 presents a modal non-parallel stability analysis of the intermediate region of the two-dimensional wake using a WKBJ method on the base flow previously derived in Chapter 2. Two scales - related to the mean flow evolution - are defined through the inverse of the Reynolds number. The multiscaling is carried out to explicitly account for the effects associated to the lateral momentum dynamics. At the first order, the disturbance is locally tuned to the property of the instability, as can be seen by the zero order theory (near-parallel parametric Orr-Sommerfeld treatment). This leads to a very synthetic analysis of the nonparallel correction on the instability characteristics. The system is perturbed by disturbances with a wavenumber that varies along the wake and which is locally equal to the wavenumber of the dominant saddle point of the zero order dispersion relation, taken at different Reynolds numbers. In this way, the Reynolds number is the only parameter. It is shown that the corrections to the frequency, temporal and spatial growth rate are remarkable in the first part of the intermediate wake. In particular, absolute instability pockets appear in the region where the WKBJ method is consistent. A comparison with global data from numerical and experimental stability studies is offered. An asymptotic analysis of the far wake is then proposed.

In Chapter 5 an asymptotic representation for the entrainment in the two-dimensional wake is presented. The representation is obtained from the asymptotic Navier-Stokes solution introduced in Chapter 2. The entrainment is defined as the longitudinal volume flow rate variation in the streamwise direction. The general n-order expansion term for the flow rate and the entrainment is given. The entrainment turns out to be maximum at the beginning of the intermediate region just downstream of the symmetric counter rotating attached eddies. Moving downstream, it decreases continuously to zero, which is the asymptotic value in the far field. It increases with the Reynolds number, which is varying in the range between 20 and 100. The spatial evolution of the entrainment depends on the Reynolds number up to a distance of almost 20 body scales. Afterwards, the Reynolds dependence becomes weak. In the Re range here considered, the entrainment can be considered negligible at a normalized distance from the body in between 50–60, that is, a distance value of the same order of magnitude of Re. This result is in agreement with the scaling adopted in Chapter 4.

Chapter 6 can be thought of as a general introduction to the initial-value problem formulation for the stability analysis. For this reason, motivation and meaningful results in literature - concerning most of the traditional tools adopted to solve an

initial-value problem - are reported. First attempts were addressed to a deeper understanding of the early transient and its possible influence on the complete temporal evolution of disturbances imposed. Then attention was focused, through the use of a moving coordinate system and transformations from the physical to the phase space, on finding exact unsteady solutions for perturbations. To this end, an innovative spatio-temporal multiscale approach, where the perturbation wavenumber is defined as the small parameter, is adopted. The three-dimensional formulation in terms of perturbation vorticity and velocity - here presented and extended in the next two chapters to the stability analysis of the two-dimensional wake - is mainly due to Criminale & Drazin (1990).

In chapter 7, the approach previously described is carried out to study the temporal dynamics of small perturbations applied to the 2D growing wake. The base flow is represented by the first order terms of the Navier-Stokes expansions solution defined in Chapter 2. The longitudinal velocity component is only considered, so that the initial-value problem is a near parallel analysis parameterized on the streamwise variable. In this regard, this study is complementary to the zero order multiscale near-parallel Orr-Sommerfeld analysis presented in Chapter 4. The viscous perturbative equations are written in the vorticity and velocity formulation. A combined Laplace-Fourier transform in the streamwise and spanwise directions is performed in order to consider a perturbation characterized by real streamwise and spanwise wavenumbers, and a uniform or damped longitudinal distribution. Various physical inputs associated to the initial condition – obliquity of the disturbance, number of oscillations of the shape function, relevant cross-stream distribution, length and spatial growth factor – are examined for a few Reynolds numbers of the order of the critical value for the onset of the first instability. The transients are observed at a few stations along the wake in the region where the entrainment process is active. The early transient evolution offers very different configurations. The more important parameters affecting these scenarios are the angle of obliquity, the symmetry of the perturbation and the spatial growth rate. The transient can last hundreds of time scales. For disturbances aligned with the flow, it can be demonstrated that the long-term behaviour is in good agreement with normal mode analysis results discussed in Chapter 4.

Chapter 8 presents a multiscale approach to study the stability of long waves through the initial-value problem formulation. The small parameter of the multiple scales analysis is the perturbation polar wavenumber. This choice is physically supported by the fact that, in some flow configurations, long waves can be destabilizing (for example Blasius boundary layer and 3D cross flow boundary layer). In

such instances, the perturbation wavenumber of the unstable wave is much less than $O(1)$. The multiscaling is applied to the stability analysis of the 2D wake, whose base flow is weakly non-parallel and approximated through both the longitudinal as well as the transversal components of the Navier-Stokes expansion solutions defined in Chapter 2. In this way, the lateral wake dynamics, that determines the wake spatial growth and the associated entrainment process, is explicitly taken into account and directly inserted into the initial-value problem. As far as small values of wavenumber (of the order of 10^{-2} or less) are considered, the agreement between multiscale at order $O(1)$ and full linear problem is good for both the early transient as well as the asymptotic fate of disturbances initially imposed.

In Chapter 9, concluding remarks as well as further developments and applications of the present work are offered. In particular, common aspects and differences between the two stability approaches are pointed out while discussing results obtained.

Chapter 2

Physical problem: the bluff-body wake

The two-dimensional bluff-body wake is an important prototype of free shear flow for the study and applications in fluid mechanics. For this reason its hydrodynamics stability has been long studied. Here, in particular, the two-dimensional wake behind an infinite circular cylinder is considered. In this chapter some general aspects concerning the description of the physical system will be introduced (§2.1). Afterwards, details on the analytical formulation of the base flow will be given (§2.2). The matching criteria and the general structure of the (inner and outer) expansions describing the mean velocity field are discussed (§2.2.1). The detailed expressions of the inner and the outer flows are given in §2.2.2. Then, in §2.3, the boundary layer model is assumed to approximate the bluff-body wake profile and the formal expression of the inner flow is given.

2.1 Base flow evolution with the Reynolds number

Qualitative aspects of the base flow evolution past a finite body in an open domain are considered. In particular, the interest is aimed on the transition from the steady to the unsteady state. The following is an introductory description mainly based on experimental observations.

The body generating the wake is a circular cylinder with diameter D. The free stream speed U_0 is the velocity that would occur without the body and that is effectively observed far from it. The cylinder is considered infinitely high, so that

the influence of its extremities can be neglected, and the same behaviour is assumed at any section normal to the cylinder axis.
For small Reynolds number values, the flow is symmetric upstream and downstream the body. The two regions are quite specular. The streamlines are influenced by the presence of the cylinder, even at many diameters far from it. The velocity is remarkably different from U_0. As soon as Re is increased, the symmetry disappears. When upstream, the flow tends to go all over paths closer to the body. When downstream, paths farer from it are followed. When Re is greater than 4, as upstream the streamlines are close to the body, downstream the flow departs from body before the back point of symmetry is reached. This leads to the separation of the flow and the onset of two attached vortices. In this region, the fluid is rotating according to the circular and close streamlines and is not going downstream. As the Reynolds number still increases, the vortices become bigger until a critical value of Re is reached ($Re \sim 40$).
When $Re > 40$ the flow becomes unsteady, although the conditions imposed are steady. The development of instability leads to a flow path, known as Kàrmàn vortex street. From the confined region behind the body, two rows of vortices, moving downstream with velocity lower than U_0, are forming. The vortices of each row are moving in the same direction, that is opposite to the one on the other row. The vortex streets commonly appear behind obstacles and their principal cause is the instability of the flow. The process for which a vortex street takes place is known as vortex shedding. In fact, as $Re > 100$, a periodic separation from the cylinder of the vortices, that are going to form the Kàrmàn vortex street, is observable. This phenomenon is quite continuous as, when a vortex is moving away from the body, another one is already replacing it.

By comparing the oscillograms with velocity fluctuations at different downstream stations, it can be seen that, for the same Re values, the irregularities become more remarkable moving away from the cylinder. The presence of subsequent instabilities leads to the break of the vortex street and the formation of a turbulent wake. In this situation, the transition to a turbulent flow occurs.
Two types of secondary instabilities can be identified. The first arises when $Re \sim 200$ and acts all over the vortex street. The second occurs when $Re > 400$ and takes place downstream the separation points from the body. The latter is the principal cause of transition when $Re > 400$, as it appears close to the body. In fact, there is a wide range of Reynolds number values, from 400 to about $3{\cdot}10^5$, for which the situation remains almost the same. The main instability forms the vortex street and the secondary one acts like a disturbance, causing a turbulent wake.

When $Re \sim 3{\cdot}10^5$, important changes related to the boundary layer flow are observed. Up to this value the flow is laminar, beyond it transition to turbulence occurs. In the range $3{\cdot}10^5 < Re < 3{\cdot}10^6$, transition happens in a quite complicate way. The laminar flow close to the cylinder moves away from the wall as it is entering into the two symmetrical vortices. The transition occurs quickly and the turbulent flow is coming nearer to the wall again, close to where the laminar separation happened. Beyond $Re = 3{\cdot}10^6$, transition occurs in the boundary layer. There is no more laminar separation and subsequent turbulent reconnection.
However, in both cases, the turbulent boundary layer separates. The flow is moving away from the wall to form the wake before the back stagnation point is reached. Actually, this phenomenon happens even before when the boundary layer remains laminar. When $Re > 3{\cdot}10^5$, the wake is narrower than for lower Re values. When $Re > 3{\cdot}10^5$ the flow entering into the wake is already turbulent and the transition just behind the body is eliminated.

2.2 Base flow formulation

The analytical expressions of the velocity components of the base flow are here presented in detail. The Reynolds number ranges from a value of 20 to a value of 100, that is the order of magnitude for the onset of the first instability.
The base flow is considered steady, incompressible and viscous, and described by the continuity and Navier-Stokes equations

$$\frac{\partial U}{\partial x} + \frac{\partial V}{\partial y} = 0, \tag{2.1}$$

$$U\frac{\partial U}{\partial x} + V\frac{\partial U}{\partial y} + \frac{\partial P}{\partial x} - \frac{1}{Re}\nabla^2 U = 0, \tag{2.2}$$

$$U\frac{\partial V}{\partial x} + V\frac{\partial V}{\partial y} + \frac{\partial P}{\partial y} - \frac{1}{Re}\nabla^2 V = 0, \tag{2.3}$$

where x is the coordinate parallel to the free stream velocity and y is normal, while $(U(x,y),V(x,y))$ and $P(x,y)$ are the velocity components and pressure respectively. The independent spatial variable x is defined from 0 to $+\infty$, y from $-\infty$ to $+\infty$. All physical quantities are normalized with respect to the free stream velocity U_0, the spatial scale of the flow D and the density.

The wake behind the cylinder is divided into two regions, inner and outer flows, both satisfying the Navier-Stokes model. A full Navier-Stokes solution is, in fact, a more acceptable outer flow model than a potential solution. At the same time,

the analysis is not adopting the rapid decay principle. This a priori assumption often leaded to complicate analytical expressions (see Goldstein 1933, Stewartson 1957, Imai 1951, Chang 1961, Kida 1984), as logarithmic terms had to be included to maintain the exponential nature of the lateral decay. The problem is complete with the specification of the boundary conditions which exclude the near wake and involve symmetry to the longitudinal coordinate and uniformity in the far field (see Figure 1 for a sketch of the laminar wake).

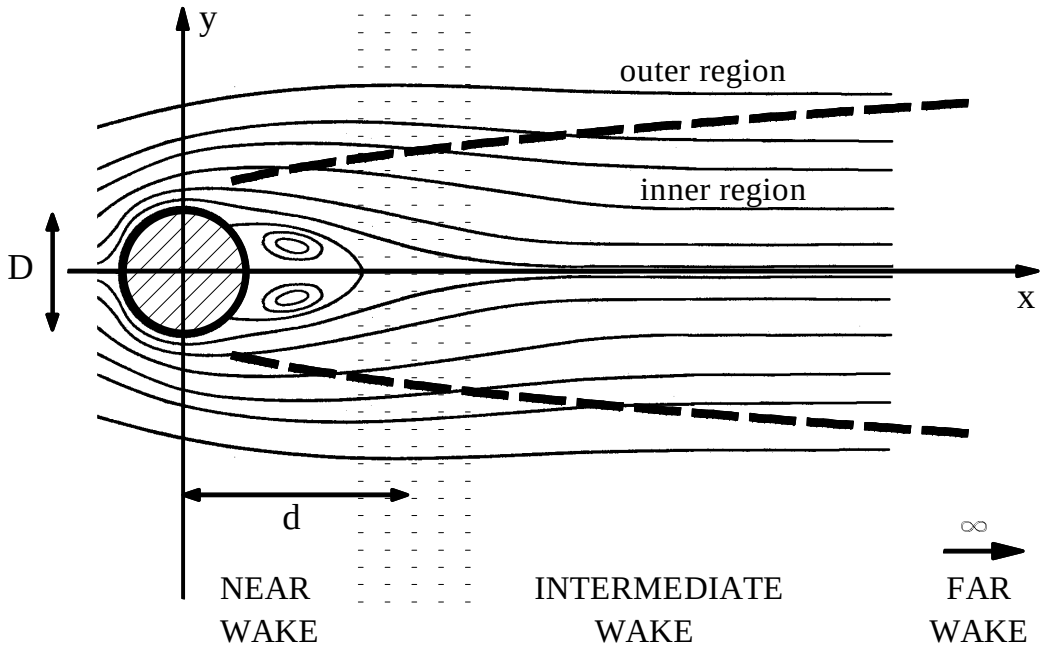

Figure 2.1. Sketch of the 2D laminar wake behind the cylinder.

The inner flow is required to be a thin layer described by the Navier-Stokes model, to keep its momentum constant along the x direction, and to entrain external fluid. The outer flow is considered as a Navier-Stokes flow which symmetrically wraps the inner flow and satisfies $U \to U_0$, $V \to 0$, $P \to P_\infty$ for $y \to \pm\infty$. The domain is composed of the intermediate and far wake

$$d < x < \infty; \;\; -\infty < y < +\infty$$

where d is the distance, which decreases with Re, from the center of the body beyond which the thin shear layer hypothesis is valid. The intermediate flow region is assumed to begin at $x = d$. The parameter d, namely a function of both Re and the shape of the body, should not depend to any great extent on the details of the actual shape. It usually varies from eight to four diameters for $20 < Re < 40$ (Belan and Tordella, 2002; Kovásznay, 1948).

As both the origin and the near wake are not included into the analysis, it is necessary to introduce field information, that gives one of the accessory conditions along the x coordinate (see Stewartson 1957), as follows

$$\begin{aligned} U(x_*,y;Re) &= U_*(y;Re) \\ V(x_*,y;Re) &= V_*(y;Re) \\ P(x_*,y;Re) &= P_*(y;Re) \end{aligned} \tag{2.4}$$

These conditions are both the result of numerical simulations as well as laboratory experiments in the intermediate field. The second condition along x is the uniformity condition at infinity.

It is now opportune to point out some important features that characterize the present approach with respect to the previous analyses in literature (Goldstein, 1933; Stewartson, 1957; Imai, 1951; Chang, 1961; Kida, 1984).

On one hand, the introduction of the intermediate region allows the adoption of the thin shear layer hypothesis for the inner flow. On the other hand, it supports a differentiation of behaviour of the intermediate flow with respect to its infinite asymptotic.

The adoption of boundary conditions (2.4) gives a higher degree of field information than the use of integral quantities, such as the drag or the lift coefficients.

The Navier-Stokes model can easily approximate the order of the pressure variations, that turn out to be of the fourth order. The pressure variations were usually overestimated at the second order in previous studies (Chang, 1961; Kida, 1984).

The use of the Navier-Stokes equations, without restrictive hypotheses and valid throughout the domain, shows rapid decay and irrotationality at first and second order for the inner and the outer flows, respectively. At the higher orders, which mainly influence the intermediate region, the decay is algebraic for the inner flow and, thus, the outer flow becomes weakly rotational.

2.2.1 Matching rules and structure of the expansion solution

The matching of the inner and outer solutions is not performed directly on the pressure but on its gradient, which is the actual physical quantity involved into the equations. In order to consider that the flow non-parallelism implies a streamwise evolution of the field, it is imposed

$$\lim_{y\to 0} \partial_x P_o = \lim_{y\to\infty} \partial_x P_i \ , \quad \text{for } x \text{ fixed.} \tag{2.5}$$

where the subscripts o and i indicate outer and inner variables, respectively. As the wake dynamics mainly involves the convection and the diffusion of vorticity, it is considered physically more significant to impose the second matching condition on the vorticity rather than velocity

$$\lim_{y\to 0} \Omega_o = \lim_{y\to\infty} \Omega_i, \quad \text{for } x \text{ fixed.} \tag{2.6}$$

In this way restrictive conditions of irrotationality are not imposed on the outer flow and, at the same time, an irrotational configuration is not *a priori* excluded for the outer region.
The entrainment – the transport of external fluid into the inner region – is taken into account by imposing the matching between the inner and the outer transversal velocities, that is

$$\lim_{y\to 0} V_o = \lim_{y\to\infty} V_i \ , \quad \text{for } x \text{ fixed.} \tag{2.7}$$

The structure of the inner and outer expansion solutions is sought in the class of inverse coordinate expansions that satisfies the boundary conditions at infinity and allows a partial variable separation so that a sequence of linear systems of inhomogeneous differential equations for the two sets of variables (U_i,V_i,P_i), (U_o,V_o,P_o) is obtained. For the inner flow, the quasi-similar transformation is introduced

$$\xi = x, \ \ \eta = x^{-1/2} y. \tag{2.8}$$

The introduction of the expansion hypothesis

$$f_i = \quad f_{i0}(\eta) + x^{-1/2} f_{i1}(\eta) + x^{-1} f_{i2}(\eta) + \cdots \tag{2.9}$$

for the inner variables satisfies the uniformity condition at infinity. At the same time, the system $\vec{\mathcal{I}}_n(f_{in},\eta,\partial_\eta,\partial_\eta^2) = \vec{\mathcal{J}}_n(f_{i0},....,f_{i(n-1)},\eta,\partial_\eta,\partial_\eta^2; Re)$, obtained by substituting (2.8) and (2.9) into Eqs. (2.2)-(2.1), results to be linear at each order. Due to the variable separation, the non-linear terms in (2.2) only include the products of quantities of an order of less than n. These terms will eventually end up in the inhomogeneous term.
The expansion hypothesis makes the second relation in (2.4) useless as, once $U_i(x,y)$ is known, $V_i(x,y)$ is obtained by the continuity equation. This avoids the use of experimental V profiles which often suffer from the inaccuracy related to the smallness of the transversal velocity values ($V << U$). The quasi-similarity is due to the fact that every term in the expansion (2.9) is self-similar, while their sum is not (a transformation is self-similar if it is invariant with respect to different scales).

For the outer flow the variable transformation is introduced

$$r = (x^2 + y^2)^{1/2}, \;\; s = y/x \tag{2.10}$$

together with the expansion hypothesis for the three variables (U_o,V_o,P_o)

$$f_o = f_{o0}(s) + r^{-1/2} f_{o1}(s) + r^{-1} f_{o2}(s) + \cdots \tag{2.11}$$

which satisfies the uniformity conditions at infinity. If (2.10) and (2.11) are substituted into (2.2)-(2.1), both the non-linear and the diffusive terms include only quantities of orders of less than $n-1$ at each order. This reduces the differential order of the transformed equations by one and makes them linear. The inhomogeneous linear ordinary differential system is of the third order of the form $\vec{\mathcal{O}}_n(f_{on},s,\partial_s) = \vec{\mathcal{P}}_n(f_{o0},...,f_{o(n-1)},s,\partial_s; Re)$.

As the system for the inner flow is of the fourth order, four constants of integration are introduced. Two of these can be determined by the symmetry of the domain. For the outer flow, three constants of integration are needed. The latter constants, together with the remaining two of the inner field, are determined through the field boundary conditions (2.4) – which are actually two conditions on the variables U and P since the transversal velocity profile V, as previously mentioned, is unnecessary – and the three matching conditions (2.5)-(2.7).

2.2.2 Inner and outer expansions

The inner expansion is defined in the region

$$x > d(Re)\ ,\ |y| \lesssim \mathcal{Y}(x)\ \Rightarrow\ \frac{y}{x} \to 0\ \text{ as }\ x \to \infty, y \to \infty\,, \tag{2.12}$$

where $\mathcal{Y}(x)$ represents the boundary between the inner and the outer regions (see dashed curves in Fig. 2.1). According to (2.9), an inner expansion solution of the Navier-Stokes equations is proposed, so that the velocity and the pressure expansions are

$$\left\{\begin{array}{ll} U_i = & \phi_0(\eta) + x^{-1/2}\phi_1(\eta) + x^{-1}\phi_2(\eta) + \cdots \\ V_i = & \chi_0(\eta) + x^{-1/2}\chi_1(\eta) + x^{-1}\chi_2(\eta) + \cdots \\ P_i = & \pi_0(\eta) + x^{-1/2}\pi_1(\eta) + x^{-1}\pi_2(\eta) + \cdots \end{array}\right. \tag{2.13}$$

The continuity equation assures that $\chi_0 \equiv 0$. This is confirmed by the uniformity condition at infinity, which also determines the other two coefficients at order zero: $\phi_0(\eta) = 1,\ \pi_0(\eta) = P_\infty/\rho U_\infty^2$. From continuity it can also be verified that $\chi_1(\eta) \equiv 0$. Thus the velocity component $V_i = x^{-1}\chi_2(\eta) + ..\ \approx O(x^{-1})$. In general, coefficients χ_n can be obtained directly from the continuity equation through the coefficients ϕ_{n-1}.

By substituting the change of coordinate (2.8) and the expansion form (2.13) in the Navier-Stokes equation in the x-direction, a general ordinary differential equation for ϕ_n, $n \geq 1$, is obtained:

$$\mathcal{L}_n\,\phi_n \equiv \frac{1}{Re}\phi_n'' + \frac{\eta}{2}\phi_n' + \frac{n}{2}\phi_n = M_n \tag{2.14}$$

where the inhomogeneous term M_n is sum of three parts:

$$M_n = T_n + P_{g\,n} + S_{d\,n}. \tag{2.15}$$

The first one, T_n, comes from the non-linear term $(\mathbf{U}\cdot\nabla)\,\mathbf{U}$ in the Navier-Stokes equation in x-direction. It can be seen that $T_0 = T_1 = 0$, $T_2 = -\frac{1}{2}\phi_1^2$ and, for $n \geq 3$,

$$T_n = -\frac{n}{4}\sum_{i=1}^{n-1}\phi_i\phi_{n-i} + \sum_{i=1}^{n-2}\left(-\frac{\eta}{2}\phi_i'\phi_{n-i} + \phi_i'\chi_{n-i}\right). \tag{2.16}$$

The terms $P_{g\,n}$ and $S_{d\,n}$ correspond to the pressure gradient component $\partial_x P$ and the streamwise diffusion term $\partial_x^2 U/Re$, respectively. In the simpler boundary layer model both these terms are identically equal to zero at any order and, for this reason, considered as high order Navier-Stokes corrections. It is found that $P_{g\,n} = 0$ for n = 1,2,3 and $S_{d\,0} = S_{d\,1} = S_{d\,2} = 0$, $S_{d\,3} = (4Re)^{-1}(3\phi_1 + 5\eta\phi_1' + \eta^2\phi_1'')$. For $n \geq 4$, both the terms $S_{d\,n}$ and $P_{g\,n}$ are non-zero and it is possible to write them as functions of ϕ_0,...ϕ_{n-1}, together with their derivatives at previous orders (for details see Tordella & Belan 2003).

Thus, a hierarchy of ordinary differential systems can be expressed as

$$\left\{\begin{array}{l} \phi_0' = 0, \mathcal{L}_n\,\phi_n = M_n,\ n \geq 1 \\ \chi_0' = 0, \chi_n' = \frac{\eta}{2}\phi_{n-1}' + \frac{n-1}{2}\phi_{n-1},\ n \geq 1 \\ \pi_n' = 0,\ n = 0,.,3; \\ \pi_n' = \Pi_n(\phi_0,...\phi_{n-1}, \chi_0,...\chi_{n-1}),\ n \geq 4 \end{array}\right. \tag{2.17}$$

where, as previously noted, $\phi_0 = 1$, $\chi_0 = 0$, $\pi_0 = p_\infty/(\rho U^2)$, $\pi_1 = \pi_2 = \pi_3 = 0$. The first equation can be solved directly for ϕ_n (Belan & Tordella, 2002), so that

$$\phi_n(\eta) \;=\; A^n \mathrm{e}^{-\frac{Re}{4}\eta^2}\left[C_n\,{}_1\mathrm{F}_1\left(\frac{1-n}{2}, \frac{1}{2}; \frac{Re}{4}\eta^2\right) + Re\mathrm{Hr}_{n-1}(\eta)F_n(\eta)\right] \tag{2.18}$$

where A is related to the drag coefficient C_D ($A = \frac{1}{4}(Re/\pi)^{1/2}c_D(Re)$, see Belan & Tordella, 2002), ${}_1\mathrm{F}_1$ is the confluent hypergeometric function, $\mathrm{Hr}_{n-1}(\eta) = \mathrm{H}_{n-1}(\frac{1}{2}Re^{1/2}\eta)$, where H_n are Hermite polynomials, and

$$F_n(\eta) \;=\; \int \frac{\mathrm{e}^{\frac{Re}{4}\eta^2}}{\mathrm{Hr}_{n-1}^2(\eta)} G_n(\eta)\mathrm{d}\eta; \tag{2.19}$$

$$G_n(\eta) \;=\; A^{-n}\int M_n(\eta)\mathrm{Hr}_{n-1}(\eta)\mathrm{d}\eta\ . \tag{2.20}$$

For $n \geq 3$, these integrals can be numerically evaluated or approximated using special functions. Once ϕ_n is known, the second equation in (2.17) gives

$$\chi_n \;=\; \frac{\eta}{2}\phi_{n-1} + \frac{n-2}{2}\Phi_{n-1} \tag{2.21}$$

where $\Phi_n = \int_0^\eta \phi_n(\zeta)\mathrm{d}\zeta$. The π_n are obtained by directly integrating the relevant equation in (2.17).

The outer expansion is defined in the region behind the body and outside the wake, that is

$$x > d(Re)\ ,\ |y| \gtrsim \mathcal{Y}(x) \Rightarrow \frac{y}{x} \to \text{cost} \neq 0 \ \text{ as } \ x \to \infty, y \to \infty\,; \tag{2.22}$$

According to (2.11), the expansions for the velocity and pressure outer fields are

$$\begin{cases} U_o = & U_0(s) + r^{-1/2}U_1(s) + r^{-1}U_2(s) + \cdots \\ V_o = & V_0(s) + r^{-1/2}V_1(s) + r^{-1}V_2(s) + \cdots \\ P_o = & P_0(s) + r^{-1/2}P_1(s) + r^{-1}P_2(s) + \cdots \end{cases} \tag{2.23}$$

By substituting into the Navier-Stokes and continuity equations, a hierarchy of ordinary differential systems is obtained. The general system of order n can be rewritten as follows

$$\begin{cases} U_n' = -\frac{n}{2}s_-^2(U_n/s + V_n + P_n/s) + U_n^* \\ V_n' = -\frac{n}{2}s_-^2 P_n + V_n^* \\ P_n' = \frac{n}{2}s_-^2 V_n + P_n^* \end{cases} \tag{2.24}$$

where U_n^*, V_n^*, P_n^* are inhomogeneous terms and

$$s_\pm = \ (1+s^2)^{\pm 1/2}\,. \tag{2.25}$$

2.3 Wake profile approximation through the inner expansions: the boundary layer model

The inner and outer expansions are then used to form the composite expansion f_{cn} according to the rule $f_{cn} = f_{in} + f_{on} - (f_{on})^{in}$, where $(f_{on})^{in}$ is the common part of f_{in} and f_{on}, and can be calculated as the inner expansion of the outer expansion, or vice versa. In the context of the present stability analysis, the wake is studied through the boundary layer model. This means that only the inner field of the previous expansions is used. The reason of this choice is that, although for this simpler model the pressure field is constant, the entrainment is very efficiently accounted for by the outer limit of the V field which has non-zero values very close to those

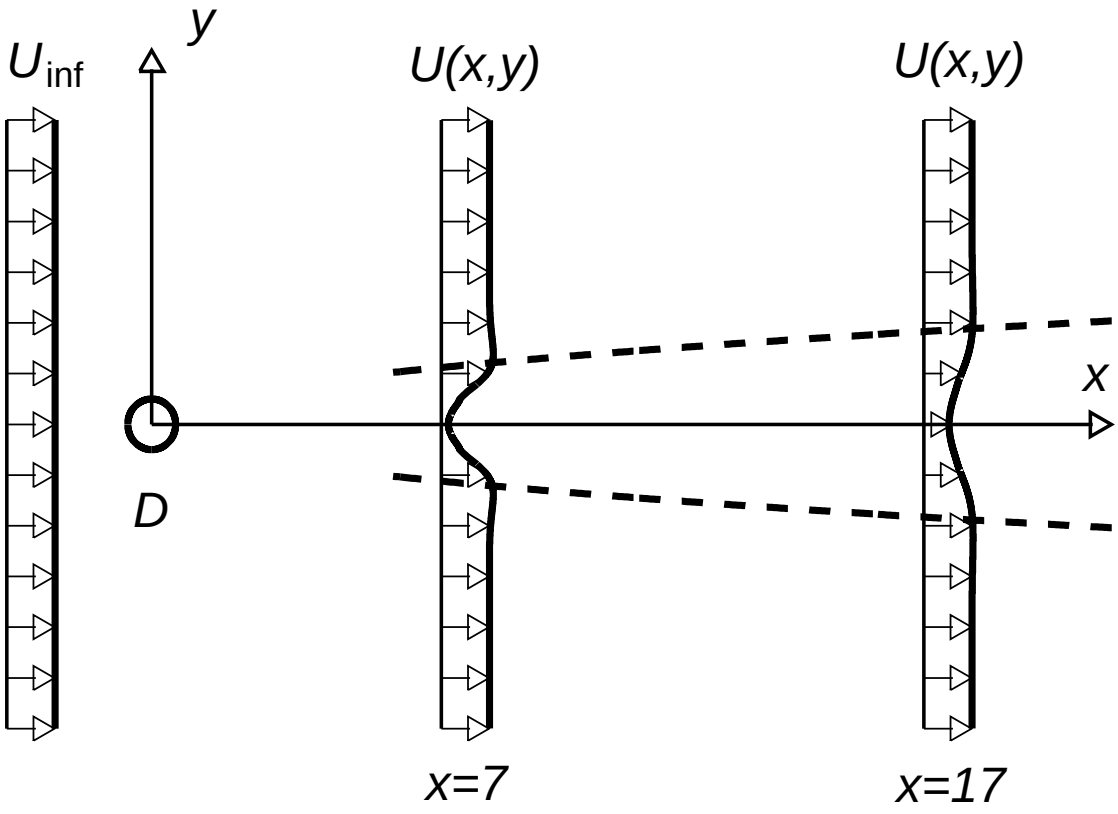

Figure 2.2. Longitudinal velocity profiles at $Re = 60$ and at stations $x = 7$, $x = 17$.

issued by the Navier-Stokes model. Moreover, the boundary layer model allows the general order term of the expansion to be analytically determined.

Before giving the detailed expression of the velocity field used to describe the wake profile, some aspects of the obtained Navier-Stokes solutions have to be pointed out.

First, it should be noted the analytical simplicity of the expansion solution, also due to the matching which, based on criteria that involve the joining of the longitudinal pressure gradient, vorticity and entrainment velocity, simplifies the system of equations at higher orders. This makes the solution suitable to accurately approximate the wake profile in the stability analysis.

Second, the solutions have been obtained relaxing the exponential decay principle for the inner layer, whose addition to the governing equations, on one hand, restricts

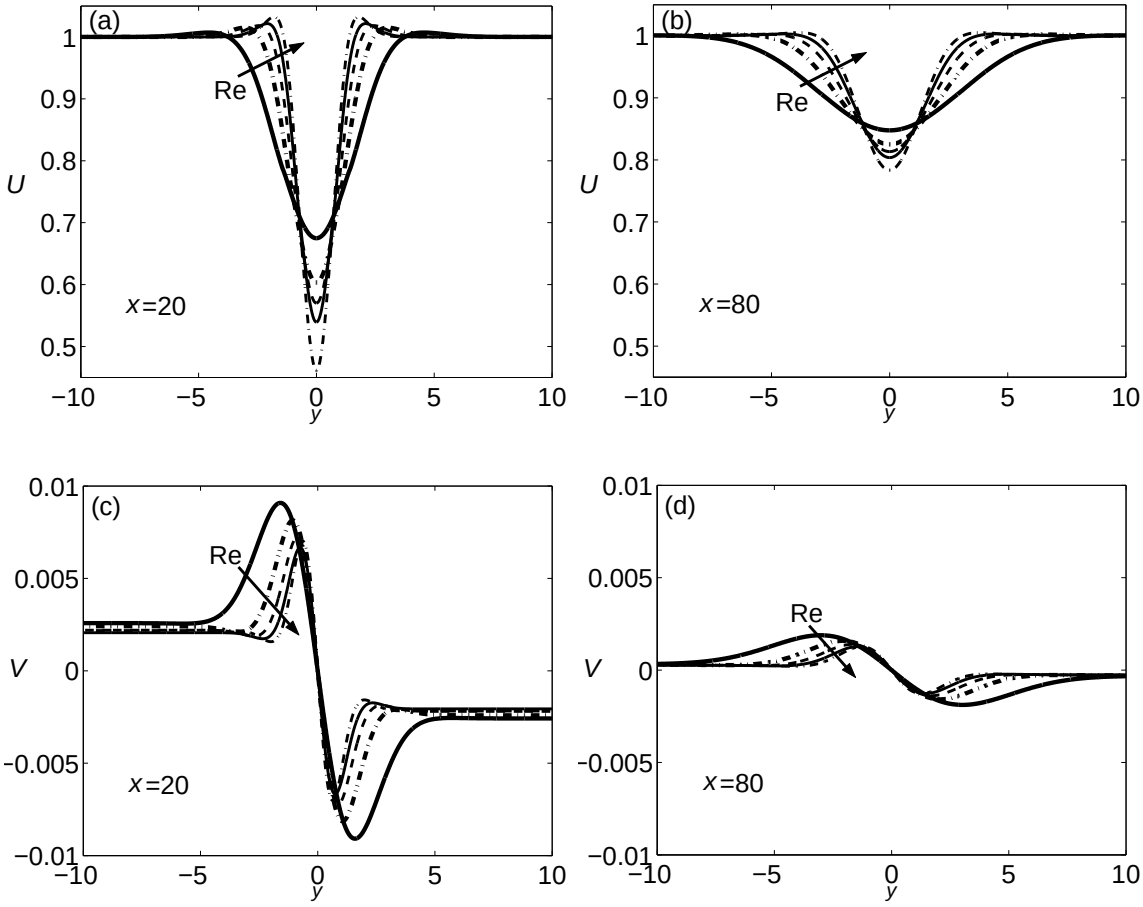

Figure 2.3. Velocity profiles at the downstream stations $x = 20$, $x = 80$ and for Re = 20,40,60,80 and 100. Longitudinal velocity U: (a) $x = 20$, (b) $x = 80$, transversal velocity V: (c) $x = 20$, (d) $x = 80$.

their generality, while on the other makes the introduction of logarithmic terms in the expansion necessary. The present approach however did not prevent the matching to show the properties of rapid decay and irrotationality at the first and second orders for the inner and the outer flows, respectively. At the higher orders, a fast algebraic decay of the inner layer is obtained. The outer flow, up to the order r^{-2}, linearly convects momentum and, from the order $r^{-5/2}$, nonlinearly convects and diffuses it.

Here we list in sequence the inner expansions for the streamwise and the transversal velocity (U and V, respectively) up to the third order. In Fig. 2.2 the longitudinal velocity profiles are shown for two differing downstream stations ($x = 7$ and $x = 17$) at $Re = 60$. In Fig. 2.3 the velocity profiles (U,V) at the downstream stations

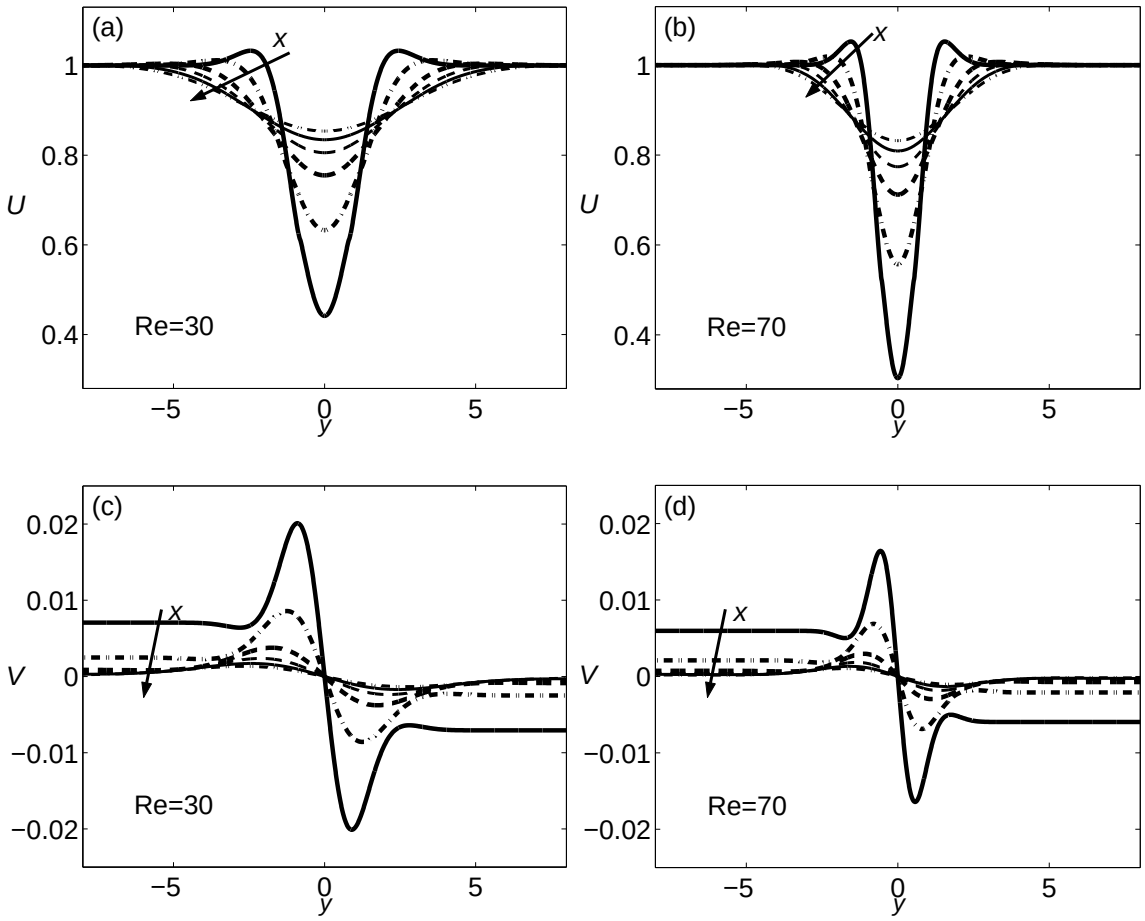

Figure 2.4. Velocity profiles for $Re = 30{,}70$ plotted at stations $x = 10{,}20{,}40{,}60{,}80$ and 100. Longitudinal velocity U: (a) $Re = 30$, (b) $Re = 70$, transversal velocity V: (c) $Re = 30$, (d) $Re = 70$.

$x = 20$, $x = 80$ and for $Re = 20{,}40{,}60{,}80$ and 100 are plotted. In Fig. 2.4 the velocity profiles (U,V) for $Re = 30{,}70$ at the stations $x = 10{,}20{,}40{,}60{,}80$ and 100 are plotted. The explicit expressions are

$$\begin{aligned} U(x,y) &= \phi_0(x,y) + \phi_1(x,y)x^{-1/2} \\ &\quad +\phi_2(x,y)x^{-1} + \phi_3(x,y)x^{-3/2} \qquad (2.26) \\ V(x,y) &= \chi_0(x,y) + \chi_1(x,y)x^{-1/2} \\ &\quad +\chi_2(x,y)x^{-1} + \chi_3(x,y)x^{-3/2} \qquad (2.27) \end{aligned}$$

Zero order, n=0

$$\phi_0(x,y) = C_0 \tag{2.28}$$
$$\chi_0(x,y) = 0 \tag{2.29}$$

with $C_0 = 1$.

First order, n=1

$$\phi_1(x,y) = -AC_1 \mathrm{e}^{-Rey^2/(4x)} \tag{2.30}$$
$$\chi_1(x,y) = 0 \tag{2.31}$$

with $C_1 = 1$.

Second order, n=2

$$\begin{aligned}\phi_2(x,y) &= -\frac{1}{2}A^2\mathrm{e}^{-Rey^2/(4x)}[C_2 {}_1\mathrm{F}_1(-\frac{1}{2},\frac{1}{2};\frac{Rey^2}{4x}) \\ &\quad +\mathrm{e}^{-Rey^2/(4x)} + \frac{1}{2}\frac{y}{\sqrt{x}}\sqrt{\pi Re}\,\mathrm{erf}(\frac{1}{2}\sqrt{\frac{Re}{x}}y)] \end{aligned}\tag{2.32}$$
$$\chi_2(x,y) = -\frac{A}{2}\frac{y}{\sqrt{x}}\mathrm{e}^{-Rey^2/(4x)} \tag{2.33}$$

with $C_2 = -2.75833 + 0.21237 \cdot Re - 0.00353 \cdot Re^2 + 0.00002 \cdot Re^3$.

Third order, n=3

$$\phi_3(x,y) = A^3\mathrm{e}^{-Rey^2/(4x)}(2 - Re\frac{y^2}{x})[\frac{1}{2}C_3 - ReF_3(x,y)] \tag{2.34}$$
$$\begin{aligned}\chi_3(x,y) &= -\frac{A^2}{2}\{C_2[-\frac{1}{2}\frac{1}{\sqrt{x}}\int_0^y [\mathrm{e}^{-Re\zeta^2/(4x)} {}_1\mathrm{F}_1(-\frac{1}{2},\frac{1}{2};\frac{Re\zeta^2}{4x})]d\zeta \\ &\quad -\frac{1}{2}\frac{y}{\sqrt{x}}\mathrm{e}^{-Rey^2/(4x)} {}_1\mathrm{F}_1(-\frac{1}{2},\frac{1}{2};\frac{Rey^2}{4x})] \\ &\quad -\frac{1}{2}\frac{y}{\sqrt{x}}\mathrm{e}^{-Rey^2/(2x)} - \sqrt{\frac{\pi}{2Re}}\,\mathrm{erf}(\sqrt{\frac{Re}{2x}}y) \\ &\quad +(\frac{1}{2}\sqrt{\frac{\pi}{Re}} - \frac{\sqrt{\pi Re}}{4}\frac{y^2}{x})\mathrm{e}^{-Rey^2/(4x)}\mathrm{erf}(\frac{1}{2}\sqrt{\frac{Re}{x}}y)\end{aligned}\tag{2.35}$$

with $C_3 = -2.26605 + 0.15752 \cdot Re - 0.00265 \cdot Re^2 + 0.00001 \cdot Re^3$.

Chapter 3

The combined spatio-temporal normal mode stability theory

In this chapter the linear stability analysis is introduced and carried on through the classical modal treatment. The essentials of the normal mode theory are presented for two-dimensional viscous incompressible steady parallel flows. After the perturbed system is introduced and the resulting equations are linearized, a partial differential equation is obtained to describe the spatio-temporal evolution of the perturbation (see §3.2). The normal mode theory is presented and, subsequently, the Orr-Sommerfeld equation is derived by introducing the stability characteristics (§3.3). The dispersion relation is defined and the concepts of convective and absolute instability are discussed in §3.4. Some general aspects and significant results on three-dimensionality of the perturbations and on the discrete and continuous spectra are given in §3.5 and in §3.6, respectively.

3.1 Introduction

Traditionally, investigations of disturbances in shear flows have been characterized using classical linear stability analysis. This concept is well founded and is, in principle, correctly recognized as an initial-value problem. However, instead of considering the complete temporal evolution of the perturbations and analyzing the physical cause of a possible instability, the attention has been widely focused on determining whether or not the flow is asymptotically unstable. If only the question of stability is to be answered, the modal analysis turns out to be a powerful and

synthetic means. First contributions have been given by Orr (1907a,b) and Sommerfeld (1908) who separately derived the now-famous Orr-Sommerfeld equation. More recently, significant results in literature for the bluff-body wake stability have been offered by, among others, Mattingly & Criminale (1972), Triantafyllou et al. (1986), Hultgren & Aggarwal (1987), Huerre & Monkewitz (1990).

The modal theory to study the stability of the flow is based on the perturbative analysis. Once the base flow is known, small oscillations are imposed and their asymptotic fate is considered. If they are damped the flow is stable, while if they are amplified the flow is unstable. In the framework of the modal analysis, the solution of the linearized perturbative equations turns into the resolution of an eigenvalue problem, the Orr-Sommerfeld equation.

3.2 Perturbed flow and linearized disturbance equations

It is now assumed the base flow to be steady, parallel, incompressible and viscous. It is described by the physical quantities

$$\begin{cases} U = & U(y) \\ V = & 0 \\ P = & P(x,y). \end{cases} \tag{3.1}$$

The perturbed flow can be decomposed into a steady part and a fluctuating component that oscillates about the base flow

$$\begin{cases} u(x,y,t) = & U(y) + \tilde{u}(x,y,t) \\ v(x,y,t) = & \tilde{v}(x,y,t) \\ p(x,y,t) = & P(x,y) + \tilde{p}(x,y,t) \end{cases} \tag{3.2}$$

where the tilde superscripts indicate fluctuation components that are small with respect to the corresponding mean system quantities ($|\tilde{u}/U| \ll 1$ e $|\tilde{p}/P| \ll 1$). By writing the continuity and the Navier-Stokes equations for the perturbed flow and then subtracting from these the corresponding ones for the base flow, one obtains the following

$$\partial_x \tilde{u} + \partial_y \tilde{v} = 0 \tag{3.3}$$

$$\partial_t \tilde{u} + U\partial_x \tilde{u} + U'\tilde{v} + \partial_x \tilde{p} + \tilde{u}\partial_x \tilde{u} + \tilde{v}\partial_y \tilde{u} = \frac{1}{Re}\nabla^2 \tilde{u} \tag{3.4}$$

$$\partial_t \tilde{v} + U\partial_x \tilde{v} + \partial_y \tilde{p} + \tilde{u}\partial_x \tilde{v} + \tilde{v}\partial_y \tilde{v} = \frac{1}{Re}\nabla^2 \tilde{v}, \tag{3.5}$$

where $U' = dU/dy$.

The system of equations (3.3)-(3.5) is non-linear with respect to the disturbance terms. The non-linear terms are products of the fluctuating velocities and their derivatives. If the oscillation has frequency ω, these terms will have frequency 0 o 2ω. This interaction will either modify the base flow (mean-flow distortion) and feedback to the fluctuating components or introduce higher harmonics. Such difficulties are overcame if it is assumed that the products of the fluctuations and their derivatives have small amplitudes. The terms $\tilde{u}\partial_x \tilde{u}$, $\tilde{v}\partial_y \tilde{u}$, $\tilde{u}\partial_x \tilde{v}$ and $\tilde{v}\partial_y \tilde{v}$ are negligible in comparison with the other terms as a small disturbance multiplied by a small disturbance results in a term of smaller order of magnitude and no longer influences the equations to this order of approximation. The linear system is

$$\partial_x \tilde{u} + \partial_y \tilde{v} = 0 \tag{3.6}$$

$$\partial_t \tilde{u} + U\partial_x \tilde{u} + U'\tilde{v} + \partial_x \tilde{p} = \frac{1}{Re}\nabla^2 \tilde{u} \tag{3.7}$$

$$\partial_t \tilde{v} + U\partial_x \tilde{v} + \partial_y \tilde{p} = \frac{1}{Re}\nabla^2 \tilde{v}. \tag{3.8}$$

The perturbations applied to the system will evolve independently because the non-linear terms, that would permit interaction, have been neglected. The same fundamental property of linearity occurs in other fields (acoustics, electromagnetism, ...), but non-linear equations must often be retained to capture the essential physics. Luckily, the solution of the linear system is sufficient to describe problems where small oscillations influence the base flow. Moreover, it should be reminded that the infinitesimal perturbations cannot be removed and are always present in any physical system.

Due to the assumption of small disturbances, the solution of the original problem can be approximated with the one of the linear system. However, as soon as the perturbation energy grows, the non-linear equations are required to correctly capture the perturbative evolution. For this reason, only the onset – and not the following temporal evolution – of a possible instability is the aim of the linear stability theory.

By differentiating (3.7) with respect to y and (3.8) with respect to x and subtracting the resulting equations to eliminate the pressure gradient terms, a system composed by the continuity equation (3.6) and by the following third order equation

$$\partial_t(\partial_y \tilde{u} - \partial_x \tilde{v}) + U\partial_x(\partial_y \tilde{u} - \partial_x \tilde{v}) + U''\tilde{v} = \frac{1}{Re}\nabla^2(\partial_y \tilde{u} - \partial_x \tilde{v}). \tag{3.9}$$

is obtained. Defining the streamfunction ψ as $\tilde{u} = \partial_y \psi$, $\tilde{v} = -\partial_x \psi$, the continuity equation (3.6) is automatically satisfied and the resulting single partial differential equation for ψ is found to be

$$(\partial_t + U\partial_x)\nabla^2\psi - U''\partial_x\psi = \frac{1}{Re}\nabla^4\psi, \tag{3.10}$$

where $\nabla^4 = \nabla^2 \cdot \nabla^2$. This fourth order partial differential equation for ψ can be solved, in principle, subject to appropriate initial and boundary conditions. Equation (3.10) is sometimes referred to as the Orr-Sommerfeld equation in partial differential equation form.

3.3 Normal mode hypothesis and Orr-Sommerfeld equation

The linearity of the system is immediately exploited by seeking solutions in terms of complex functions. In this way, a variable separation is introduced and a reduction from a partial differential equation (3.10) to an ordinary differential equation is allowed. Normal mode solutions of the form

$$\begin{aligned}
\tilde{u}(x,y,t) &= \frac{1}{2}(\hat{u} + \hat{u}^*) = \frac{1}{2}(\mathbf{u}(y)e^{i(hx-\sigma t)} + \mathbf{u}(y)^* e^{-i(h^* x - \sigma^* t)}),\\
\tilde{v}(x,y,t) &= \frac{1}{2}(\hat{v} + \hat{v}^*) = \frac{1}{2}(\mathbf{v}(y)e^{i(hx-\sigma t)} + \mathbf{v}(y)^* e^{-i(h^* x - \sigma^* t)}),\\
\tilde{p}(x,y,t) &= \frac{1}{2}(\hat{p} + \hat{p}^*) = \frac{1}{2}(\mathbf{p}(y)e^{i(hx-\sigma t)} + \mathbf{p}(y)^* e^{-i(h^* x - \sigma^* t)}),
\end{aligned} \tag{3.11}$$

are to be found. The quantities $\hat{u}$, $\hat{v}$, $\hat{p}$ indicate the complex normal mode, while $\mathbf{u}(y)$, $\mathbf{v}(y)$, $\mathbf{p}(y)$ are functions of the y only and the $*$ quantities are the complex conjugates. Therefore, the sum of the normal mode and its complex conjugate is the real disturbance quantity. The perturbative quantities can be treated separately as the system is linear. In principle, since the complex conjugate values can be obtained from the quantities themselves, it is only necessary to solve for the complex quantities $\hat{u}$, $\hat{v}$, $\hat{p}$. To be solutions for the perturbations, the modal expansions (3.11) have to satisfy the system (3.6)-(3.8). In this way the partial differential equations system (independent variables x, y, t) reduces to a ordinary differential equations system (independent variable y).

Moreover, the amplitude and the phase of the oscillations can be expressed through the use of complex functions, as the eigenvectors $\mathbf{u}(y)$, $\mathbf{v}(y)$, $\mathbf{p}(y)$. For any disturbance, in fact, the amplitude of the cosine and the amplitude of the sine components are to be given. This is done through the real and the imaginary parts of the above complex functions, respectively. With a single complex quantity, the two values (phase and amplitude) characterizing the oscillation can be expressed.

In the above relations $h = k + is$ is identified as the complex wavenumber in x-direction, where k is the wavenumber of the perturbation (wavelength $\lambda = 2\pi/k$) and s is the spatial growth rate. The complex frequency is $\sigma = \omega + ir$, where ω identifies the frequency of the perturbative wave and r is the temporal growth rate. The wave velocity is defined as $c = c_r + ic_i = \sigma/h$, while the phase velocity is $v_p = \omega/k$.
In the more general spatio-temporal stability analysis, both h and σ are complex. The amplitudes of the perturbative functions $\tilde{u}$, $\tilde{v}$ and $\tilde{p}$ are proportional to e^{-sx+rt}. For the temporal evolution, if $r > 0$ for one mode, the corresponding perturbation exponentially grows until the non-linearities become relevant to the system. The mode is unstable. If $r = 0$ the mode is marginally stable, while if $r < 0$ the mode is stable. In general, as a small perturbation can excite all the modes, it is sufficient that $r > 0$ for only one mode to have an unstable configuration for the flow. On the contrary, it is necessary that $r < 0$ for all the modes to have a stable configuration. Similar considerations can be made for the spatial evolution. If $s < 0$ for one mode the flow is spatially unstable. On the contrary, if $s \geq 0$ for all the modes the flow is spatially stable.
To separately consider the temporal and the spatial stability it is sufficient to let $s = 0$ and $r = 0$, respectively.

Let the streamfunction ψ be represented by a normal mode form

$$\psi(x,y,t) = \frac{1}{2}(\hat{\psi} + \hat{\psi}^*) = \frac{1}{2}(\phi(y)e^{i(hx-\sigma t)} + \phi(y)^* e^{-i(h^* x - \sigma^* t)}). \tag{3.12}$$

By substituting (3.12) into the equation (3.10), the following equation holds

$$(U - c)(\phi'' - h^2\phi) - U''\phi = \frac{1}{ihRe}(\phi'''' - 2h^2\phi'' + h^4\phi), \tag{3.13}$$

known as the Orr-Sommerfeld equation. From the partial differential equation (3.10), an ordinary differential equation of the fourth order is found. Proper boundary conditions have to be given for the closure. For bounded flows, the boundary conditions require that ϕ and ϕ' vanish at the walls. For unbounded flows, ϕ and ϕ' must vanish if $|y| \to \infty$.

If the fluid is taken as inviscid ($Re \to \infty$), a second order differential equation

$$(U - c)(\phi'' - h^2\phi) - U''\phi = 0, \tag{3.14}$$

was first derived by Rayleigh (1880) and known as Rayleigh equation. Although often referred as the "inviscid Orr-Sommerfeld" equation, the Rayleigh equation is not a special case ($Re \to \infty$) of the Orr-Sommerfeld equation as it was derived more than 25 years before it.

3.4 Dispersion relation: convective and absolute instability

The Orr-Sommerfeld eigenvalue problem can be expressed as

$$[A(h,Re) + cB(h)]\phi = 0, \tag{3.15}$$

where A and B are square and, in general, complex matrices. In principle, a non-trivial solution of the homogeneous system can be obtained by imposing that

$$det[A(h,Re) + cB(h)] = 0. \tag{3.16}$$

However, the analytical solution of the problem is given only for very simple base flow profiles (e.g. piecewise linear profiles). Numerical means are usually required for more complicate velocity profiles.

From the general solution of the Orr-Sommerfeld equation at a fixed Re, the dispersion relation between the wavenumber and the frequency can be obtained

$$D(h,\sigma; Re) = 0. \tag{3.17}$$

and the explicit form holds

$$\sigma = \sigma(h; Re). \tag{3.18}$$

The dispersion relation gives significant information about the stability characteristics h and σ, as a discrete set of eigenvalues σ_n (with h and Re parameters) can be found. Moreover, this expression is fundamental for a deeper stability analysis involving the velocity group definition and the saddle point perturbative hypothesis. First, the complex group velocity $v_g = \partial\sigma/\partial h$ is defined as the velocity of a wave packet evolving in time and space. Second, a saddle point of the dispersion relation occurs when the velocity group v_g vanishes, that is

$$\frac{\partial\sigma(h; Re)}{\partial h} = 0. \tag{3.19}$$

In these regions of the phase space, the perturbation can grow in time as there is a local increase of energy.
In this context, the instability is defined as *convective* if $r < 0$ for all the modes and if, for at least one mode, $s < 0$ with group velocity v_g equal to zero. If the coordinate system is moving with the phase velocity of the wave the perturbation is amplified, but it remains small at a fixed point as time passes. The disturbance is convected away.
The instability is *absolute* if, for at least one mode, $r > 0$ and the group velocity v_g vanishes. The perturbation is locally growing in time.

The linear theory allows to describe the onset of instability as, when a perturbation establishes, its first behaviour is exponential. However, the subsequent temporal evolution is modified by the non-linear dynamics. This interaction makes the perturbations assume a behaviour which is no longer exponential. Therefore, the linearized equations are useful to study the onset and a possible development of the instability, and not to consider its following evolution.

3.5 Three-dimensionality and Squire's theorem

Up to now, only two-dimensional disturbances have been analyzed. The normal mode theory can be extended from two to three dimensions considering a perturbation velocity field with a z-direction component, ($\tilde{u}(x,y,z,t)$, $\tilde{v}(x,y,z,t)$, $\tilde{w}(x,y,z,t)$). An additional complex wavenumber in the spanwise direction is then introduced in the phase space. The three-dimensional Orr-Sommerfeld equation – expressed in terms of the transversal velocity and no longer in terms of the streamfunction of the perturbation – can be obtained similarly to the two-dimensional one.
Squire (1933) recognized that, through a simple transformation now known as Squire transformation, the three-dimensional Orr-Sommerfeld equation can be reduced to the same form as the two-dimensional Orr-Sommerfeld equation. First, this implies that a three-dimensional problem can be transformed into a two-dimensional one. Second, for parallel flows, only the two-dimensional problem has to be studied for determining stability, as two-dimensional and three-dimensional quantities are linked together through the Squire transformation. Third, the two-dimensional and three-dimensional problems have the same formulation, except that the two-dimensional problem has a lower value of the Reynolds number. Finally, the wave velocity c remains unscaled for the three-dimensional and the two-dimensional problems. All these remarks are summed up in the following theorem

Theorem 3.5.1. *Squire's Theorem (1933): If an exact two-dimensional parallel flow admits an unstable three-dimensional disturbance for a certain value of the Reynolds number, it also admits a two-dimensional disturbance at a lower value of the Reynolds number.*

In other words the theorem could also be stated as, "The minimum Reynolds number for instability will be higher for an oblique three-dimensional wave than for a purely two-dimensional one." Or, "To each unstable three-dimensional perturbation there corresponds a two-dimensional one with a lower Reynolds number (and with a higher longitudinal wavenumber)." Therefore, in the framework of the normal mode theory, only two-dimensional perturbations will be considered.
Anyhow, it should be reminded that the Squire theorem only applies to parallel flows. For more complicated flows, such as three-dimensional or curved mean flows, three-dimensional perturbations have to be considered. Moreover, theorem (3.5.1) does not exclude the possibility that, for sufficiently high Reynolds number values, an unstable oblique wave can occur even if the corresponding two-dimensional one (with the same longitudinal wavenumber k) is stable.

3.6 Discrete and continuous spectra

Finding the most unstable mode, for fixed values of the parameters (e.g. Re) of the dispersion relation, is enough for the stability question to be answered. If instead the complete temporal evolution is the aim of the analysis, then all the modes must be known. The transient becomes critical and cannot be evaluated without this information. Moreover, to consider the most general perturbation, the discrete spectrum given by the relation dispersion has to be joined by the continuous one. Even if in the following normal mode analysis (see §4) the main goal will be to determine whether or not the flow is unstable, it is worth mentioning some significant results on the discrete and continuous spectra.

The discrete spectrum is, in general, a (finite or infinite) set of discrete temporal modes of the Orr-Sommerfeld equation. For profile on a bounded domain, DiPrima & Habetler (1969) showed that this set is complete. Any initial disturbance can be expanded in terms of normal modes and thus the complete solution can be expressed in terms of them. For unbounded domains, general completeness theorems do not exist. However, Miklavčič & Williams (1982) and Miklavčič (1983) proved rigorously that if the mean flow decays exponentially to a constant in the freestream, then only a finite number of eigenvalues exists for a fixed Re, while if the mean flow decays

algebraically, then there exists an infinite discrete set of eigenvalues. In the first case, a continuum must exist for a complete set to span the space solution, while in the latter case no continuum exists.
Moreover, for unbounded flows, most of the numerical works to date (see Criminale et al. 2003) suggest that there is only a finite number of discrete modes (in same cases only one). Since a finite set of modes on the unbounded domain is not complete, it cannot be used to describe an arbitrary perturbation. The continuous spectrum must be considered. Grosch & Salwen (1978) and Salwen & Grosch (1981) showed (not rigorously) that for unbounded flows the set consisting of the discrete modes and the continuum is complete. According to this result, to complete the solution the continuum part has to be included. This can be exploited considering the Orr-Sommerfeld equation with bounded solutions at infinity. For the discrete set ϕ and ϕ' are required to vanish when $y \to \infty$, while for the continuous spectrum ϕ and ϕ' are required to be bounded when $y \to \infty$.

Chapter 4

Multiscale analysis of the wake instability through a synthetic perturbative hypothesis

In this chapter, the stability of the two-dimensional non-parallel wake (previously derived, see §2.3) is analyzed using a multiscale method. After an introduction with a brief state of the art (see §4.1), the base flow is expressed through the new slow variables introduced by the multiscale (see §4.2.1). A spatio-temporal multiscaling is then performed so that the non-parallel effects of the mean flow are directly introduced into the modal stability analysis (§4.2.2). A synthetic hypothesis based on the dominant saddle points of the local dispersion relation is considered to excite the system (§4.2.3). Results, in particular the appearance of absolute instability regions in the first pert of the intermediate wake, and a comparison with global data from numerical and experimental stability studies are offered in §4.2.4. An asymptotic analysis of the far wake is then proposed in §4.3. Concluding remarks are given in §4.4.

4.1 Introduction

The two-dimensional bluff-body wake is a spatially developing flow where self-sustained oscillations occur (see, among others, Mattingly & Criminale 1972, Zebib 1987, Triantafyllou et al. 1986, Huerre & Monkewitz 1990, Oertel 1990). The disturbances, modelled as viscous and incompressible, grow linearly and two-dimensionally in a region of absolute instability that is downstream to the back stagnation point

of the body generating the wake. This region is preceded and followed by a region of convective instability (Monkewitz 1988, Yang & Zebib 1989, Hannemann & Oertel 1989, Pier 2002). The perturbation concentrates in the absolute instability region and tunes to a frequency that corresponds to a global mode, usually selected according to criteria based on the saddle points of the dispersion relation (see, for instance, Chomaz et al. 1991, Monkewitz et al. 1993).
In literature, the base flow is usually considered as locally parallel and the analysis is decomposed into a sequence of equivalent problems. At every longitudinal station downstream the body, the wake profile is approximated through a parallel flow with the same average velocity profile (e.g. Mattingly & Criminale 1972, Triantafyllou et al. 1986, Hultgren & Aggarwal 1987). This is a restrictive assumption, as the transversal dynamics of the system is present neither in the base flow nor in the perturbative equations. Instead, when the base flow evolution is slow compared to the disturbance quantities, the structure of the equations suggests the non-parallel aspects to be inserted through a perturbation approach based on the multiscale analysis. Two scales are usually considered: a long scale for the mean flow variations, and a short scale where the perturbations vary. At the first order, the multiscale allows a differential equation to be written for the wave modulation, which gives the corrections on the stability characteristics. If the multiscale is on the spatial variable, the modulation equation is ordinary and the corrections are on the wavenumber (Tordella & Belan 2005). If the multiscale is on both the spatial and the temporal variables, a partial differential equation for the modulation is obtained (see Bouthier 1972).

4.2 Multiscale approach for the stability analysis

The recognition of the bluff-body intermediate and far wake as a system which slowly evolves with respect to the unsteady fluctuating field leads to the introduction of the slow spatial and temporal variables

$$x_1 = \varepsilon x, \;\; t_1 = \varepsilon t, \tag{4.1}$$

where $\varepsilon = \dfrac{1}{Re}$, according to the thin shear layer assumption for the wake with $Re \in$ [30,100]. The multiple scales method – often referred to as WKBJ (Wentzel-Kramers-Brillouin-Jeffreys) method – relies on the introduction of the small dimensionless parameter ε, the inverse of the Reynolds number, which characterizes the

non-parallelism of the base flow and allows its decomposition. Thus, in terms of the base flow stream function Ψ, the hypothesis $\Psi = \Psi(x_1,y)$ is made. In this way, the (intermediate and far) wake is actually a system which shows a slow streamwise evolution (see §4.2.1).
The hypothesis is accompanied by the assumption that this evolution can influence the stability characteristics through a spatio-temporal modulation of the perturbative wave, which turns into a correction on the complex wavenumber and frequency. The multiscale approach results in an expanded perturbative equation which, here, will be truncated and solved up to the first order of accuracy with regards to ε (see §4.2.2).
In the present study, the disturbance is considered as a variable wave which, at every longitudinal station, corresponds to the most unstable mode. In other words, the perturbative wave has a wavenumber equal to that of the dominant saddle point of the local dispersion relation. This allows the slow streamwise variation to be incorporated into the coefficients of the modulation equation, where the only remaining parameter is the Reynolds number (see §4.2.3).
This results in the determination of the complex wave modulation and downstream distribution (order 0 and order 1) of the stability characteristics values associated to the dominant saddle point of each intermediate section. The longitudinal distributions of the frequency can be compared to global numerical and experimental values, and information about the wake regions where the two data match is obtained (see 4.2.4).

4.2.1 Base flow

The inner solution of the asymptotic Navier-Stokes expansions up to $O(x^{-3/2})$ is assumed to be an approximation of the wake profile (see §2.3) and the adimensional velocity components (U,V) can be written as

$$U = 1 + x^{-1/2}\phi_1(\eta) + x^{-1}\phi_2(\eta) + x^{-3/2}\phi_3(\eta) \tag{4.2}$$
$$V = x^{-1}\chi_2(\eta) + x^{-3/2}\chi_3(\eta). \tag{4.3}$$

According to what previously mentioned, the base flow is a slowly evolving system and is assumed to be expanded through the small parameter ε

$$\Psi(x_1,y) = \Psi_0(x_1,y) + \varepsilon\Psi_1(x_1,y) + \cdots \tag{4.4}$$

Since the quasi-similar transformation (2.8) becomes $\eta = (Re\, x_1)^{-1/2} y$, the velocity components of the base flow can now be expressed as

$$U(x_1,y) = \partial_y \Psi = U_0(x_1,y) + \varepsilon U_1(x_1,y) + \cdots \tag{4.5}$$
$$V(x_1,y) = -\partial_x \Psi = -\varepsilon \partial_{x_1} \Psi = \varepsilon V_1(x_1,y) + \cdots \tag{4.6}$$

By only considering the integer powers of ε up to the first order, Eqs. (4.2), (4.3) can assume the multiscale structure (4.5), (4.6). For the longitudinal component U, it turns out that

$$\begin{aligned} U &= 1 + Re^{-1/2} x_1^{-1/2} \phi_1(y/\sqrt{Re\, x_1}) + Re^{-1} x_1^{-1} \phi_2(y/\sqrt{Re\, x_1}) \\ &\quad + Re^{-3/2} x_1^{-3/2} \phi_3(y/\sqrt{Re\, x_1}) \\ &= \left[1 + Re^{-1/2} x_1^{-1/2} \phi_1(\eta)\right] + \varepsilon \left[x_1^{-1} \phi_2(\eta) + Re^{-1/2} x_1^{-3/2} \phi_3(\eta)\right] , \end{aligned} \tag{4.7}$$

so that

$$U_0 = 1 + Re^{-1/2} x_1^{-1/2} \phi_1 \tag{4.8}$$
$$U_1 = x_1^{-1} \phi_2 + Re^{-1/2} x_1^{-3/2} \phi_3 \, . \tag{4.9}$$

The transversal component V, at the same order of approximation, is given by

$$\begin{aligned} V &= Re^{-1} x_1^{-1} \chi_2(x_1,y) + Re^{-3/2} x_1^{-3/2} \chi_3(x_1,y) \\ &= \varepsilon \left[x_1^{-1} \chi_2(\eta) + Re^{-1/2} x_1^{-3/2} \chi_3(\eta)\right] \end{aligned} \tag{4.10}$$

so that

$$V_1 = x_1^{-1} \chi_2 + x_1^{-3/2} Re^{-1/2} \chi_3 \tag{4.11}$$

4.2.2 Orr-Sommerfeld equation through the multiscaling

For the two-dimensional non-parallel wake the linearized perturbation equation (3.10) becomes

$$\partial_t \nabla^2 \psi + (\partial_x \nabla^2 \Psi) \psi_y + \Psi_y \partial_x \nabla^2 \psi - (\partial_y \nabla^2 \Psi) \psi_x - \Psi_x \partial_y \nabla^2 \psi = \frac{1}{Re} \nabla^4 \psi \, , \tag{4.12}$$

with boundary conditions

$$\lim_{|y|\to\infty} \psi(x,y,t) = 0, \tag{4.13}$$

$$\lim_{|y|\to\infty} \partial_y\psi(x,y,t) = 0, \tag{4.14}$$

and where $\Psi(x,y)$ and $\psi(x,y,t)$ are the stream functions for the base flow and the perturbation, respectively. The following perturbation hypothesis is then introduced (Nayfeh 1973; Saric & Nayfeh 1975)

$$\psi = \varphi(x,y,t;\varepsilon)\,\mathrm{e}^{i\theta(x,t;\varepsilon)} = [\varphi_0(x_1,y,t_1) + \varepsilon\varphi_1(x_1,y,t_1) + \cdots]\,\mathrm{e}^{i\theta(x,t;\varepsilon)}. \tag{4.15}$$

According to the Whitham (1974) theory,

$$\partial_x\theta = h_0 = k_0 + is_0 \tag{4.16}$$

$$\partial_t\theta = -\sigma_0 = -(\omega_0 + ir_0), \tag{4.17}$$

where $\theta = h_0x - \sigma_0t$. The quantities $h_0 = k_0 + is_0$ and $\sigma_0 = \omega_0 + ir_0$, as defined in §3.3, are the complex wavenumber and the complex frequency, respectively. k_0 is the wavenumber and s_0 is the spatial growth rate, while ω_0 is the frequency and r_0 is the temporal growth rate of the perturbation. In terms of the slow variables (x_1,t_1) and θ, the spatial and temporal derivatives transform as

$$\partial_x \to h_0\partial_\theta + \varepsilon\partial_{x_1}, \quad \partial_t \to -\sigma_0\partial_\theta + \varepsilon\partial_{t_1}. \tag{4.18}$$

By applying this transformation to the linearized perturbation equation (4.12), a hierarchy of ordinary differential equations, truncated at the first order in ε, is obtained.

The zero order equation (ε^0) is the homogeneous Orr-Sommerfeld equation, where x_1 and the Reynolds number Re are parameters,

$$\mathcal{A}\varphi_0 = \sigma_0\mathcal{B}\varphi_0 \tag{4.19}$$

$$\varphi_0 \to 0 \text{ as } |y| \to \infty \tag{4.20}$$

$$\partial_y\varphi_0 \to 0 \text{ as } |y| \to \infty\,. \tag{4.21}$$

with $\mathcal{A} = \left\{(\partial_y^2 - h_0^2)^2 - ih_0 Re\left[U_0(\partial_y^2 - h_0^2) - U_0''\right]\right\}$, $\mathcal{B} = -iRe(\partial_y^2 - h_0^2)$. It is useful to write $\varphi_0(x_1,t_1,y) = A(x_1,t_1)\zeta_0(x_1,y)$, where A is the spatio-temporal modulation determined at the next order. Thus, the eigenvalue problem (4.19-4.21) becomes

$$\begin{aligned} \mathcal{A}\zeta_0 &= \sigma_0\mathcal{B}\zeta_0 && (4.22)\\ \zeta_0 &\to 0 \text{ as } |y| \to \infty && (4.23)\\ \partial_y\zeta_0 &\to 0 \text{ as } |y| \to \infty\,. && (4.24) \end{aligned}$$

By numerically solving the system (4.22)-(4.24), the eigenfunction ζ_0 and a discrete set of eigenvalues $\sigma_{0n}(x_1; h_0, Re)$ are obtained. By selecting the eigenvalue with the largest imaginary part a first approximation of the dispersion relation $\sigma_0 = \sigma_0(x_1; h_0, Re)$ is found. According to the Briggs (1964) criterium, a further analysis of this relation, discussed later in §4.2.3, gives the loci of the branching points.

The first-order theory ($O(\varepsilon^1)$) gives the non-homogeneous Orr-Sommerfeld equation, which is parametric in x_1 and Re

$$\begin{aligned} \mathcal{A}\varphi_1 &= \sigma_0\mathcal{B}\varphi_1 + \mathcal{M}\varphi_0 && (4.25)\\ \varphi_1 &\to 0 \text{ as } |y| \to \infty && (4.26)\\ \partial_y\varphi_1 &\to 0 \text{ as } |y| \to \infty\,. && (4.27) \end{aligned}$$

where $\mathcal{A}$ and $\mathcal{B}$ are the operators defined above, and the linear differential operator $\mathcal{M}$ defined as

$$\begin{aligned} \mathcal{M} = \Big\{ & \left[Re(2h_0\sigma_0 - 3h_0^2U_0 - U_0'') + 4ih_0^3\right]\partial_{x_1} && (4.28)\\ & +(Re\,U_0 - 4ih_0)\partial^3_{x_1yy} + -Re\,V_1(\partial_y^3 - h_0^2\partial_y) + Re\,V_1''\partial_y && (4.29)\\ & +ih_0Re\left[U_1(\partial_y^2 - h_0^2) - U_1''\right] + Re(\partial_y^2 - h_0^2)\partial_{t_1}\Big\}, && (4.30) \end{aligned}$$

is a function of the zero-order dispersion relation and eigenfunction as well as of the base flow. It accounts for entrainment effects through the explicit presence of velocity transversal component V_1. Equation (4.25)-(4.27) can be now used to obtain the modulation function $A(x_1,t_1)$, which was left undetermined at the zero order, and to obtain the first order corrections of the stability characteristics.
By means of $\varphi_0(x_1,t_1,y) = A(x_1,t_1)\zeta_0(x_1,y)$, $\mathcal{M}\varphi_0$ is equal to $\mathcal{M}A\zeta_0$, and can be rewritten as

$$\begin{aligned}\mathcal{M}A\zeta_0 &= \Big\{\partial_{x_1}A\left[M_1+M_2\partial_y^2\right]+\partial_{t_1}A\left[M_7+M_8\partial_y^2\right] \\ &\quad +A\left[M_1\partial_{x_1}+M_2\partial^3_{x_1yy}+M_3+M_4\partial_y+M_5\partial_y^2+M_6\partial_y^3\right]\Big\}\zeta_0 \\ &= \hat{\mathcal{M}}\zeta_0 \end{aligned} \tag{4.31}$$

where the coefficients M_j are

$$M_1 = Re(2h_0\sigma_0 - 3h_0^2U_0 - U_0'') + 4ih_0^3 \tag{4.32}$$
$$M_2 = Re\,U_0 - 4ih_0 \tag{4.33}$$
$$M_3 = -ih_0Re(\partial_y^2+h_0^2)U_1 \tag{4.34}$$
$$M_4 = -Re(\partial_y^2+h_0^2)V_1 \tag{4.35}$$
$$M_5 = ih_0Re\,U_1 \tag{4.36}$$
$$M_6 = Re\,V_1 \tag{4.37}$$
$$M_7 = -Re\,h_0^2 \tag{4.38}$$
$$M_8 = Re\,. \tag{4.39}$$

It should be noticed that, in the case of spatial multiscale, coefficients M_7, M_8 do not exist and this leads to the simple ordinary differential equation $d_{x1}A(x_1) = ih_1(x_1)A(x_1)$, where h_1 depends on the M_j, $j = 1,...,6$ (see Tordella & Belan 2005). To avoid secular terms in the solution of (4.25)-(4.27), the non-homogeneous term in equation (4.25) should be orthogonal to each solution of the adjoint homogenous problem. This problem can be written considering the hermitian conjugate equation

$$\tilde{\mathcal{A}}\tilde{\zeta_0} = \sigma_0^*\tilde{\mathcal{B}}\tilde{\zeta_0}\,,$$

where * indicates the complex conjugate quantity, and

$$\begin{aligned}\tilde{\mathcal{A}} &= \left\{(\partial_y^2-h_0^{*2})^2 - \mathrm{i}h_0^*Re\left[(\partial_y^2-h_0^{*2})u_0-\partial_y^2u_0\right]\right\} \\ \tilde{\mathcal{B}} &= \mathrm{i}Re(\partial_y^2-h_0^{*2})\,.\end{aligned}$$

The same equation can be rewritten in the complex conjugate form

$$\mathcal{A}^+\zeta_0^+ = \sigma_0\mathcal{B}\zeta_0^+$$

where

$$\mathcal{A}^+ = \left\{(\partial_y^2 - h_0^2)^2 - \mathrm{i}h_0 Re\left[(\partial_y^2 - h_0^2)u_0 - \partial_y^2 u_0\right]\right\},$$

$\mathcal{B} = \tilde{\mathcal{B}}^*$ and ζ_0^+ is the eigenfunction of the adjoint homogeneous problem. The orthogonality condition is expressed as

$$(\tilde{\zeta_0},\hat{\mathcal{M}}\zeta_0) \equiv \int_{-\infty}^{\infty} \zeta_0^+ \hat{\mathcal{M}}\zeta_0 \mathrm{d}y = \int_{-\infty}^{\infty} \zeta_0^+ \mathcal{M}A\zeta_0 \mathrm{d}y = 0\ . \tag{4.40}$$

This leads to an evolution equation for the modulation A

$$\begin{aligned}(\partial_{x_1}A)\int_{-\infty}^{\infty}\zeta_0^+\left[M_1+M_2\partial_y^2\right]\zeta_0\mathrm{d}y + (\partial_{t_1}A)\int_{-\infty}^{\infty}\zeta_0^+\left[M_7+M_8\partial_y^2\right]\zeta_0\mathrm{d}y\\ +A\int_{-\infty}^{\infty}\zeta_0^+\left[M_1\partial_{x_1}+M_2\partial^3_{x_1yy}+M_3+M_4\partial_y+M_5\partial_y^2+M_6\partial_y^3\right]\zeta_0\mathrm{d}y = 0\end{aligned} \tag{4.41}$$

which is a partial differential equation for x_1 and t_1, and has complex and variable coefficients. By substituting $A(x_1,t_1)$ with $e^{a(x_1,t_1)}$ (see Bouthier 1972) and going back to the original coordinates x and t, the equation (4.41) can be written as

$$\partial_t a + p(x)\partial_x a + \varepsilon q(x) = 0 \tag{4.42}$$

where coefficients

$$p(x) = \frac{\int_{-\infty}^{\infty}\zeta_0^+\left[M_1+M_2\partial_y^2\right]\zeta_0\,\mathrm{d}y}{\int_{-\infty}^{\infty}\zeta_0^+\left[M_7+M_8\partial_y^2\right]\zeta_0\,\mathrm{d}y} \tag{4.43}$$

and

$$q(x) = \frac{\int_{-\infty}^{\infty}\zeta_0^+\left[M_1\partial_{x_1}+M_2\partial^3_{x_1yy}+M_3+M_4\partial_y+M_5\partial_y^2+M_6\partial_y^3\right]\zeta_0\,\mathrm{d}y}{\int_{-\infty}^{\infty}\zeta_0^+\left[M_7+M_8\partial_y^2\right]\zeta_0\,\mathrm{d}y} \tag{4.44}$$

are not singular.

The modulation equation (4.42) is numerically solved specifying proper initial and boundary conditions. The considered spatial domain extends from a few body-scales D downstream from the body to the far field (in the present computations

$x_i < x < x_f$, where $x_i = 3$ and $x_f = 60$). Since the differential equation is of the first order for the variable x, only one boundary condition has to be imposed. The modulation equation is required to satisfy to asymptotic uniformity in the far field $x = x_f$, that is the Neumann condition

$$(\partial_x a)_{x=x_f} = 0, \forall\ t. \tag{4.45}$$

A natural choice for the initial condition is

$$a_{x,t=0} = (const)\,(1+i). \tag{4.46}$$

The solution at the first order is $\varphi_1(x_1,y,t_1) = A(x_1,t_1)\zeta_1(x_1,y)$ while for the complete problem (order 0 + order 1) is

$$\psi = (\varphi_0 + \varepsilon\varphi_1)e^{i\theta} = A(x_1,t_1)(\zeta_0 + \varepsilon\zeta_1)e^{i\theta} = (\zeta_0 + \varepsilon\zeta_1)e^{i\theta + i\theta_1}\ . \tag{4.47}$$

By defining $a = i\theta_1$ and the complete phase as $\Theta = \theta + \theta_1$, the solution (4.47) can be written as

$$\psi = (\zeta_0 + \varepsilon\zeta_1)e^{i\Theta}\ . \tag{4.48}$$

The Whitham theory can be also applied to the complete phase, obtaining

$$\partial_x\Theta = h = k + is \tag{4.49}$$
$$\partial_t\Theta = -\sigma = -(\omega + ir), \tag{4.50}$$

where h and σ are the complex wavenumber and the complex frequency of the complete problem, respectively. Using relation (4.18), one has

$$h = \partial\Theta/\partial x = h_0\partial\Theta/\partial\theta + \varepsilon\partial\Theta/\partial x_1 = h_0 + \varepsilon\partial\theta_1/\partial x_1 \tag{4.51}$$
$$\sigma = -\partial\Theta/\partial t = -\sigma_0\partial\Theta/\partial\theta + \varepsilon\partial\Theta/\partial t_1 = -\sigma_0 + \varepsilon\partial\theta_1/\partial t_1. \tag{4.52}$$

The first order corrections of the instability characteristics are thus obtained as

$$h_1 = \partial\theta_1/\partial x_1 = k_1 + is_1, \sigma_1 = -\partial\theta_1/\partial t_1 = \omega_1 + ir_1\ . \tag{4.53}$$

Once a (or equivalently θ_1) is numerically known, the corrections of the stability characteristics h_1 and σ_1 are obtained by numerical differentiation of the same solution a.

In particular, the solution is known on a discrete spatial domain x_1,x_2....x_N, and can be integrated forward in time in t_0,t_1,...t_M. However, the temporal derivatives are computed at the first temporal step t_0, as the linear stability analysis can only describe the onset of the instability and not its following temporal evolution, which is influenced by the interaction of the growing non-linearities.

Moreover, it should be recalled that the first order analysis does not influence the dispersion relation approximation and the subsequent saddle points research, which are both determined at the zero order. The perturbation hypothesis based on the saddle points sequence determines, at the first order, an *a posteriori* correction on the stability characteristics previously approximated at the zero order.

4.2.3 Saddle point perturbative hypothesis

Coefficients $p(x)$ and $q(x)$ of the modulation equation (4.42) are functions of the disturbance and of the base flow. The base flow is only present in p through the zero-order longitudinal velocity U_0, while the first order longitudinal and transversal velocities U_1 and V_1 are present in q. The distributions of the real and imaginary parts of coefficients p and εq are here computed by inserting in h_0 and σ_0 the values of the dominant saddle point of the zero order dispersion relation taken at each x position along the wake. For a visualization, see the multidimensional map for frequency $\omega_0(k_0,\ s_0)$ and temporal growth rate $r_0(k_0,s_0)$ in Fig 4.2, and the two-dimensional level curves for frequency (dashed lines) and temporal growth rate (solid lines) in Fig. 4.1, for $Re = 35$ and $x = 4$.

The distributions of coefficients p and εq (real and imaginary parts) are instead shown in Fig. 4.3 for Re = 35, 50 and 100.

In so doing, the disturbance is locally tuned, through the modulation function, to the property of the instability as can be seen from the zero-order theory (near-parallel parametric Orr-Sommerfeld treatment). This leads to a synthetic analysis of the non-parallel correction on the instability characteristics. In such a way, the parametrization with respect to the longitudinal position in the wake (Belan and Tordella 2006) (see Fig. 4.7) is not necessary since the evolution of the zero order dispersion relation is directly inserted into the variable coefficients of the modulation equation. The streamwise variation of the instability characteristics is deduced from

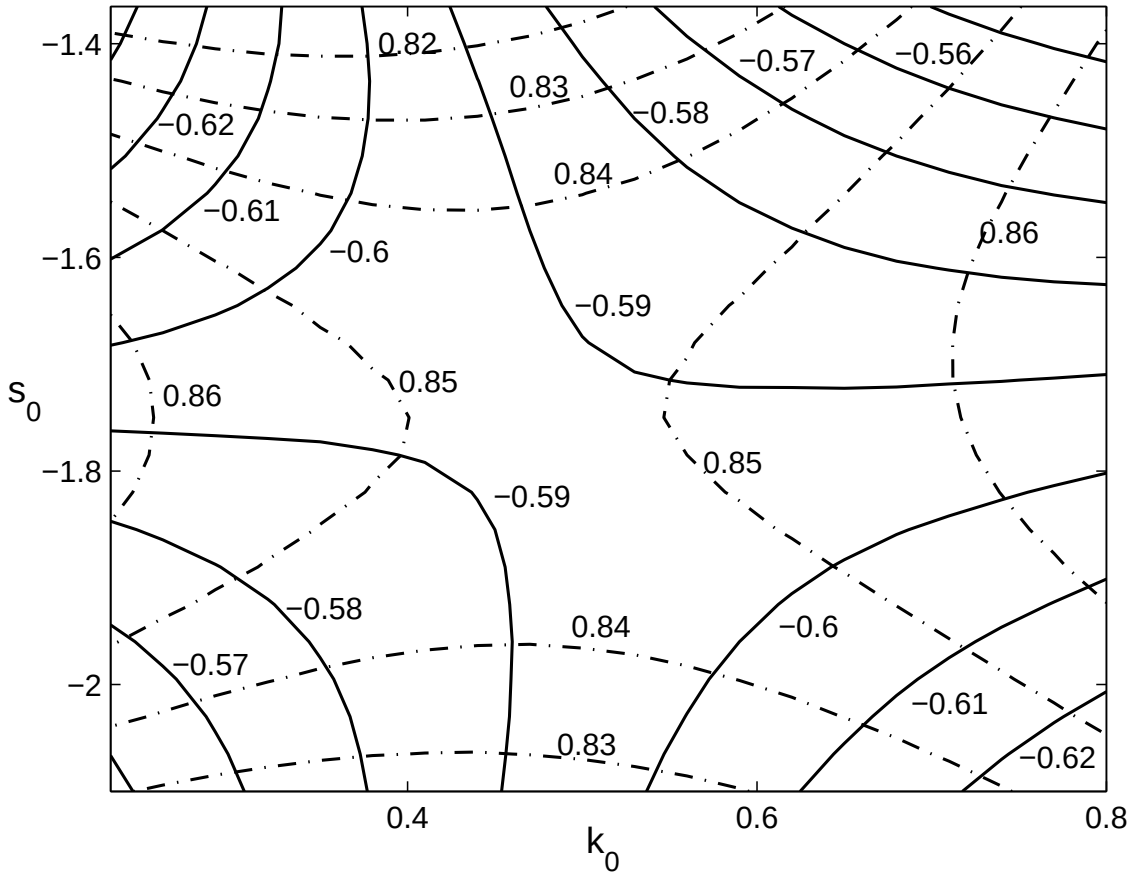

Figure 4.1. Saddle point level curves for $Re = 35$, $x = 4$. ω_0=cost (dashed curves), r_0=cost (solid curves).

the spatial and temporal derivatives of the modulation function. With this new approach, the system is considered as locally perturbed by waves with a wavenumber that varies along the wake and which is equal to the wavenumber of the dominant saddle point of the zero order dispersion relation, taken at different Reynolds numbers. Since the perturbation is no more parameterized with respect to a given wave number, the Reynolds number remains the only parameter of the present stability analysis. The branching points distribution along the longitudinal coordinate and for $Re = 35$,50 and 100, is given in Table 4.1.

As the Orr-Sommerfeld problem (4.22-4.25) solution is necessarily computed on a numerical bounded domain instead of on the theoretical unbounded one, the determination of the saddle points is sensitive to the extension of the actual numerical

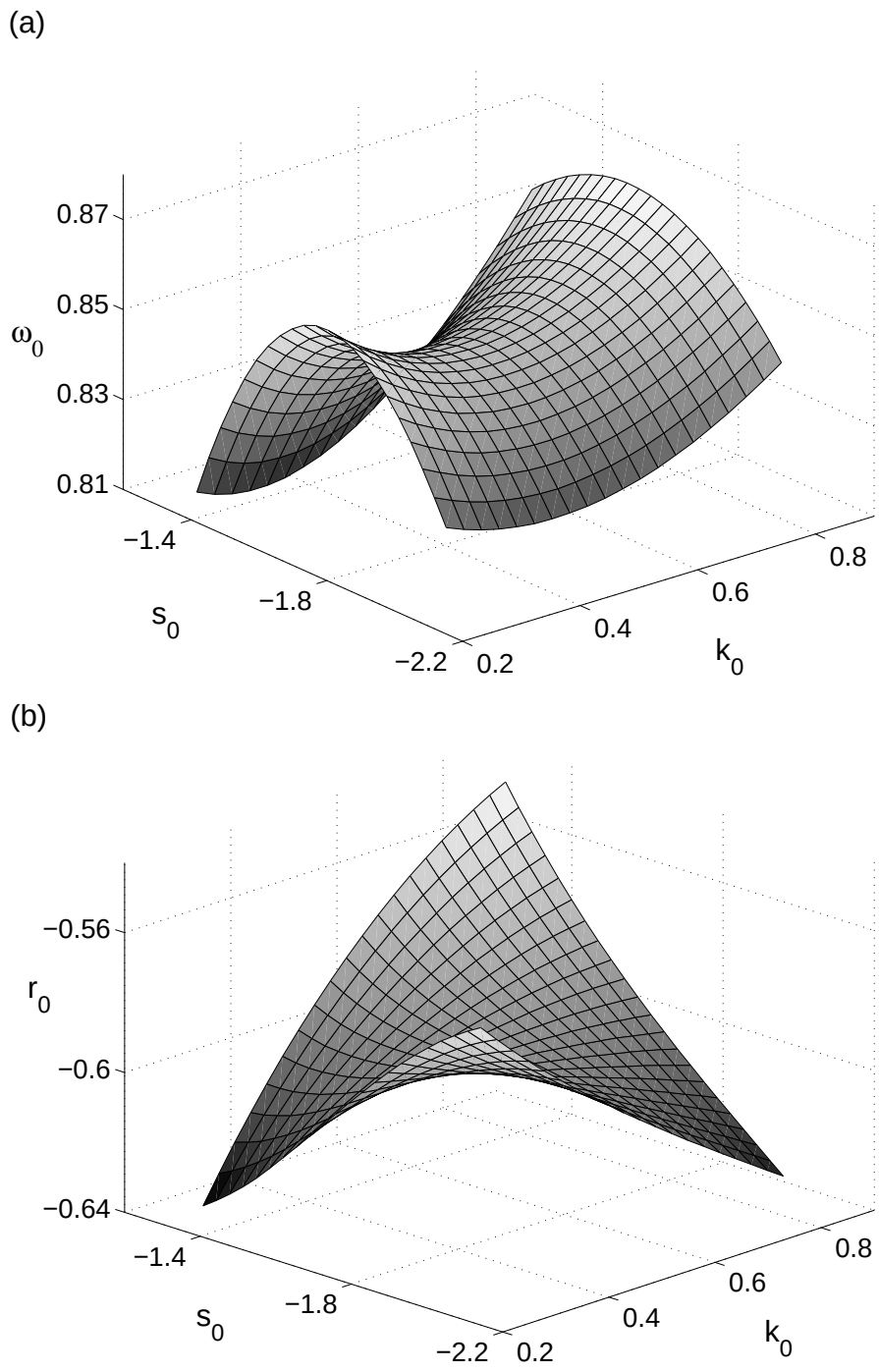

Figure 4.2. Multidimensional map: (a) $\omega_0(k_0, s_0)$ and (b) $r_0(k_0,s_0)$; Re=35, x=4.

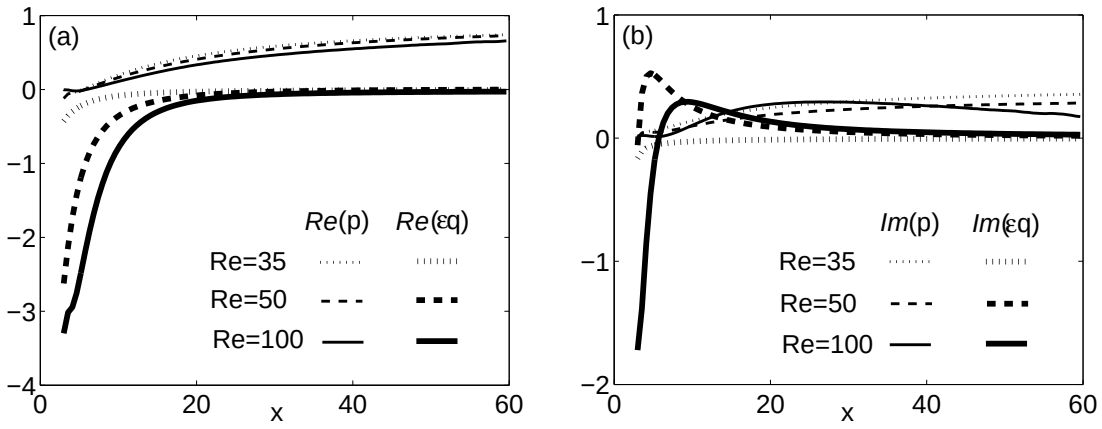

Figure 4.3. Real (a) and imaginary (b) part of the modulation equation coefficients.

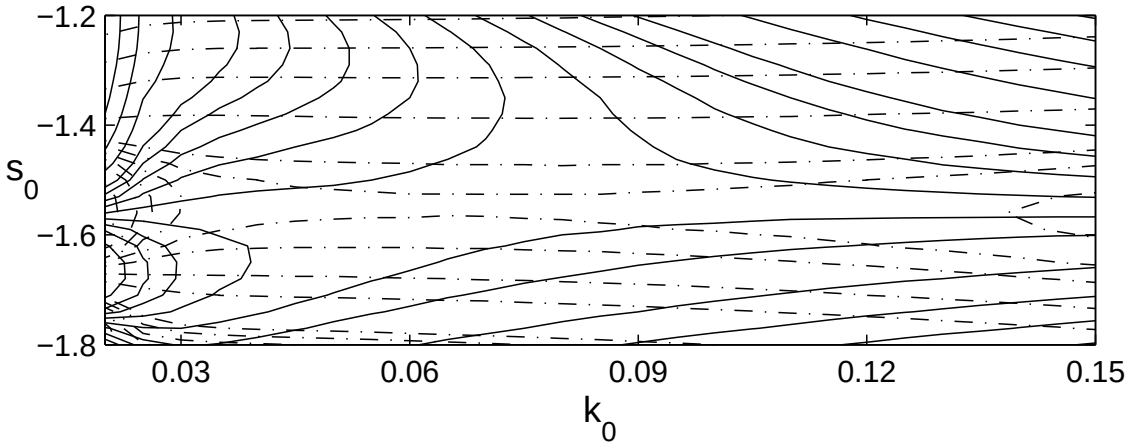

Figure 4.4. Saddle point level curves for $Re = 50$, $x = 7$. ω_0=cost (dashed curves), r_0=cost (solid curves).

domain and to the number and choice of the collocation points.
Moreover, problems arise when small values of k_0 are reached because singularities are present on the s_0 axis in the complex wave number plane. This aspect already becomes important at a few diameters behind the cylinder, since the wavenumber rapidly decreases with the longitudinal coordinate x. See Fig. 4.4 ($Re = 50$, $x = 7$), where the saddle point research is already affected by singularities present at $k_0 = 0$.

For these reasons, by minimizing the relative error between the data and the curves, truncated Laurent series have been used to extrapolate the saddle point

x	Re = 35	Re = 50	Re = 100
3.00	h_0 = 0.9730 -i1.9040	h_0 = 1.3850 -i2.2160	h_0 = 2.9000 -i1.5960
	σ_0 = 1.0194 -i0.4861	σ_0 = 1.2504 -i0.4567	σ_0 = 1.5825 +i0.1513
4.10	h_0 = 0.4167 -i1.7171	h_0 = 0.6254 -i2.0754	h_0 = 2.3544 -i2.2444
	σ_0 = 0.8388 -i0.6022	σ_0 = 1.0430 -i0.6286	σ_0 = 1.5138 -i0.1695
5.20	h_0 = 0.2242 -i1.5156	h_0 = 0.3505 -i1.8620	h_0 = 1.6796 -i2.5098
	σ_0 = 0.6857 -i0.6486	σ_0 = 0.8681 -i0.7067	σ_0 = 1.3992 -i0.3818
6.30	h_0 = 0.1381 -i1.3477	h_0 = 0.2232 -i1.6712	h_0 = 1.2244 -i2.4207
	σ_0 = 0.5769 -i0.6597	σ_0 = 0.7366 -i0.7368	σ_0 = 1.2755 -i0.5357
7.40	h_0 = 0.0929 -i1.2123	h_0 = 0.1547 -i1.5125	h_0 = 0.9249 -i2.2238
	σ_0 = 0.4951 -i0.6545	σ_0 = 0.6361 -i0.7433	σ_0 = 1.1537 -i0.6304
9.60	h_0 = 0.0500 -i1.0129	h_0 = 0.0874 -i1.2736	h_0 = 0.5789 -i1.8246
	σ_0 = 0.3810 -i0.6249	σ_0 = 0.4951 -i0.7254	σ_0 = 0.9426 -i0.7106
12.35	h_0 = 0.0280 -i0.8474	h_0 = 0.0516 -i1.0718	h_0 = 0.3657 -i1.4590
	σ_0 = 0.2917 -i0.5794	σ_0 = 0.3838 -i0.6842	σ_0 = 0.7469 -i0.7209
16.20	h_0 = 0.0154 -i0.6996	h_0 = 0.0301 -i0.8895	h_0 = 0.2235 -i1.1465
	σ_0 = 0.2172 -i0.5211	σ_0 = 0.2889 -i0.6253	σ_0 = 0.5645 -i0.6888
22.80	h_0 = 0.0075 -i0.5537	h_0 = 0.0159 -i0.7082	h_0 = 0.1218 -i0.8782
	σ_0 = 0.1504 -i0.4457	σ_0 = 0.2001 -i0.5447	σ_0 = 0.3853 -i0.6225
32.15	h_0 = 0.0038 -i0.4446	h_0 = 0.0087 -i0.5717	h_0 = 0.0675 -i0.7166
	σ_0 = 0.1058 -i0.3766	σ_0 = 0.1370 -i0.4686	σ_0 = 0.2563 -i0.5532
44.80	h_0 = 0.0020 -i0.3671	h_0 = 0.0051 -i0.4743	h_0 = 0.0392 -i0.6271
	σ_0 = 0.0774 -i0.3204	σ_0 = 0.0940 -i0.4056	σ_0 = 0.1692 -i0.4951
59.65	h_0 = 0.0012 -i0.3170	h_0 = 0.0033 -i0.4112	h_0 = 0.0251 -i0.5820
	σ_0 = 0.0608 -i0.2808	σ_0 = 0.0672 -i0.3609	σ_0 = 0.1157 -i0.4542

Table 4.1. Distribution of the saddle points along the longitudinal coordinate.

behavior from data at the lower x values. These data are more accurate, because the values of k_0 are not too small at these longitudinal stations. The extrapolating curves obtained are in agreement with the asymptotic analysis of the stability characteristics, see §4.3, Fig. 4.9.

Assuming that k_0 is non-negative, its extrapolating function is $k_0(x) = \sum_i c_i^k x^{-i}$,$i$ = 1,2,.... For the other stability characteristics (s_0, ω_0, r_0), the extrapolating functions are $s_0(x) = \sum_i c_i^s x^{-i+1}$, $\omega_0(x) = \sum_i c_i^\omega x^{-i+1}$, $r_0(x) = \sum_i c_i^r x^{-i+1}$,$i$ = 1,2,....

The Laurent series coefficients for the stability characteristics are given in tables 4.2 and 4.3, while in table 4.1 the longitudinal evolution of the extrapolating curves for the stability characteristics is shown. The domain of validity is $3 < x < 60$

Re	$k_0(x) = \sum_i c_i^k x^{-i}$	$s_0(x) = \sum_i c_i^s x^{-i+1}$
35	c_1^k = 0.0205 c_2^k = 2.7405 c_3^k = 15.1650 c_4^k = 8.1000	c_1^s = -0.1610 c_2^s = -9.5190 c_3^s = 12.8700
50	c_1^k = 0.1100 c_2^k = 4.8450 c_3^k = 20.0700 c_4^k = 5.4000	c_1^s = -0.2140 c_2^s = -12.0660 c_3^s = 18.1800
100	c_1^k = 0.7175 c_2^k = 45.8525 c_3^k = 38.3850 c_4^k = -312.3000	c_1^s = -0.0005·10^3 c_2^s = -0.0007·10^3 c_3^s = -0.2271·10^3 c_4^s = 1.2726·10^3 c_5^s = -1.8436·10^3

Table 4.2. Complex wavenumber extrapolating curve of the downstream distribution of the dominant saddle points.

Re	$\omega_0(x) = \sum_i c_i^\omega x^{-i+1}$	$r_0(x) = \sum_i c_i^r x^{-i+1}$
35	c_1^ω = 0.0187 c_2^ω = 2.0880 c_3^ω = 28.5906 c_4^ω = -201.5260 c_5^ω = 601.3316 c_6^ω = -688.1536	c_1^r = -0.1403 c_2^r = -9.4102 c_3^r = 65.0415 c_4^r = -230.5392 c_5^r = 472.4563 c_6^r = -420.4417
50	c_1^ω = -0.0114 c_2^ω = 4.5533 c_3^ω = 9.1532 c_4^ω = -78.4682 c_5^ω = 205.6623 c_6^ω = -220.1156	c_1^r = -0.1999 c_2^r = -10.8650 c_3^r = 79.9060 c_4^r = -285.3133 c_5^r = 576.7085 c_6^r = -502.1086
100	c_1^ω = 0.0000 c_2^ω = 0.0081·10^3 c_3^ω = 0.0531·10^3 c_4^ω = -0.5530·10^3 c_5^ω = 1.6819·10^3 c_6^ω = -1.7701·10^3	c_1^r = -0.0003·10^3 c_2^r = -0.0092·10^3 c_3^r = 0.0405·10^3 c_4^r = 0.2403·10^3 c_5^r = -1.5176·10^3 c_6^r = 2.1540·10^3

Table 4.3. Complex frequency extrapolating curve of the downstream distribution of the dominant saddle points.

and the Reynolds number values are Re = 35,50,100. In Fig. 4.5, some significant data (symbols) computed in the early spatial domain and the relative extrapolating curves for the stability characteristics are shown in the spatial range $3 < x < 30$.

4.2.4 Results

The first-order correction of the instability characteristics is obtained through relation (4.53), after the modulation equation (4.42) is solved with the associated accessory conditions, (4.45) and (4.46).
It can be seen, in Fig. 4.6, that the correction of the characteristics values - at the saddle points - increases with the Reynolds number. At the subcritical Reynolds number, Re = 35, the lowest value here considered, the correction is negligible throughout the intermediate and far domain.

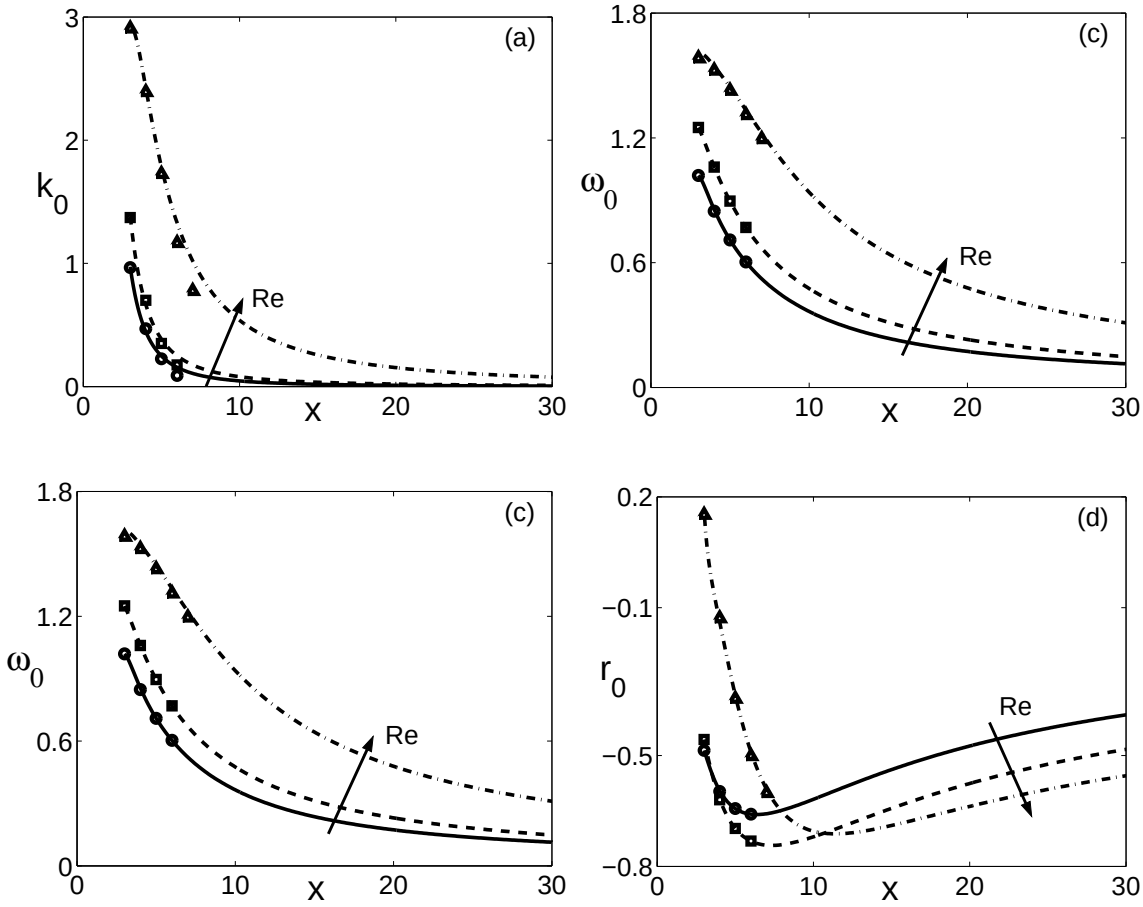

Figure 4.5. Instability characteristics at order zero: (a) wavenumber, (b) spatial growth rate, (c) angular frequency (pulsation), (d) temporal growth rate; $Re = 35{,}50{,}100$. Computed data (symbols) and extrapolating curves.

Another general feature, which is Reynolds number independent, is the vanishing of the first-order correction as $x \to \infty$. In the first part of the intermediate wake, $3 < x < 20$, the multiscaling correction instead increases the values of all the four characteristics. The perturbation wave has, here, shorter wavelength and temporal period, and an increase of spatial and temporal growth rates is observed, see Fig. 4.6. While an increase of the temporal growth rate r means a wave configuration that is more unstable in the absolute sense, an increase of the spatial growth rate s results in a perturbation configuration that is convectively more stable.

The largest variations between the complete and the zero-order results are shown

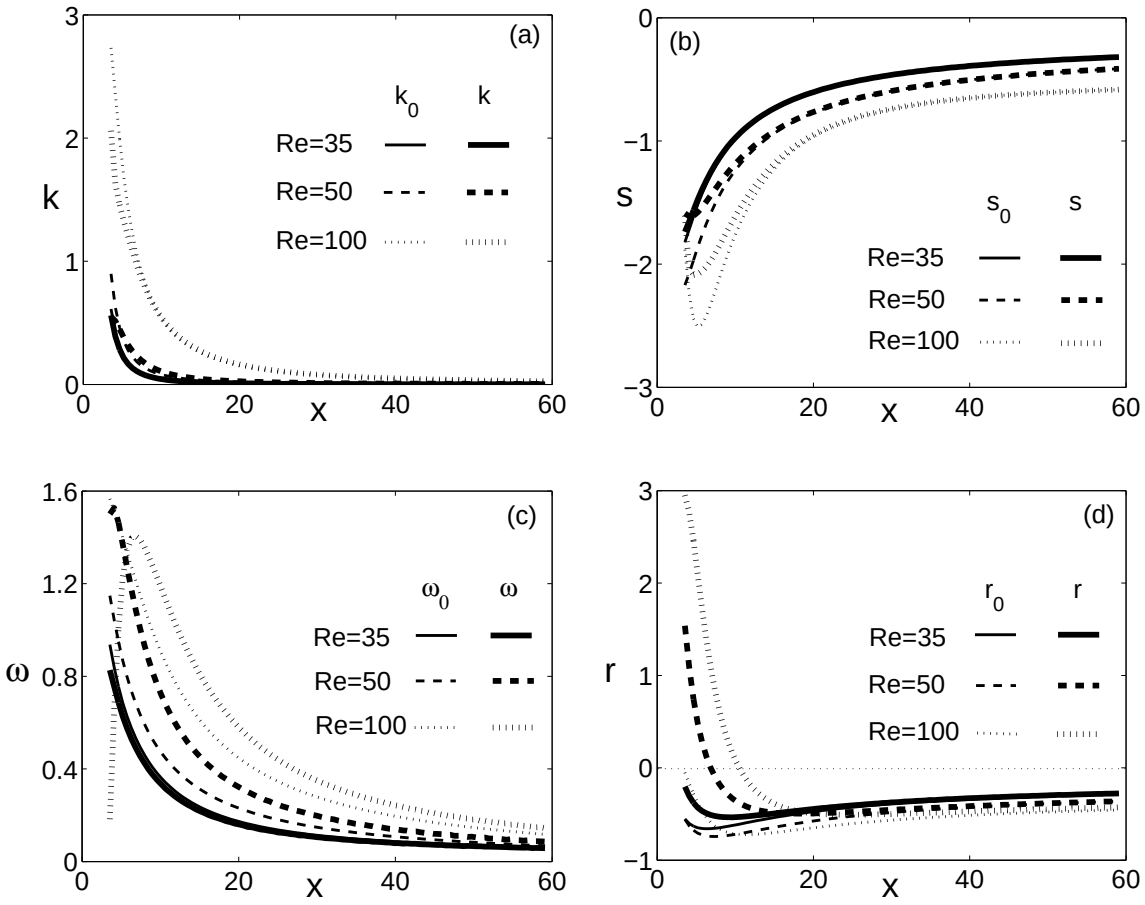

Figure 4.6. Instability characteristics: (a) wavenumber, (b) spatial growth rate, (c) angular frequency (pulsation), (d) temporal growth rate; $Re = 35{,}50{,}100$.

by the pulsation ω and the temporal growth factor r, see Fig. 4.6(c,d). In fact, for these quantities, corrections of the order of $50 \sim 100\%$ can be observed in the first 15 diameters downstream to the body. At $Re = 100$, the complete pulsation exhibits a point of relative maximum for $x \sim 7$. The temporal growth factor r becomes positive, for both $Re = 50$ and 100, in the first part of the intermediate wake region. Thus, at these Reynolds numbers, absolute instability pockets appear which extend to $x \sim 7$ and $x \sim 10$, respectively. The instability turns out to be convective throughout the spatial domain. In the meantime, the analysis leads to marginal conditions of convective and absolute stability for the asymptotic wake (s,$r \to 0$ as $x \to \infty$, respectively) for all the Reynolds number considered ($Re = 35{,}50{,}100$).

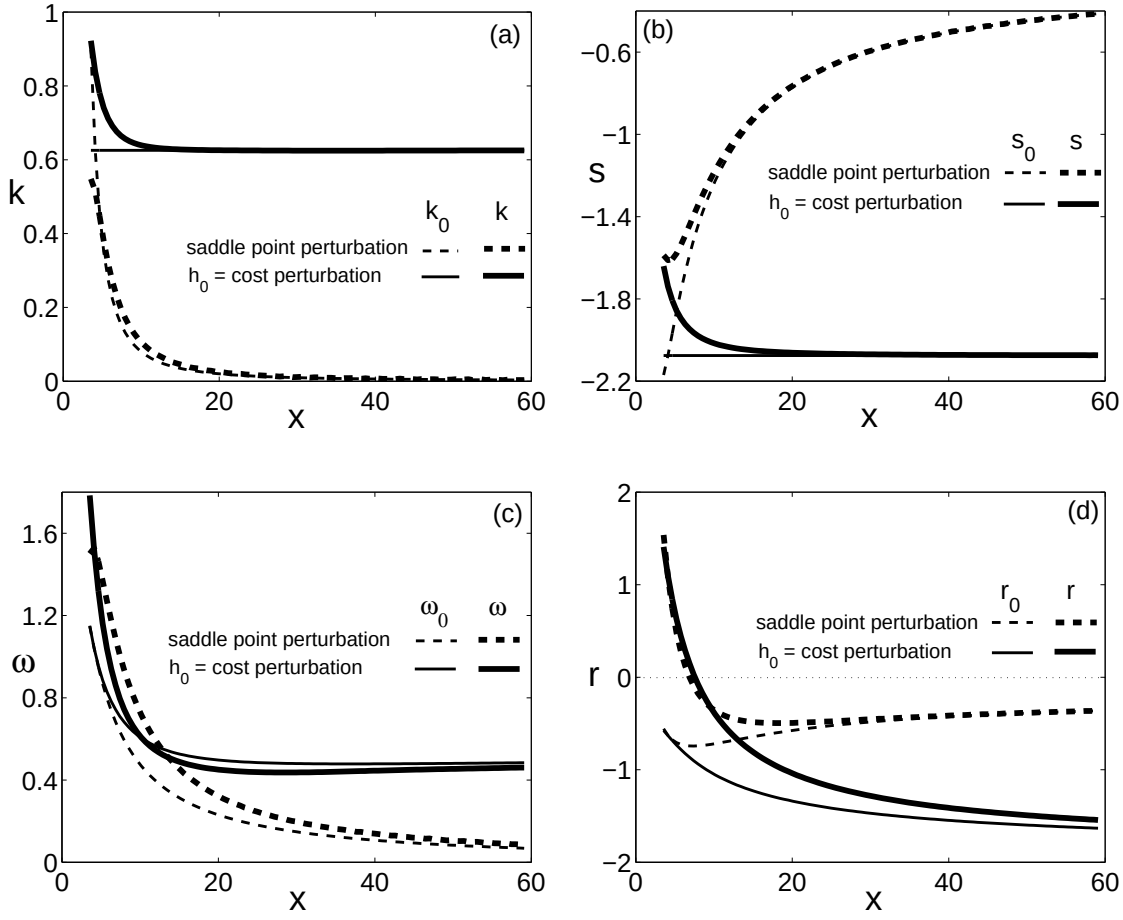

Figure 4.7. Comparison between the instability characteristics with the present perturbation hypothesis (spatial sequence of saddle points) and the perturbation with $h_0(x = 4.10)$=cost at Re=50: (a) wave number, (b) spatial growth rate, (c) pulsation, (d) temporal growth rate.

This latter result on marginal stability will be later confirmed by the asymptotic analysis (see §4.3).

It should be noted that the first order corrections are really relevant, especially for the complex frequency, in the near wake for increasing values of the Reynolds number. The order of correction can easily reach 100% or more in this region, and this means that here the non-parallelism effects are no longer negligible. Moreover, corrections have to be much smaller than the original values to be acceptable. Thus, instability characteristics values for longitudinal coordinates about $x < 5 - 7$ only

offer a qualitative behaviour but are, in no way, valid for the stability analysis. As previously said, indeed, the near wake region falls outside the domain of the present analysis. Going downstream, the first order corrections become smaller but still important, at least in the intermediate wake. In the far wake, they are vanishing. Considering the spatial evolution of first order corrections with respect to zero order values, an extension of the multiscale to second order corrections seems unnecessary. The $O(\varepsilon^2)$ corrections would not affect results so much in the region where parallel flow theory is valid, and they would be completely useless where first order corrections are already too big.

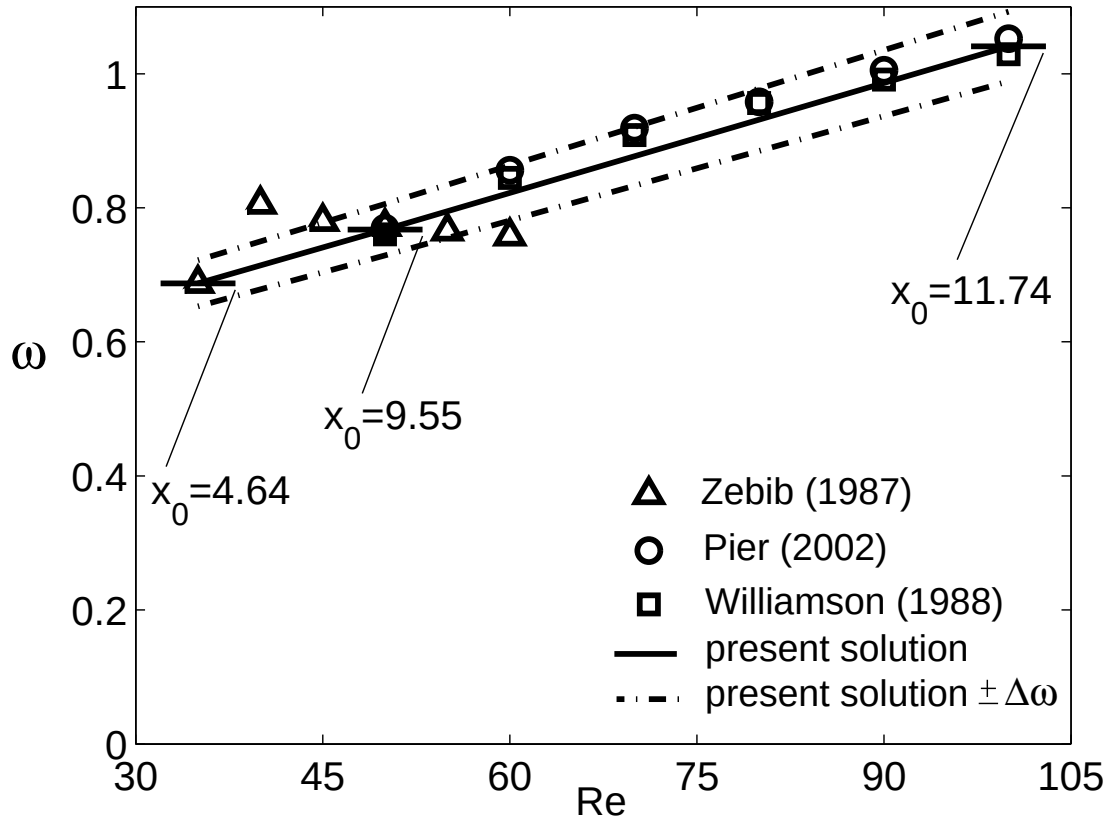

Figure 4.8. Comparison between the global pulsation data according to Pier (2002), Zebib (1987), Williamson (1988) and present solution (accuracy $\Delta\omega = 0.05$).

Fig. 4.7 shows a comparison between the results of the present perturbation hypothesis and those obtained considering the system disturbed by a wave with a complex wave number which is kept constant downstream to the wake (Belan and Tordella, 2006), and equal to the zero-order value shown at the saddle point in

$x = 4.10$, see Fig. 4.7(a,b). One can see that the two perturbation hypothesis yield the same results close to $x = 4.10$, but differ downstream, where, in latter case, the perturbation is no longer locally tuned to the most unstable wave number, which results in forcing the system to the chosen wave number in the positions of the wake that are different from $x = 4.10$. A similar behavior is observed if the position of the forcing point is moved along the wake. It can thus be concluded that the present perturbation, being tuned to the natural sequence along the longitudinal coordinate of the proper wave numbers, is an efficient tool to highlight the evolution of the stability properties in the intermediate wake.

Data from the global results obtained by Pier (2002, DNS simulations), Williamson (1988, laboratory observations), and Zebib (1987, numerical experiments) are included in Fig. 4.8. In this figure the x positions pointed out represent the wake sections where the longitudinal distribution of pulsation obtained with the present method match the global pulsation obtained in these numerical and laboratory experiments. These regions, for $Re = 50$ and 100, are very close to the ones where the temporal growth rate r is observed to change its sign leading to absolutely unstable configurations (see Fig. 4.6(d)). A linear interpolation on the frequency points determined is proposed. The experimental data fall within an accuracy of $\pm 5\%$ around the pulsation interpolating curve that grows with the Reynolds number.

4.3 Eigenfunction and eigenvalue asymptotic theory

Based on the Orr-Sommerfeld problem properties at zero order, an asymptotic analysis of the stability characteristics k_0, s_0, ω_0, r_0 is here presented in the limit $x \to \infty$.

The present nonparallel stability analysis shows that the saddle point wave numbers k_0 decay rapidly as $x \to \infty$. Thus we can assume this decay as a hypothesis of behavior of the solutions of equation (4.22). In the same equation, the base flow longitudinal component U_0 appears together with its second y derivative $\partial_y^2 U_0$. The relevant asymptotic forms are

$$U_0 = 1 + x^{-1/2}\phi_1(yx^{-1/2}) = 1 - \frac{A}{e^{\frac{Rey^2}{4x}}\sqrt{x}} \sim O(1) \tag{4.54}$$

$$\partial_y^2 U_0 = \frac{ARe}{2e^{\frac{Rey^2}{4x}}x^{\frac{3}{2}}} - \frac{ARe^2y^2}{4e^{\frac{Rey^2}{4x}}x^{\frac{5}{2}}} \sim O(x^{-3/2}). \tag{4.55}$$

It can be seen that $\partial_y^2 U_0$ is negligible in comparison to U_0, therefore operator $\mathcal{A}$, which is present in (4.19) and (4.22), becomes

$$\mathcal{A} = \left\{(\partial_y^2 - h_0^2)^2 - ih_0 Re\, U_0\, (\partial_y^2 - h_0^2)\right\}. \tag{4.56}$$

Now the eigenvalue problem (4.22) with the relevant boundary conditions can be rewritten in the form

$$\left\{\partial_y^2 - h_0^2 - ih_0 Re\, U_0\right\} f = -iRe\sigma_0 f, \tag{4.57}$$

$$f \to 0 \text{ as } |y| \to \infty. \tag{4.58}$$

where

$$f(x,y) = (\partial_y^2 - h_0^2)\varphi_0(x,y). \tag{4.59}$$

It is useful to rewrite the base flow in the form $U_0 = 1 + g(x,y)$, where $g(x,y) = -Ax^{-1/2}e^{-\frac{Re\, y^2}{4\, x}}$ is the well-known asymptotic gaussian law for velocity defect in the wakes. Parameter $P = ih_0 Re$ and the generalized eigenvalue $w = iRe\sigma_0 - ih_0 Re - h_0^2$ are also introduced. The eigenvalue problem (4.57) finally becomes

$$\left(-\partial_y^2 + P\, g\right) f = w f, \tag{4.60}$$

with the same boundary conditions. In this equation, $P = ih_0 Re \sim -s_0 Re$ is a real parameter according to the hypothesis $k_0 \sim 0$. One can observe that (4.60) is the stationary Schrödinger equation. Moreover, if we assume $s_0 < 0$, in agreement with the numerical results described in §4.2.4, positive values are obtained for the P parameter. Product $Pg(x,y)$ at a given x is therefore a negative function throughout, that vanishes as $|y| \to \infty$. This makes the eigenvalue problem (4.60) become the famous 1D 'potential well' problem, which has been widely treated in theoretical physics (see Messiah, 1960).

Some properties of this problem should be mentioned at this point: the operator in (4.60) is now self-adjoint and thus the eigenvalues w are real. The eigenvalue spectrum has a discrete part $\{w_0, w_1, w_2 ...\}$, and all these eigenvalues satisfy the inequality

$$g_{min} < w_n < 0, \tag{4.61}$$

where $g_{min} = -Ax^{-1/2}$ is the axial value of g (wake center). There is also a continuous spectrum in the range $w > 0$, but its physical meaning lies outside the aim of the present analysis.

These properties lead to interesting consequences. First, since w is real

$$\Im\{w\} = \Im\{iRe\sigma_0 - ih_0Re - h_0^2\} = -k_0(Re + 2s_0) + Re\omega_0 = 0, \tag{4.62}$$

so that $k_0 \sim 0$ implies

$$\omega_0 \sim 0, \tag{4.63}$$

that is, if the saddle point wave numbers k_0 vanish rapidly, the pulsation ω_0 should also vanish rapidly. This result is in good agreement with the present numerical computations, see figure 4.6.

Second, since $k_0 \sim 0$, the inequality (4.61) shows that

$$g_{min} < -r_0Re + s_0(Re + s_0) < 0. \tag{4.64}$$

However, in the limit $x \to \infty$, $g_{min} \to 0$. Thus, $-r_0Re + s_0(Re + s_0) \sim 0$ and a relation between the asymptotic behavior of the temporal and spatial growth rates can be found:

$$r_0 \sim s_0 + s_0^2/Re. \tag{4.65}$$

Since finite values for an asymptotic uniform flow at infinity are unphysical, because uniformity means absence of spatial and temporal scales, and since positive infinite values for r_0 are *a priori* excluded, it can be evinced that both r_0,$s_0 \to 0$.

In the asymptotic limit, this result is in good agreement with the numerical computations, as shown in Fig. 4.9 where the computations are compared with the simple curves $r_0 = s_0 + s_0^2/Re$ (unitary proportionality constant).
Moreover, it should be noted that the only hypotheses made for the asymptotic analysis are on the wavenumber k_0, which is supposed to rapidly decay as $x \to \infty$, and on the spatial growth rate s_0, which is required to be negative throughout the spatial domain. The two assumptions lead, in the far wake, to an asymptotic behaviour for the complex frequency, which is in good agreement with the numerical results of the zero order dispersion relation. Thus, the marginal conditions for convective and absolute stability shown by the multiscale Orr-Sommerfeld results in the far wake are confirmed by the present asymptotic analysis.

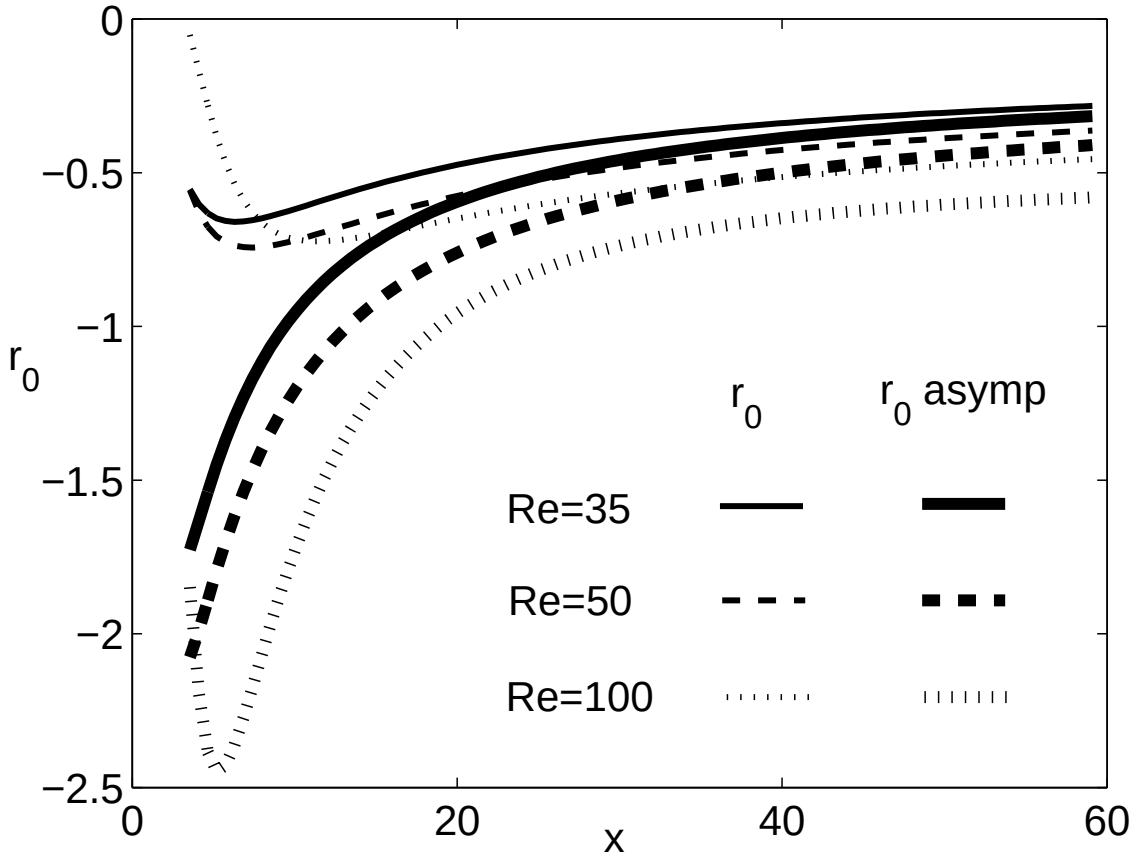

Figure 4.9. Temporal growth rate, $r_0(x)$. Comparison between the asymptotic behaviour $r_0 = s_0(x) + s_0(x)^2/Re$ and present solution at order zero (extrapolated curves, see Tables 4.2 and 4.3); Re = 35, 50, 100.

4.4 Concluding remarks

The spatially varying disturbance used here to represent the amplitude modulation turns out to be a synthetic way of pointing out the behaviour of the convective instability in the intermediate and far bluff-body wake. This disturbance is tuned to the local proper wavenumbers along the wake and is associated to a classical spatial and temporal WKBJ analysis carried out on the two-dimensional base flow previously derived in §2.3. The multiscaling explicitly accounts for the non-parallel effects associated to the lateral momentum dynamics, at a given Reynolds number.

The first-order corrections allow absolute instability pockets to be determined in the first part of the intermediate wake. These pockets are present when the Reynolds

number Re is equal to 50 and 100, but are absent when Re is as low as 35. This is in general agreement with the standard notion of a critical Reynolds number of about 47 for the onset of the first observable instability.

The size of the correction increases with Re and is larger for the pulsation and the temporal growth factor than for the spatial growth factor. It is negligible for the wavenumber.

The pulsation variation with Re of the wake region where the temporal growth factor is almost equal to zero is in good agreement with experimental global flow data in literature. Another result of the present study is that the convective instability, observable throughout the domain at both zero and complete orders, asymptotically sets on a condition of marginal stability. All the four instability characteristics vanish at infinity downstream the body generating the wake flow.

The far wake asymptotic behavior, shown by this WKBJ analysis and independently obtained through an analysis based on the properties of the Orr-Sommerfeld problem, is in good agreement with the numerical computations and highlights the same marginal stability condition as $x \to \infty$.

Chapter 5

Streamwise evolution of the entrainment in the steady 2D bluff-body wake

The analytical description of the two-dimensional bluff-body wake is not only a powerful means to analyze the non-parallel effects on the stability, but it can also be useful to consider phenomenons, associated to the lateral momentum transport, as the entrainment of the external fluid into the wake region.
In this chapter an asymptotic representation for the entrainment in the 2D steady wake is presented. After the entrainment process is introduced for laminar and turbulent flows (see §5.1), a formal definition of entrainment will be deduced as the longitudinal volume flow rate variation, through the analytical Navier-Stokes expansion derived in §2.3. The first four orders of the expansion coefficients are listed (see §5.2). The streamwise behaviour of the entrainment is presented in §5.3. Two possible lateral integration limits are discussed: the displacement thickness and the wake thickness, which is explicited through the introduction of a threshold ϵ. The concluding remarks are given in §5.4.

5.1 Introduction

The dynamics of entrainment and mixing is of considerable interest in engineering applications such as pollutant dispersal or combustion, but it is also relevant in geophysical and atmospherical situations. In all these cases, flows tend to be complex. In most of them, entrainment is a time dependent multistage process both in the

laminar or turbulent regime of motion.

The entrainment of an ambient fluid in a shear flow is a convective-diffusive process, which is widespread in the physical domain when the Reynolds number is greater than a few decades. It is a key aspect associated to the lateral dynamics of spatially evolving flows. However, quantitative data concerning the entrainment spatial evolution are not very frequent in literature and are difficult to determine experimentally. In fact, it is not easy to obtain quantitative experimental observations either in the laboratory or in the numerical simulation context. In some cases, as fluid entrainment by isolated vortex rings, theoretical studies (Maxworthy 1972) are followed by experimental observations (Baird, Wairegi and Loo 1977; Müller and Didden 1980; Dabiri and Gharib 2004).

It should be noted that, in literature, more attention has been focused on complex unsteady and highly turbulent configurations than to their laminar counterparts.
In unsteady configurations, the entrainment process is related to repeated cycles of viscous diffusion and circulatory transport. In turbulent flows, the external fluid is first included by the highly stretched and twisted inner turbulent motion (large-scale stirring) and is then mixed, at the molecular level, by the action of the small-scale velocity fluctuations. To this end, see for instance the recent experimental works on free jets by Grinstein 2001, or on a plane turbulent wake by Kopp, Giralt and Keffer 2002.
In steady laminar flows, the stretching dynamics is generally absent or close to its onset. In this case, the entrainment is mainly governed by the balance between the longitudinal and lateral nonlinear convective transport and the lateral molecular diffusion.

Here, the entrainment variations with the Reynolds number ($Re \in [20,100]$) and the longitudinal coordinate will be discussed. It increases with the Reynolds number but, after about 20 diameters downstream the body, the dependence becomes weak. The entrainment will turn out to be maximum at the beginning of the intermediate region and it will be vanishing in the far wake. In the Re range here considered, the entrainment is negligible beyond about $50 - 60$ diameters downstream the body, a distance which is of the same order of magnitude of Re. This result is in agreement with the multiscaling approach adopted in the wake stability analysis to represent the slow system variation (see §4.2).

5.2 Volumetric flow rate and entrainment

Recalling the inner expansion in §2.2.2, the base flow velocity components are

$$U(x,y) = \phi_0(x,y) + \phi_1(x,y)x^{-1/2} \ldots = \sum_{n=0}^{N} \phi_n(x,y)x^{-n/2} \tag{5.1}$$

$$V(x,y) = \chi_0(x,y) + \chi_1(x,y)x^{-1/2} \ldots = \sum_{n=0}^{N} \chi_n(x,y)x^{-n/2} \tag{5.2}$$

The normalized volumetric flow rate Q can be defined as

$$\begin{aligned} Q(x) &= \frac{1}{2z_w\delta}\int_{-z_w}^{z_w}\int_0^{\delta} U(x,y)dydz \\ &= \frac{1}{2z_w\delta}\Big(\int_{-z_w}^{z_w}\int_0^{\delta}\phi_0(x,y)dydz + x^{-1/2}\int_{-z_w}^{z_w}\int_0^{\delta}\phi_1(x,y)dydz \\ &\quad + x^{-1}\int_{-z_w}^{z_w}\int_0^{\delta}\phi_2(x,y)dydz + \ldots\Big) \\ &= q_0(x) + q_1(x)x^{-1/2} + q_2(x)x^{-1} + \ldots = \sum_{n=0}^{N} q_n(x)x^{-n/2} \end{aligned} \tag{5.3}$$

where $\delta = \delta(x,Re)$ is a measure of the half inner wake thickness, z_w is an arbitrary spanwise length and

$$q_n(x) = \frac{1}{2z_w\delta}\int_{-z_w}^{z_w}\int_0^{\delta}\phi_n(x,y)dydz = \frac{1}{\delta}\int_0^{\delta}\phi_n(x,y)dy. \tag{5.4}$$

Since the wake is symmetric around the x coordinate, the adimensionalized longitudinal velocity U is integrated in the transversal direction between 0 and δ.

The wake width δ is a function of x and Re and it can be defined in terms of the displacement thickness of the boundary-layer theory (see Belan & Tordella 2002, eq.(40))

$$\delta(x,Re) = \frac{2}{1-u(x,y=0;Re)}\int_0^{\infty}(1-u(x,y;Re))dy \tag{5.5}$$

If the wake width is approximated using the longitudinal velocity up to $n = 1$, $U(x,y) = \phi_0(x,y) + x^{-1/2}\phi_1(x,y) = 1 - Ax^{-1/2}\mathrm{e}^{-Rey^2/(4x)}$, one obtains

$$\delta(x,Re) = \frac{2}{Ax^{-1/2}}\int_0^{\infty}(Ax^{-1/2}\mathrm{e}^{-Rey^2/(4x)})dy = 2\sqrt{\frac{\pi}{Re}}x^{1/2}, \tag{5.6}$$

see Fig. 5.1. The approximated asymptotic behavior $\delta \sim x^{1/2}$ can then be obtained.

The wake width can alternatively be defined by introducing the parameter ϵ, so that

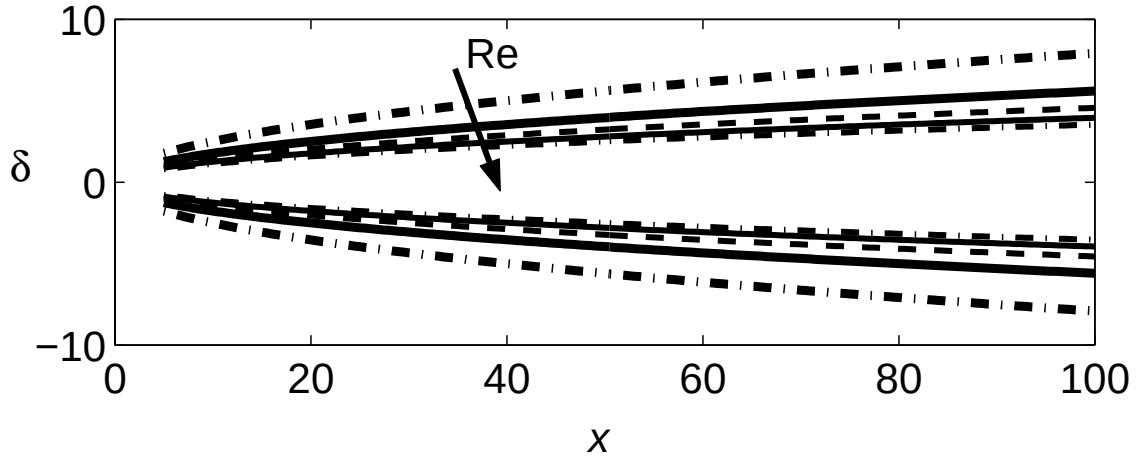

Figure 5.1. Wake displacement thickness δ in (5.5)–(5.6) as a function of x for $Re = 20$,40,60,80,100.

$$|1 - U(x,y_w; Re)| = \epsilon, \tag{5.7}$$

Thus, we can define the physical width y_w as the half-wake thickness where condition (5.7) is met, with $0 < \epsilon \leq 0.1$. At the $n = 1$ order, the wake width is

$$y_w(x; \epsilon,Re) = \frac{2}{\sqrt{Re}}[x\log(\frac{A}{\epsilon\sqrt{x}})]^{1/2}. \tag{5.8}$$

See Fig. 5.2, where the dependence on ϵ of the wake width is shown in parts (a, b) and where a comparison between definitions (5.5) and (5.7) is presented on the volumetric flow rate in parts (c, d).

The entrainment is the physical quantity taking into account the volumetric flow rate variation in the streamwise direction, and is defined as $E(x) = \dfrac{dQ(x)}{dx}$. Using expansion (5.3), one obtains

$$\begin{aligned} E(x) &= \frac{dQ(x)}{dx} \\ &= \sum_{n=0}^{N}[t_n(x) - \frac{n-2}{2}\, q_{n-2}(x)]x^{-n/2} \\ &= \sum_{n=0}^{N} e_n(x)x^{-n/2} \end{aligned} \tag{5.9}$$

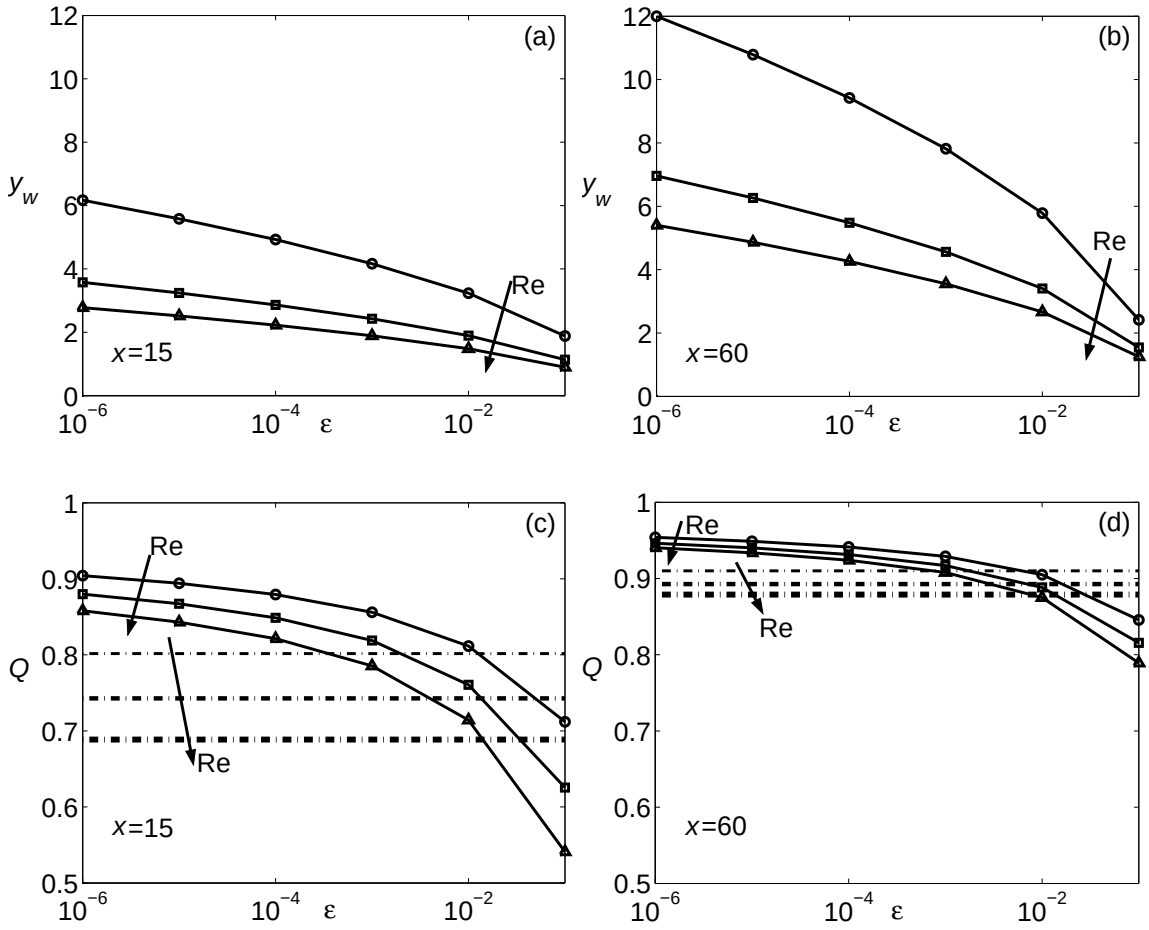

Figure 5.2. Wake width y_w, in (5.7)–(5.8), as function of ϵ for $Re = 20$, $Re = 60$, $Re = 100$ at $x = 15$ (part a) and $x = 60$ (part b). In parts (c, d) the volumetric flow rate Q is shown as function of ϵ according to y_w definition (5.7)–(5.8) (solid curves with symbols) and δ definition (5.5)–(5.6) (dashed curves) for $Re = 20$, $Re = 60$, $Re = 100$. Downstream stations $x = 15$ (c) and $x = 60$ (d).

where

$$t_n(x) = \frac{dq_n(x)}{dx} = \frac{d}{dx}(\frac{1}{\delta}\int_0^{\delta}\phi_n(x,y)dy) \tag{5.10}$$

and where the sequence of the coefficients of the flow rate expansion (5.3) is enlarged to include the elements $q_{-2} = 0$ and $q_{-1} = 0$.

The expression for coefficients $\phi_n(x,y)$ is

$$\phi_0(x,y) = 1, \tag{5.11}$$

which satisfies the boundary condition on U as $x \to \infty$, and

$$\begin{aligned}\phi_n(x,y) &= A^n \mathrm{e}^{-Rey^2/(4x)}[C_{n1}\mathrm{F}_1(\frac{1-n}{2},\frac{1}{2};\frac{Rey^2}{4x}) \\ &\quad +Re\mathrm{Hr}_{n-1}(x,y)F_n(x,y)],\ n \geq 1,\end{aligned} \tag{5.12}$$

see §2 for details on the involved functions and the constants C_n (see also Belan & Tordella, 2002; Tordella & Belan, 2003). Once ϕ_n are known, coefficients χ_n can be obtained through the continuity equation, so that

$$\chi_0(x,y) = 0, \tag{5.13}$$

which satisfies the boundary condition on V as $x \to \infty$, and

$$\chi_n(x,y) = \frac{1}{2\sqrt{x}}[y\phi_{n-1}(x,y) + (n-2)\int_0^y \phi_{n-1}(x,\zeta)d\zeta],\ n \geq 1. \tag{5.14}$$

The entrainment $E(x)$ can thus be directly related to the transversal velocity V through coefficients χ_n, as

$$e_n(x) = t_n(x) - \frac{n-2}{2}q_{n-2}(x) \tag{5.15}$$

with

$$t_n(x) = \sqrt{\frac{Re}{\pi}}\frac{d}{dx}\{\int_0^\delta y^{-n}\int_0^y [\zeta^{n-1}\frac{\partial}{\partial\zeta}\chi_{n+1}(x,\zeta)]d\zeta dy\} \tag{5.16}$$

and

$$q_n(x) = \sqrt{\frac{Re}{\pi}}\int_0^\delta y^{-n}\int_0^y [\zeta^{n-1}\frac{\partial}{\partial\zeta}\chi_{n+1}(x,\zeta)]d\zeta dy. \tag{5.17}$$

5.2.1 Expansion of the first four orders

Here we list in sequence the flow rate (5.3) and the entrainment (5.9) up to the third order. The explicit expressions are

$$Q(x) = q_0(x) + q_1(x)x^{-1/2} + q_2(x)x^{-1} + q_3(x)x^{-3/2} \tag{5.18}$$

$$E(x) = t_0(x) + t_1(x)x^{-1/2} + t_2(x)x^{-1} + (t_3(x) - \frac{1}{2}q_1(x))x^{-3/2} \tag{5.19}$$

Zero order, n=0

$$q_0(x) = 1 \tag{5.20}$$
$$t_0(x) = 0 \tag{5.21}$$

First order, n=1

$$q_1(x) = -\frac{A}{\delta}\int_0^\delta \mathrm{e}^{-Rey^2/(4x)}dy = -\frac{A}{2}\mathrm{erf}(\sqrt{\pi}) \tag{5.22}$$
$$t_1(x) = -A\frac{d}{dx}(\frac{1}{\delta}\int_0^\delta \mathrm{e}^{-Rey^2/(4x)}dy) = 0 \tag{5.23}$$

Second order, n=2

$$\begin{aligned} q_2(x) = & -\frac{A^2}{2\delta}\int_0^\delta \{\mathrm{e}^{-Rey^2/(4x)}[C_{21}\mathrm{F}_1(-\frac{1}{2},\frac{1}{2};\frac{Rey^2}{4x}) \\ & +\mathrm{e}^{-Rey^2/(4x)} + \frac{1}{2}\frac{y}{\sqrt{x}}\sqrt{\pi Re}\mathrm{erf}(\frac{1}{2}\sqrt{\frac{Re}{x}}y)]\}dy \end{aligned} \tag{5.24}$$
$$\begin{aligned} t_2(x) = & -\frac{A^2}{2}\frac{d}{dx}(\frac{1}{\delta}\int_0^\delta \{\mathrm{e}^{-Rey^2/(4x)}[C_{21}\mathrm{F}_1(-\frac{1}{2},\frac{1}{2};\frac{Rey^2}{4x}) \\ & +\mathrm{e}^{-Rey^2/(4x)} + \frac{1}{2}\frac{y}{\sqrt{x}}\sqrt{\pi Re}\mathrm{erf}(\frac{1}{2}\sqrt{\frac{Re}{x}}y)]\}dy) \end{aligned} \tag{5.25}$$

Third order, n=3

$$q_3(x) = \frac{A^3}{\delta}\int_0^\delta \{\mathrm{e}^{-Rey^2/(4x)}(2-Re\frac{y^2}{x})[\frac{1}{2}C_3 - ReF_3(x,y)]\}dy \tag{5.26}$$
$$t_3(x) = A^3\frac{d}{dx}(\frac{1}{\delta}\int_0^\delta \{\mathrm{e}^{-Rey^2/(4x)}(2-Re\frac{y^2}{x})[\frac{1}{2}C_3 - ReF_3(x,y)]\}dy) \tag{5.27}$$

5.3 Streamwise evolution of the entrainment process

The asymptotic behaviour of the expansion solutions (5.1)-(5.2) in the lateral far field is important to determine the entrainment spatial evolution. At finite values of x, the coefficient function ϕ for the streamwise velocity decays to zero as a Gaussian law for $n = 1$ and as a power law of exponent -2 for $n = 2$ and of exponent -3 for

$n \geq 3$. The coefficient function χ for the transversal velocity goes to zero for $n = 0,1$ and to a constant value for $n \geq 2$. This allows V to vanish as $x^{-3/2}$ for $x \to \infty$. When $x \to \infty$ this solution coincides with the Gaussian representation given by the Oseen approximation. It can be concluded that, at Reynolds numbers as low as the first critical value and where the non-parallelism of the streamlines is not yet negligible, the division of the field into two basic parts, an inner vortical boundary layer flow and an outer potential flow, is spontaneously shown up to the first order of accuracy ($n = 1$). At higher orders in the expansion solution, the vorticity is first convected and then diffused in the outer field. This is the dynamical context in which the entrainment process takes place.

Figure 5.3 shows the volumetric flow rate $Q = Q(x,Re)$ and the entrainment $E = E(x,Re)$ obtained from expansions (5.3), (5.9). It can be observed that these quantities significantly depend on the flow control parameter up to a distance of nearly 20 body scales. In fact, at $x = 5$, by varying $Re \in [20,100]$, Q varies from 0.62 to 0.24. An increase of Re by a factor 5 produces a decrease of Q by a factor of about 2.5. However, this factor at $x \sim 22$ reduces to 1.1, see Fig. 5.3(a). An opposite situation is observed for the entrainment, which is the derivative of the volumetric flow rate, see Fig. 5.3(b). An increase of Re from 20 to 100 produces, at $x = 5$, an increase of E by a factor of about 3. By moving further downstream, the decrease of Q and the increase of E with Re continue to reduce to just a few percent at about $x \in [50,60]$. At this distance the volumetric flow rate is close to 90% of the far field unitary value. Correspondingly, the entrainment process is practically exhausted. It is interesting to observe that this distance happens to be of the same order of magnitude of Re. This means that the multiple scales used in the multiscaling stability analysis to represent the slow time and space wake evolution - $\tau = \varepsilon t$ and $\xi = \varepsilon x$, where $\varepsilon = \dfrac{1}{Re}$ (see §4.2) - are linked to the exhaust of the entrainment process. The unitary values of the slow temporal and spatial scales are reached where the entrainment vanishes.

It should be noted that the behaviour shown by the entrainment is qualitatively close to the trend shown by the wavenumber and pulsation evolution of the dominant saddle points of the zero order dispersion relation yielded by the nonparallel Orr-Sommerfeld stability analysis (see §4.2.3-4.2.4 and for details Tordella, Scarsoglio and Belan 2006, ; Belan and Tordella 2006). In relation to this observation, the values of Q and E at $Re = 50$ and 100 for which the instability becomes absolute are pointed out in Fig. 5.3 (triangle and circle symbols). It is interesting to note that these highlighted positions ($x \sim 10$) are close to the beginning of the intermediate wake where the spatial evolution is intense, but inside the region where the thin

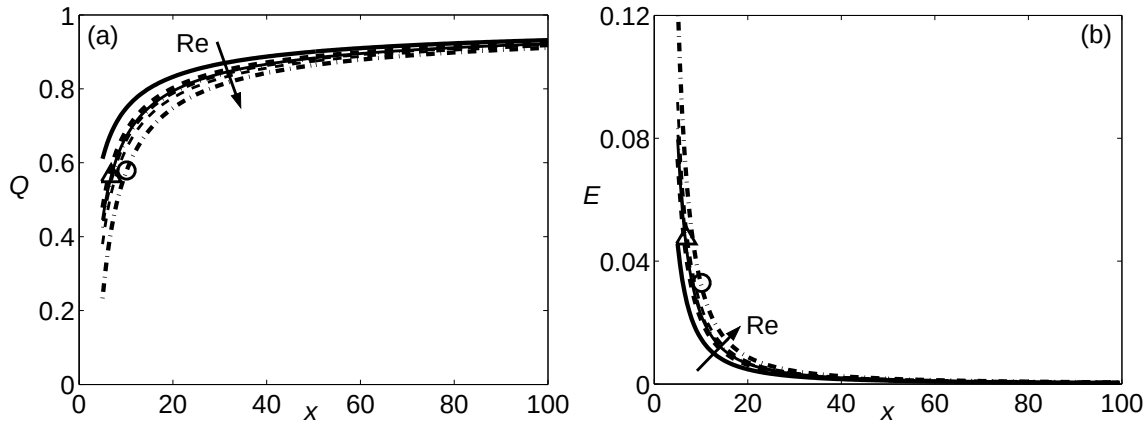

Figure 5.3. Downstream distribution of the volumetric flow rate Q (a) and entrainment E (b) for Re = 20,40,50,60,80 and 100. Integration carried out using the δ wake width definition in (5.5)–(5.6). The triangle ($Re = 50$) and the circle ($Re = 100$) are values related to the wake regions where absolute instability occurs, according to a recent Orr-Sommerfeld spatio-temporal multiscale analysis (see §4.2.4 and for details Tordella, Scarsoglio and Belan 2006; Belan and Tordella 2006).

shear layer hypothesis is valid. This aspect *a posteriori* makes the use of the WKBJ method, for the stability analysis in slowly varying flows, self-consistent.

The choice of the lateral integral scales that can be used to determine integral quantities such as the volumetric flow rate and the entrainment is here discussed. An intuitive quantity in this regard is the wake width y_w which, in order to be defined, needs the introduction of an arbitrary threshold, see (5.8)-(5.7) and Fig. 5.2. Selecting a very small threshold ϵ would be meaningless because it would imply a transversal length of integration going to infinity, which would not allow the finite flow rate variations associated to the wake momentum defect to be estimated.

An alternative to the wake width y_w is the displacement thickness δ, an integral quantity often used in the boundary layer theory and which is directly associated to the momentum defect in the wake, see (5.5)-(5.6). Figures 5.2 and 5.4 show that the results obtained using the displacement thickness δ are very close to the results obtained using a threshold equal to 0.01 (a position where the streamwise component of the velocity reaches 99% of the free stream velocity). As known, the displacement thickness is a very common definition used in boundary layer literature and engineering applications.

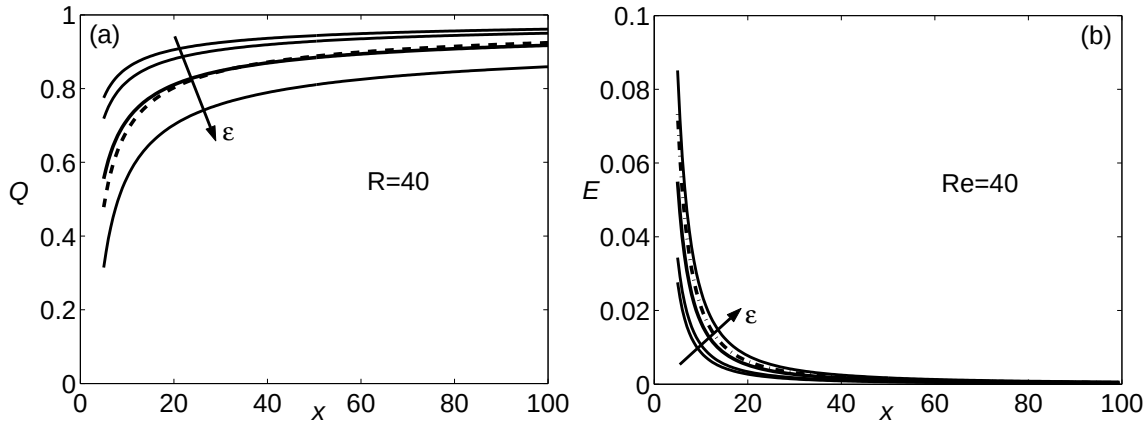

Figure 5.4. (a) Volumetric flow rate Q and (b) entrainment E as function of x for $Re = 40$. Integration carried out using y_w wake width definition in (5.7)–(5.8), solid curves with $\epsilon = 10^{-6}$,10^{-4},10^{-2},10^{-1}. The dashed curves represent Q and E obtained using the displacement thickness δ, in (5.5)–(5.6).

5.4 Concluding remarks

The entrainment distribution in the intermediate and far laminar wake has been analytically determined as an asymptotic expansion, using the Navier-Stokes expansion solutions for the inner field of the wake that successfully match an external Navier-Stokes field (see §2). The general n-order term of the expansion is explicitly obtained.

The entrainment is intense downstream the separation region, where the two-symmetric standing eddies are situated. Here, the maximum of the distribution is reached and the dependence on the Reynolds number is clear: the entrainment trebles when Re is increased from 20 to 100. The subsequent downstream evolution presents a continuous decrement of the entrainment which, in the case of a wake flow, has to vanish in the far field. The decrease is almost concluded for all the Re here considered at an average distance from the body of $50 - 60$ diameters, which is a value of the same order of magnitude as the control parameter Re. This result means that the Reynolds number dependence becomes weak when moving downstream and disappears in the far field. Moreover, it confirms the validity of the multiscaling approach often adopted in wake stability analyses (see §4.2) and carried out using the multiple spatial and temporal scales. The slow temporal and spatial scales τ,ξ are usually taken equal to $\tau = \varepsilon t$ and $\xi = \varepsilon x$, where $\varepsilon = \dfrac{1}{Re}$.

According to the present analysis, the physical scales $\tau \sim 1, \xi \sim 1$ correspond to the downstream region where the entrainment process is considered to be extinguished.

Chapter 6

Transient dynamics and asymptotic behaviour: the initial-value problem

In this chapter, the three-dimensional initial-value problem concepts for the linear stability study of a steady shear parallel flow are introduced. Although the stability analysis has been widely recognized as an initial-value problem, the temporal dynamics of the perturbations has only recently become an important topic in stability theory. The motivation, meaningful results in literature and the basis of the initial-value problem formulation are given in §6.1 and §6.2. The next two sections will be mainly dealing with a brief introduction to a traditional tool to solve an initial-value problem, that is the Laplace transform (see §6.3), and with the goal, through a moving coordinate system and the Fourier transform, to find explicit unsteady solutions for perturbations (see §6.4). The three-dimensional formulation here presented will be then developed and extended to study the stability of the growing wake in §7. An innovative spatio-temporal multiscale approach, where the small parameter will be defined through the perturbation polar wavenumber, is presented in §6.5 and then carried on for the weakly non-parallel wake stability in §8.

6.1 Introduction

Attention on the early transient behaviour of the perturbations has been widely developing only in recent years, even if both Kelvin (1887 a, b) and Orr (1907 a, b) had already recognized that the early transient contained important information.

First, because of the many complexities in the mathematics formulation and the lack of adequate computing in the early stages of the development, it was practically impossible to find either exact or approximate solutions. Second, traditional studies did not indicate that the transient dynamics could have any influence on the ultimate behaviour and it was simply ignored. Nowadays, it is becoming clear that the purpose of modal formulation computations is of predicting the asymptotic fate, and that in the early transient important events for the stability analysis can occur. In fact, a transient growth can take place long before the exponential growth. In principle, this behaviour could cause perturbation amplitude that violates the assumption of linearity and promote rapid transition, phenomenon known as by-pass transition.

It should be noted that the leading equations in stability analysis have different properties than those that are common in initial-value and boundary-value problems. In fact the principal one, the Orr-Sommerfeld equation, is of the fourth order and not self-adjoint. The Orr-Sommerfeld equation does not have a set of known functions that can be used to express arbitrary perturbations. There are means to form inner products (see Drazin & Reid 1984) in this case, but only for the viscous channel flow the discrete spectrum is complete (see DiPrima & Habetler 1969). In the inviscid case, only the continuous spectrum exists (see Case 1960, 1961; Criminale, Long & Zhu 1991). The boundary layer (Mack 1976) and the unbounded flows, that exponentially decay to a constant in the free stream, have a finite number of discrete modes. Anyhow, the presence of the continuous spectrum is a recognition of the fact that there can be algebraic growth rather than just exponential.

Moreover, the attention mainly focused on the transient growth does not prevent the present formulation from capturing the perturbation asymptotic fate. Through the initial-value problem formulation, in fact, the complete temporal evolution of arbitrary perturbations is known. Beyond the transient, the asymptotic temporal limit can be reached and compared with the results given by the Orr-Sommerfeld analysis (see §7.4).

On the one hand, the normal mode theory turns out to be a synthetic means, as the Reynolds number is the only parameter, of answering to the question of whether or not the flow is stable in the long time scale (see §3 and §4). On the other hand, only ascertaining that there may be at least one positive eigenvalue is not sufficient to conclude that the flow is unstable (see Grosch & Salwen, 1978 and Salwen & Grosch, 1981), as the continuous spectrum must be examined.

The initial-value problem formulation developed in the following will be dealing with

more parameters than the modal analysis (the most affecting ones are the symmetry, the obliquity and the wavenumber of the perturbation) and can be thought of as an extended alternative for evaluating the system response to arbitrary three-dimensional disturbances. In fact, the direct calculation of the continuous spectrum is no longer necessary as the transient behaviour, that is consequence of such a spectrum, is unequivocally captured by the alternate scheme.
Moreover, based on this formulation, an optimization procedure - which will not be developed here - can be determined without using a variational method. The optimization scheme indicates the initial conditions that can lead to the largest relative perturbation energy growth at a certain time (for details see results for channel flows in Criminale *et al.*, 1997).

6.2 The initial-value problem

The stability analysis will be considering arbitrary three-dimensional perturbations. There are two principal reasons to generalize the formulation including oblique waves. First, the Squire theorem is formulated within the modal stability analysis and applies to the asymptotic fate of disturbances. Nothing can be concluded on their early growth. Second, as noted in §3.5, the Squire theorem does not rule out the possibility that, for high enough Reynolds number, an unstable oblique oscillation can occur even though the purely two-dimensional one (with the same longitudinal wavenumber) is damped. This point is referred to by Watson (1960) as well as Betchov & Criminale (1967), but has not been exploited to date.
To this end, before carrying on with the fundamentals of the initial-value problem, the Squire equation in partial differential equation form is introduced

$$(\partial_t + U\partial_x)\widetilde{\omega}_y + U'\partial_z\widetilde{v} = \frac{1}{Re}\nabla^2\widetilde{\omega}_y, \tag{6.1}$$

where $\widetilde{\omega}_y = \partial_z\widetilde{u} - \partial_x\widetilde{w}$ is the transversal component of the perturbation vorticity. This second order not self-adjoint equation can be obtained - by considering a general three-dimensional disturbance velocity field $(\widetilde{u}(x,y,z,t),\widetilde{v}(x,y,z,t),\widetilde{w}(x,y,z,t))$ - through the same linearity assumption as in §3.2 and is necessary for the stability analysis of three-dimensional perturbations. Moreover, the partial differential Orr-Sommerfeld equation (3.10) can be alternatively expressed as

$$(\partial_t + U\partial_x)\nabla^2\widetilde{v} - U''\partial_x\widetilde{v} = \frac{1}{Re}\nabla^4\widetilde{v}, \tag{6.2}$$

in terms of the perturbation transversal velocity $\widetilde{v}$.

From the mathematical complexities of the Orr-Sommerfeld equation - which does not have a detailed set of known functional solutions and whose operator is of the fourth order and not self-adjoint - and the Squire equation, it can be concluded that there are algebraic as well as exponential solutions in time. There are two main reasons for this. First, the eigenfunctions of the Orr-Sommerfeld and the Squire equations are mutually non-orthogonal as the operators are not self-adjoint, and this can cause algebraic growth for early time (see Sommerfeld 1949). Second, a possible resonance between the Orr-Sommerfeld and Squire solutions can lead to algebraic dependence. In the Squire equation, the inhomogeneous term is proportional to the normal velocity component and is usually referred to as the lift-up term (Landhal 1980). This equation can be resonant if there is a matching of the frequencies of the respective modes of the normal velocity with the dependent variable of the equation. Resonance has been demonstrated to be possible for channel flow (Gustavsson & Hultgren 1980; Gustavsson 1981; Benney & Gustavsson 1981) but does not occur for the boundary layer. Resonance in the free shear flows is yet to be determined. Moreover, the use of the Laplace transform to solve an arbitrary initial-value problem (see Gustavsson 1979) showed that branch cuts as well as poles must exist when the inversion back to the real space is to be made. This implies the existence of a continuous spectrum and the transient behaviour associated.

Regardless the underlying source that is the cause, the algebraic growth translates into a linear time dependence. The perturbations can increase algebraically to quite large amplitudes and eventually decay, for viscous dissipation, after a maximum is reached in finite time. Then, any exponential growth will prevail beyond this point as time passes. For some problems, however, the transient growth can be unbounded and the assumption of linearity is overcome long before the dominance of any exponential growth. If, instead, there is no growing mode, the flow is considered stable even if the initial growth reaches an amplitude that violates the linearity assumption. These concepts will be put in the proper stability context as the formulation is presented.

The equations (6.1)-(6.2) represent the point of departure for the initial-value problem formulation. A two-dimensional Fourier decomposition in the $x-z$ plane is performed for every dependent variable, so that in the (α,γ) phase space the equations become

$$(\partial_t + i\alpha U)\triangle\hat{v} - i\alpha U''\hat{v} = \frac{1}{Re}\triangle\triangle\hat{v} \tag{6.3}$$

$$(\partial_t + i\alpha U)\hat{\omega}_y + i\gamma U'\hat{v} = \frac{1}{Re}\triangle\hat{\omega}_y \tag{6.4}$$

and can be used in a very general way to understand the initial-value problem. The angle of obliquity is $\phi = tan^{-1}(\gamma/\alpha)$ and the polar wavenumber is $k = \sqrt{\alpha^2 + \gamma^2}$. The Fourier transform assures that all the dependent variables are bounded in the x and z coordinates, which both range from $-\infty$ to $+\infty$. The remaining variable $y \in (-\infty, +\infty)$ also requires boundary conditions for the velocity to be met. However, the initial conditions are not necessarily given in terms of velocity. In fact, vorticity is the actual physical quantity describing the perturbation dynamics, and this can be seen through the kinematics relation

$$\nabla^2 \widetilde{v} = \frac{\partial \widetilde{\omega}_z}{\partial x} - \frac{\partial \widetilde{\omega}_x}{\partial z}, \tag{6.5}$$

which in the phase space becomes

$$\triangle \hat{v} = i\alpha\hat{\omega}_z - i\gamma\hat{\omega}_x = ik\hat{\omega}_\phi, \tag{6.6}$$

where $\hat{\omega}_\phi$ is the perturbation vorticity component in the ϕ direction. The equations (6.3), (6.4) and (6.6) are now clearly describing the disturbance dynamics in terms of vorticity, and this further substantiates the choice of initial conditions in terms of vorticity rather than velocity.

An important result for a correct formulation was given by Grosch & Salwen (1978) and Salwen & Grosch (1981). They showed that any solution to (6.3), together with an initial condition, can be expressed as

$$\hat{v}(\alpha,\gamma,y,t) = \sum_{j=1}^{N} A_j e^{i\omega_j t} \bar{v}_j(y) + V_c(y,t)\,, \tag{6.7}$$

where N is the number of discrete modes and is finite, A_j are the amplitude factors, ω_j are the frequencies, $\bar{v}_j(y)$ are the eigenfunctions, and $V_c(y,t)$ represents the continuum spectrum. Once an initial condition is prescribed, the amplitude factors and the continuum spectrum can be found requiring the orthogonality between the eigenfunctions and the adjoint eigenfunctions. As the system has to be numerically solved, there are some difficulties in determining the eigenfunctions. This procedure, although formally correct, is of limited use as cannot be easily applied. Thus, alternative methods for analysis will be presented in the following. However, significant results are to be noted. For the Blasius boundary layer, Salwen & Grosch (1981) showed that, in the case $\phi = \pi/2$, only the continuous spectrum exists, and therefore transient growth is possible. The early growth is completely due to three-dimensionality of perturbations. In fact, resonance is not possible for the boundary layer (Benney & Gustavsson 1981) and, for $\phi = \pi/2$, there is no contributions from

non-orthogonality of the Orr-Sommerfeld and the Squire operators. This result represents a further demonstration of the influence - on the transient growth - of three-dimensionality, which can be the cause of the perturbation algebraic growth.

6.3 Laplace transforms

A traditional tool to solve an initial-value problem is the Laplace transform in time. Significant contributions in the study of shear flows are due to Case (1960, 1961), Gustavsson (1979) and Hultgren & Gustavsson (1981). The Laplace transforms

$$\bar{v}(y,s) = \int_0^\infty \hat{v}(y,t)e^{-st} \quad \text{and} \quad \bar{\omega}_y(y,s) = \int_0^\infty \hat{\omega}_y(y,t)e^{-st}, \tag{6.8}$$

can be directly applied to equations (6.3) and (6.4), so that they become

$$(s + i\alpha U)\triangle\bar{v} - i\alpha U''\bar{v} - \frac{1}{Re}\triangle\triangle\bar{v} = [\triangle\hat{v}]_{t=0}, \tag{6.9}$$

$$(s + i\alpha U)\bar{\omega}_y + i\gamma U'\bar{v} - \frac{1}{Re}\triangle\bar{\omega}_y = \hat{\omega}_y(y,0). \tag{6.10}$$

The two leading partial differential equations are now ordinary ones, both with inhomogeneous terms. It should be noted that the specific initial conditions are directly inserted into the equations and deeply influence the stability analysis. Unluckily, only general properties can actually be found with this approach, as the ordinary differential equations (6.9) and (6.10) are the same as the modal theory ones.
The stability analysis of the Blasius boundary layer was studied by Gustavsson (1979) by means of the Laplace transform. In the evaluation of singularities in the complex plane, he found out that branch cuts as well as poles are to be considered when inverting the transform to the real time. The branch cut is the same as a singularity (condition where the coefficient of the highest derivative vanishes). The presence of these singularities implies that a continuum must exist. In this sense, important results - confirming the presence of branch cuts in the complex space when making the inversion of the Laplace transform to the real time - are also given by Case (1960, 1961) for inviscid Poiseuille flow and general inviscid problems for incompressible flows.
The use of Laplace transform is not remarkably different from the modal analysis. In literature, it turned out to be useful to prove that the transient growth must exist but, as the specific initial conditions strongly determine the subsequent dynamics, other strategies for the initial-value problem formulation are to be examined.

6.4 Moving coordinates and piecewise linear profiles: the exact solutions case

Kelvin (1887 a, b) and Orr (1907 a, b) first tried to find analytical unsteady solutions for perturbations. Beside the class of exact solutions given by Craik & Criminale (1986), more recent works (among others Criminale & Drazin 1990, 2000; Criminale, Long & Zhu 1991; Bun & Criminale 1994; Criminale, Jackson & Lasseigne 1995) with equivalent bases are aimed to explicitly solve initial-value problems.

According to this approach, the fundamental mechanism is that the disturbance vorticity is advected by the base flow, while the mean vorticity is, in turn, advected by the disturbance. For viscous problems, the perturbation vorticity can also be diffused. If the mean flow is piecewise linear, then the base vorticity is piecewise constant. In the case of particular travelling waves, this condition ensures that the solutions of the full Navier-Stokes perturbative equations are exact (Craik & Criminale 1986). In a more general fashion, Criminale & Drazin (1990) showed that a set of basic solutions can be found for the linear perturbation problem. These solutions are of closed form and contain both the discrete as well as the continuous spectra allowing for arbitrary perturbations, so that the early transient and the asymptotic behavior are captured. Moreover, the inviscid formulation is no longer dealing with the critical layer concept and the perturbation scheme is, in general, regular rather than singular.

The continuity and Navier-Stokes equations for perturbations applied to a steady and incompressible flow can be expressed as

$$\nabla \cdot \widetilde{\underline{u}} = 0 \tag{6.11}$$

$$\frac{\partial \widetilde{\underline{u}}}{\partial t} + \underline{U} \cdot \nabla \widetilde{\underline{u}} + \widetilde{\underline{u}} \cdot \nabla \widetilde{\underline{u}} + \widetilde{\underline{u}} \cdot \nabla \underline{U} = -\nabla \widetilde{p} + \frac{1}{Re} \nabla^2 \widetilde{\underline{u}} \tag{6.12}$$

where the underbar denotes a vector quantity. Craik & Criminale (1986) assumed that the perturbation velocity can be written in the form

$$\widetilde{\underline{u}}(\underline{x},t) = f(\underline{x},t)\hat{\underline{u}}(t), \tag{6.13}$$

so that $\nabla \cdot \widetilde{\underline{u}} = \hat{\underline{u}} \cdot \nabla f = 0$. In this way, for reasonable functions f and $\hat{\underline{u}}$, the non-linear terms in the Navier-Stokes equations vanish identically as $\widetilde{\underline{u}} \cdot \nabla \widetilde{\underline{u}} = f\hat{\underline{u}} \cdot \nabla (f\hat{\underline{u}}) = f\hat{\underline{u}} \cdot \nabla f \otimes \hat{\underline{u}} = 0$, where $\otimes$ indicates the tensor product $\nabla f \otimes \hat{\underline{u}} = \nabla f \hat{\underline{u}}^T$. In this special case, the perturbation system turns out to be linear without requiring disturbances to be small with respect to the mean flow.

In general, the hypothesis of travelling wavelike fluctuations (6.13) is not adopted, since it is too specific as initial condition. Thus, the solution of linearized perturbative equations is consistent if oscillations are small with respect to the mean flow. Various works are aimed to obtain explicit solutions for small initial perturbations and reference can be made to Criminale & Drazin (1990). The fundamentals of the method are, on the one hand, a coordinate transformation that changes the partial differential equations to ones where the coefficients are at most functions of time and, on the other hand, the use of piecewise linear functions to model the mean profiles.

Here, the problem of the inviscid mixing layer (Bun & Criminale 1994) is illustrated as a guideline for the initial-value problem formulation. The mean flow is $\underline{U} = (\sigma y,0,0)$ and the moving coordinate transformation is defined as

$$\xi = x - \sigma y t, \tag{6.14}$$

which can be used when the mean profile can be expressed as $U_i = \sigma_{ij}(t)x_j + U_i^0(t)$. After the Fourier transform is performed in ξ and z directions for the perturbation quantities, the Rayleigh and Squire equations in the phase space are, respectively

$$\frac{\partial}{\partial t}\triangle\hat{v} = 0, \tag{6.15}$$

$$\frac{\partial\widetilde{w}}{\partial t} = \sigma sin\phi\hat{v}, \tag{6.16}$$

where

$$\triangle\hat{v} = \frac{\partial^2\hat{v}}{\partial y^2} + 2i\alpha\sigma t\frac{\partial\hat{v}}{\partial y} - (k^2 + \alpha^2\sigma^2t^2)\hat{v}, \tag{6.17}$$

and, by definition, $\hat{\omega}_y = -i\gamma\hat{u} + i\alpha\hat{w}$ and $k\widetilde{w} = -\gamma\hat{u} + \alpha\hat{w}$. The transformation (6.14) can be thought of as a moving set of coordinate that is changing position with the mean flow velocity. Due to (6.14), there is neither advection or production of perturbation vorticity throughout the spatial domain. At the same time, for the piecewise linear profile assumption the advection of the mean vorticity is only present in equation (6.16). Far field conditions are satisfied by the boundedness of the dependent variables in the phase space. In y direction, boundedness is automatically met in view of the form the equations take, while matching conditions are needed where the mean velocity changes from one linear variation to another. Equations (6.15) and (6.16) are written in terms of the velocity components, but are equations for vorticity, as the following relations $\hat{\omega}_y = ik\widetilde{w}$ and $\hat{\omega}_\phi = -\frac{i}{k}\triangle\hat{v}$ hold, where $\hat{\omega}_\phi$ (see §6.2) is the vorticity component in ϕ direction.

The simplified form of equations (6.15) and (6.16), obtained through the moving coordinate transformation (6.14) and the use of a piecewise linear profile, allows exact solutions to be obtained. In general, a vector field can be decomposed into its solenoidal, rotational and harmonic parts. As the velocity is divergence free, only the harmonic and the rotational parts remain. In the case of a three section piecewise linear mean profile, the vorticity is initially imposed in the inner shear region, while no initial value is given in the non-shear regions, thus the outer flow is irrotational. The general solution has to remain bounded when $y \to \pm\infty$, and is expressed as

$$\hat{v} = \begin{cases} A(t)e^{ky} & y \leq -y_0 \\ B(t)e^{ky-i\alpha\sigma ty} + C(t)e^{-ky-i\alpha\sigma ty} + \hat{v}_R & -y_0 < y < y_0 \\ D(t)e^{-ky} & y \geq y_0 \end{cases}$$

where the coefficients are only function of time and $\hat{v}_R$ indicates a particular rotational component. The solution is obtained requiring the continuity of $\hat{v}$ and the pressure $\hat{p}$ - which can be expressed through the momentum equations in terms of $\hat{v}$ - at the two locations $y = -y_0$ and $y = y_0$ where the base flow changes. Among other results, Bun & Criminale (1994) found that the algebraic growth can lead to non-linearity before an exponential mode occurs.

In a similar way the piecewise jet and wake (Criminale, Jackson & Lasseigne 1995) and the Couette flow (Criminale, Long & Zhu 1991) are studied in the inviscid limit. The results show that the rapid algebraic growth can evolve and three-dimensionality is not to be neglected. The boundary layer is instead analyze in the viscous case (Criminale & Drazin 2000) and the solutions, although complicate, are expressed in explicit form through the method of matched asymptotic expansions. The main results substantiate, once again, that linear disturbances can grow so much in the transient as to promote non-linear growth.

6.5 Multiple scales analysis

The approach described above is mainly focused on the determination of explicit solutions for the initial-value problem, regardless the fact that the mean flow has discontinuous derivatives. How a continuous mean flow influences the perturbation dynamics is a question that is still to be answered. To this end, an analytical means of solving initial-value problems with continuous and parallel mean profiles is presented. The problem is again described in terms of vorticity and a moving coordinate transformation simplifies the governing equations in the phase space.

Moreover, the perturbation scheme results to be regular rather than singular. The essentials of the method are illustrated for the case of the Blasius boundary layer (see Lasseigne, Jackson, Joslin & Criminale, 1999).
In the Fourier space, the Orr-Sommerfeld and Squire equations (6.3)-(6.4) are joined by the following equation

$$\nabla^2 \hat{v} = \frac{\partial^2 \hat{v}}{\partial y^2} - k^2 \hat{v} = \hat{\Gamma}. \tag{6.18}$$

Now, for $\hat{\Gamma}$,$\hat{v}$,$\hat{\omega}_y$, a transformation of the kind

$$\hat{\Gamma} = e^{ikcos(\phi)t} e^{-\varepsilon k^2 t} \overline{\Gamma} \tag{6.19}$$

holds, where $\varepsilon = 1/Re$. This is a special case of the more general moving coordinate transformation (see §6.4), as all quantities are shifted with the value of the free stream velocity. The governing equations become

$$\nabla^2 \overline{v} = \overline{\Gamma} \tag{6.20}$$

$$\frac{\partial \overline{\Gamma}}{\partial t} - \varepsilon \frac{\partial^2 \overline{\Gamma}}{\partial y^2} = ikcos(\phi)(U-1)\overline{\Gamma} - ikcos(\phi)U''\overline{v} \tag{6.21}$$

$$\frac{\partial \overline{\omega}_y}{\partial t} - \varepsilon \frac{\partial^2 \overline{\omega}_y}{\partial y^2} = ikcos(\phi)(U-1)\overline{\omega}_y - iksin(\phi)U'\overline{v} \tag{6.22}$$

When $y \to \infty$, the right hand sides of equations (6.21) and (6.22) vanish, as $U \to 1$, $U' \to 0$ and $U'' \to 0$. The two equations reduce to the heat diffusion equations in the free stream and are easily solvable. When $\phi = \pi/2$, the system can be explicitly solved throughout the domain.

In some flow configurations, long waves can be destabilizing (e.g. Blasius boundary layer and 3D cross-flow boundary layer). Results on the stability of 2D and 3D boundary layers (see, among others, Mack, 1976; Schlichting 1968; Reshotko, 1976; Reed & Saric, 1989; Saric, Reed & White, 2003) confirm this fact and show that the perturbation wavenumber k is much less than $O(1)$ when instability occurs. In fact, large wavenumber values would imply short scales that can be easily damped. Moreover, Lasseigne *et al.* (1999) noted that with the more general moving coordinate transformation - which is changing position with the mean flow velocity - the terms t, kt, k^2t^2 are present in the Laplace operator. All these points suggest that multiple times and multiple scales can be identified, and k is the ideal parameter to carry on a regular perturbation scheme. Specifically, two spatial and three temporal

scales can be identified. Spatially, the scales are y and $Y = ky$. Temporally, they are t, $\tau = kt$ and $T = k^2 t$. In the inviscid limit, the third temporal scale T is no longer needed, as it is the asymptotic limit in time for the viscous problem, see (6.19). The dependent variables $\overline{\Gamma}(y,Y,t,\tau,T;k,\phi)$, $\overline{v}(y,Y,t,\tau,T;k,\phi)$, $\overline{\omega}_y(y,Y,t,\tau,T;k,\phi)$ should be now expanded as follows

$$\begin{aligned} \overline{\Gamma} &= \overline{\Gamma}_0 + k\overline{\Gamma}_1 + k^2\overline{\Gamma}_2 + \cdots , \\ \overline{v} &= \overline{v}_0 + k\overline{v}_1 + k^2\overline{v}_2 + \cdots , \\ \overline{\omega}_y &= \overline{\omega}_{y0} + k\overline{\omega}_{y1} + k^2\overline{\omega}_{y2} + \cdots , \end{aligned} \tag{6.23}$$

with $k \ll 1$. Initial conditions at order O(1) are defined as in the full problem, and at next orders (O(k), O(k^2), $\cdots$) are equal to zero. Boundary conditions remain as stated in the full problem. It is necessary that the series expansions begin as indicated, so that all variables are at the same order of magnitude. This point can be noted from relations for $\hat{\omega}_y$ and $\hat{\omega}_\phi$, and the constraint of incompressibility that requires the velocity to be divergence free. After the expansions (6.23) are substituted into equations (6.20)-(6.22) with appropriate initial conditions, the vorticity equations become a series of forced heat equations, while the equation for the transversal velocity results in a series of equations forced at the outset. At any order, the resulting equations can be explicitly solved. For the Blasius boundary layer (see Lasseigne *et al.* 1999), a comparison between this method and the direct numerical integration of the linear partial differential equations is presented. The agreement is good, even to low orders of expansions.

Chapter 7

Temporal behaviour of small three-dimensional perturbations applied to the growing wake

The linear stability of the two-dimensional wake - whose profile is derived in §2.3 - is studied as a three-dimensional initial-value problem through the formulation presented in the previous chapter. Two main innovative features are introduced here. First, the mean flow - which is parameterized with respect to the Reynolds number and the longitudinal coordinate - is approximated through the longitudinal component of the inner Navier-Stokes expansion (see §2.3), to include the slow spatial evolution of the system in the stability analysis. Then, a complex wavenumber in streamwise direction is considered when the transformation to the phase space is performed. The leading equations are no more explicitly solvable, but numerical means are required. However, most of the general features described in Chapter 6 still hold and can be extended here.

In synthesis, Laplace and Fourier decompositions are performed in streamwise and spanwise directions, respectively. The perturbation is characterized by real streamwise and spanwise wavenumbers, and a uniform or damped spatial distribution along the longitudinal direction. Amplified streamwise distributions are not considered since the perturbation kinetic energy is required to be finite. The resulting equations in the phase space are numerically solved after appropriate initial and boundary conditions are imposed. In §7.3, an exploration of different transient configurations will be shown with particular attention to those parameters - such as the angle of obliquity, the length, the symmetry and the spatial damping rate - which most affect the early growth and the asymptotic fate. In §7.4 the perturbation asymptotic

states are reproduced and, in the longitudinal case, it can be demonstrated that the agreement with modal analysis turns out to be good for both symmetric and asymmetric initial conditions. Concluding remarks are discussed in §7.5.

7.1 Introduction

The two-dimensional wake stability has been widely studied by means of normal mode analysis (see §4.1). However, as previously stated, in this way only the asymptotic fate can be determined, regardless the transient behaviour and the underlying physical cause of any instability. Recent shear flows studies (Butler & Farrell 1992; Criminale & Drazin 1990; Criminale *et al.* 1991) have been showing the importance of the early time dynamics, which can in principle lead to non-linear growth long before an exponential mode occurs. The recognition of the existence of an algebraic growth, due - among other things - to the non-orthogonality of the eigenfunctions (Sommerfeld 1949) and a possible resonance between Orr-Sommerfeld and Squire solutions (Benney & Gustavsson 1981), recently promoted many contributions directed to study the early-period dynamics. For fully bounded flows works by Criminale *et al.* 1991, Criminale *et al.* 1997, Gustavsson 1991, Bergstrom 1993, Schmid & Henningson 1994, Schmid 2007, and for partially bounded flows works by Lasseigne *et al.* 1999, Hultgren & Gustavsson 1981, Criminale & Drazin 2000, can be cited. As for free shear flows, the attention was first aimed to obtain closed-form solutions to the initial-value inviscid problem (Bun & Criminale 1994; Criminale *et al.* 1995) by considering piecewise linear parallel basic flow profiles. Recently, by means of multiscale approach, explicit solutions have been obtained for continuous parallel base flow profiles (Blossey, Criminale & Fisher 2007).
The initial-value problem is here extended to include, in the stability analysis, a more accurate description of the mean flow. In particular, the longitudinal component of the Navier-Stokes expansion solutions described in §2.3 is considered, so that the problem is parameterized on x_0 - the longitudinal coordinate - and the Reynolds number Re. The formulation will be carried on similarly to what first proposed by Criminale & Drazin (1990). Early transient and asymptotic behaviour are examined for the base flow configurations corresponding to Reynolds numbers ($Re = 50$,100) of the order of the critical value for the onset of the first instability, and for longitudinal sections x_0 inside the intermediate region of the flow where the entrainment process is working (see §5.3). Different physical inputs - linked to the shape, the obliquity, the length and the symmetry of the perturbation - which most influence the subsequent temporal evolution are presented. In the initial-value

problem formulation, the introduction of a complex wavenumber in the streamwise direction is an innovative feature suggested by the combined spatio-temporal modal stability analysis. The imaginary part of the complex longitudinal wavenumber, which determines the longitudinal evolution of the perturbing wave, plays an important role in the whole temporal evolution of the perturbation. In fact, varying the order of magnitude of this parameter leads to actually different temporal trends. A longitudinal asymptotic comparison with modal results - carried out considering arbitrary initial conditions and not waves related to the most unstable mode - is made. It can be demonstrated that the agreement is good for both the frequency as well as the temporal growth rate.

7.2 The initial-value problem

7.2.1 Formulation

The first orders (n = 0,1,2) of the inner longitudinal component velocity field are taken as a first approximation of the base flow. The analytical expression is reported below for convenience

$$U(y;x_0,Re) = 1 - aC_1 x_0^{-1/2} \mathrm{e}^{-\frac{\mathrm{Re}}{4}\frac{\mathrm{y}}{\mathrm{x_0}}} - \frac{\mathrm{a}^2}{2}\mathrm{x_0^{-1}}\,\mathrm{e}^{-\frac{\mathrm{Re}}{4}\frac{\mathrm{y}^2}{\mathrm{x_0}}} \times \left\{ C_2\, {}_1\mathrm{F}_1\left(-\frac{1}{2},\frac{1}{2};\frac{Re}{4}\frac{y^2}{x_0}\right) + \mathrm{e}^{-\frac{\mathrm{Re}}{4}\frac{\mathrm{y}^2}{\mathrm{x_0}}} + \frac{\sqrt{\pi \mathrm{Re}}}{2}\frac{\mathrm{y}}{\sqrt{\mathrm{x_0}}}\,\mathrm{erf}\left(\frac{\sqrt{\mathrm{Re}}}{2}\frac{\mathrm{y}}{\sqrt{\mathrm{x_0}}}\right)\right\} \quad (7.1)$$

By changing the longitudinal coordinate x_0, which plays the role of parameter together with the Reynolds number, the base flow profile (7.1) will locally approximate the behaviour of the actual wake generated by the body. The wake sections taken into account are in the interval $3 \leq x_o \leq 50$. Base flow configurations corresponding to a Re of 50,100 are considered. In figure 7.1 a representation of the wake profile at differing longitudinal stations is shown.

The continuity and Navier-Stokes equations - describing the system perturbed with small disturbances - are linearized and expressed as

$$\frac{\partial \widetilde{u}}{\partial x} + \frac{\partial \widetilde{v}}{\partial y} + \frac{\partial \widetilde{w}}{\partial z} = 0 \quad (7.2)$$

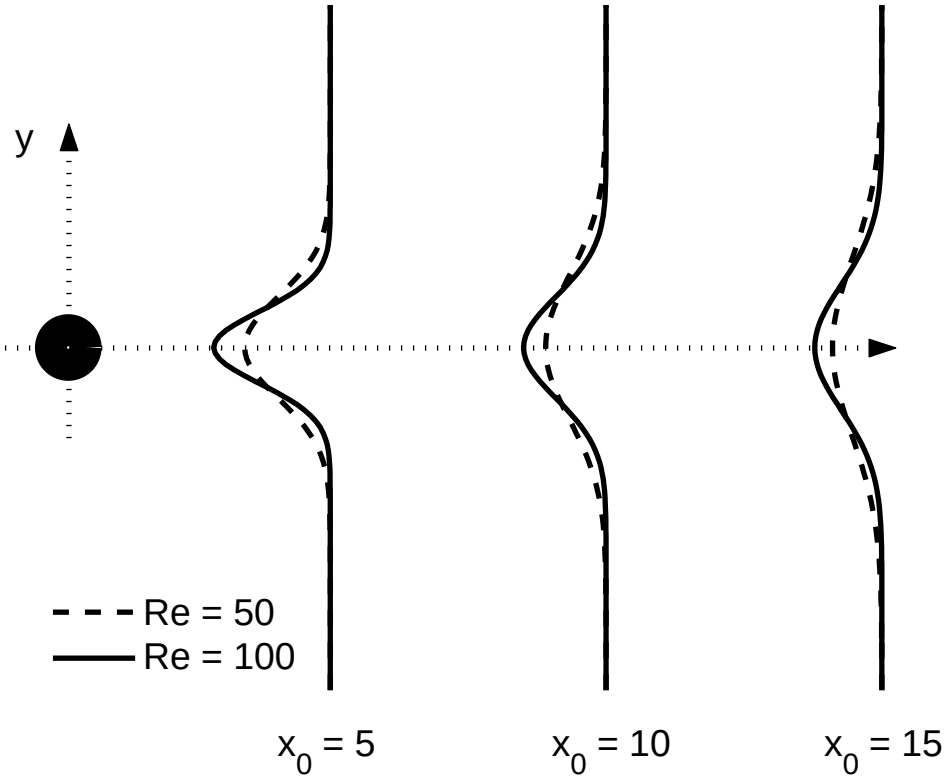

Figure 7.1. Wake profile $U(y;x_0,Re)$ at different longitudinal stations x_0 and for different Reynolds numbers.

$$\frac{\partial \widetilde{u}}{\partial t} + U\frac{\partial \widetilde{u}}{\partial x} + \widetilde{v}\frac{\partial U}{\partial y} + \frac{\partial \widetilde{p}}{\partial x} = \frac{1}{Re}\nabla^2\widetilde{u} \tag{7.3}$$

$$\frac{\partial \widetilde{v}}{\partial t} + U\frac{\partial \widetilde{v}}{\partial x} + \frac{\partial \widetilde{p}}{\partial y} = \frac{1}{Re}\nabla^2\widetilde{v} \tag{7.4}$$

$$\frac{\partial \widetilde{w}}{\partial t} + U\frac{\partial \widetilde{w}}{\partial x} + \frac{\partial \widetilde{p}}{\partial z} = \frac{1}{Re}\nabla^2\widetilde{w} \tag{7.5}$$

where ($\widetilde{u}(x,y,z,t)$, $\widetilde{v}(x,y,z,t)$, $\widetilde{w}(x,y,z,t)$) and $\widetilde{p}(x,y,z,t)$ are the perturbation velocity and pressure respectively. introduced. The independent spatial variables z and y are defined from $-\infty$ to $+\infty$, x from 0 to $+\infty$. All physical quantities are normalized with respect to the free stream velocity, the spatial scale of the flow D and the density. By combining equations (7.3)-(7.5) to eliminate the pressure terms, the linearized equations describing the perturbation dynamics become

$$(\frac{\partial}{\partial t} + U\frac{\partial}{\partial x})\nabla^2\widetilde{v} - \frac{\partial\widetilde{v}}{\partial x}\frac{d^2U}{dy^2} = \frac{1}{Re}\nabla^4\widetilde{v} \tag{7.6}$$

$$(\frac{\partial}{\partial t} + U\frac{\partial}{\partial x})\widetilde{\omega}_y + \frac{\partial\widetilde{v}}{\partial z}\frac{dU}{dy} = \frac{1}{Re}\nabla^2\widetilde{\omega}_y \tag{7.7}$$

where $\widetilde{\omega}_y$ is the transversal component of the perturbation vorticity. The physical quantity $\widetilde{\Gamma}$ is defined as

$$\nabla^2\widetilde{v} = \widetilde{\Gamma} \tag{7.8}$$

In so doing, the three coupled equations (7.6), (7.7) and (7.8) describe the perturbed system. Equations (7.6) and (7.7) are the Orr-Sommerfeld and Squire equations respectively, known from the classical linear stability analysis for three-dimensional disturbances and written in partial differential equation form. From kinematics, the relation

$$\widetilde{\Gamma} = \frac{\partial\widetilde{\omega}_z}{\partial x} - \frac{\partial\widetilde{\omega}_x}{\partial z} \tag{7.9}$$

physically links together the perturbation vorticity in the x and z directions ($\widetilde{\omega}_x$ and $\widetilde{\omega}_z$, respectively) and the perturbation velocity field. If equations (7.6) and (7.8) are combined together, the following equation is valid

$$\frac{\partial\widetilde{\Gamma}}{\partial t} + U\frac{\partial\widetilde{\Gamma}}{\partial x} - \frac{\partial\widetilde{v}}{\partial x}\frac{d^2U}{dy^2} = \frac{1}{Re}\nabla^2\widetilde{\Gamma} \tag{7.10}$$

which, together with (7.7) and (7.8), fully describes the perturbed system in terms of vorticity. This formulation is not that common in linear stability analysis, although the dynamics description is physically more appropriate in terms of vorticity than velocity. For piecewise linear profiles it turned out to be useful in obtaining analytical solutions (see §6.4). For continuous profiles, the governing perturbative equations cannot be analytically solved in general, but they assume a reduced form in the free stream (Blossey *et al.* 2007). Equations (7.7), (7.8) and (7.10) show that the only cause of any perturbation vorticity production is the interaction between the mean vorticity in z-direction ($\Omega_z = -dU/dy$) and the perturbation strain rates in x and z directions ($\frac{\partial\widetilde{v}}{\partial x}$ and $\frac{\partial\widetilde{v}}{\partial z}$, respectively).

7.2.2 Laplace-Fourier transforms

The perturbations are Laplace and Fourier decomposed in the x and z directions, respectively. A complex wavenumber $\alpha = \alpha_r + i\alpha_i$ along the x coordinate, as well

as, a real wavenumber γ along the z coordinate are introduced. In order to have a finite perturbation kinetic energy, the imaginary part α_i of the complex longitudinal wavenumber can only assume non-negative values. In so doing, perturbative waves can spatially decay ($\alpha_i > 0$) or remain constant in amplitude ($\alpha_i = 0$). The perturbation quantities ($\widetilde{v}$,$\widetilde{\Gamma}$,$\widetilde{\omega}_y$) involved in the system dynamics are now indicated as ($\hat{v}$,$\hat{\Gamma}$,$\hat{\omega}_y$), where

$$\hat{g}(y,t;\alpha,\gamma) = \int_{-\infty}^{+\infty}\int_{0}^{+\infty} \widetilde{g}(x,y,z,t)e^{-i\alpha x - i\gamma z}dxdz \tag{7.11}$$

indicates the Laplace-Fourier transform of a general dependent variable in the $\alpha-\gamma$ phase space and in the remaining independent variables y and t. The governing partial differential equations are

$$\frac{\partial^2\hat{v}}{\partial y^2} - (k^2 - \alpha_i^2 + 2ikcos(\phi)\alpha_i)\hat{v} = \hat{\Gamma} \tag{7.12}$$

$$\begin{aligned}\frac{\partial\hat{\Gamma}}{\partial t} = &- (ikcos(\phi) - \alpha_i)U\hat{\Gamma} + (ikcos(\phi) - \alpha_i)\frac{d^2U}{dy^2}\hat{v} \\ &+ \frac{1}{Re}[\frac{\partial^2\hat{\Gamma}}{\partial y^2} - (k^2 - \alpha_i^2 + 2ikcos(\phi)\alpha_i)\hat{\Gamma}]\end{aligned} \tag{7.13}$$

$$\begin{aligned}\frac{\partial\hat{\omega}_y}{\partial t} = &- (ikcos(\phi) - \alpha_i)U\hat{\omega}_y - iksin(\phi)\frac{dU}{dy}\hat{v} \\ &+ \frac{1}{Re}[\frac{\partial^2\hat{\omega}_y}{\partial y^2} - (k^2 - \alpha_i^2 + 2ikcos(\phi)\alpha_i)\hat{\omega}_y]\end{aligned} \tag{7.14}$$

where $\phi = tan^{-1}(\gamma/\alpha_r)$ is the perturbation angle of obliquity with respect to the x-y physical plane, $k = \sqrt{\alpha_r^2 + \gamma^2}$ is the polar wavenumber and $\alpha_r = kcos(\phi)$, $\gamma = ksin(\phi)$ are the wavenumbers in x and z directions respectively. The imaginary part α_i of the complex longitudinal wavenumber is a spatial damping rate in streamwise direction. In figure 7.2 the three-dimensional perturbative geometry scheme is shown.

From equations (7.12)-(7.14), it can be noted that there can't be either advection or production of vorticity in the free stream. Vorticity can only be diffused as just the diffusive terms remain when $y \to \infty$. Perturbation vorticity vanishes in the free stream, regardless if it is initially inserted there (if inserted, vorticity is finally dissipated in time when $y \to \infty$). This means that the velocity field is harmonic if $y \to \infty$.

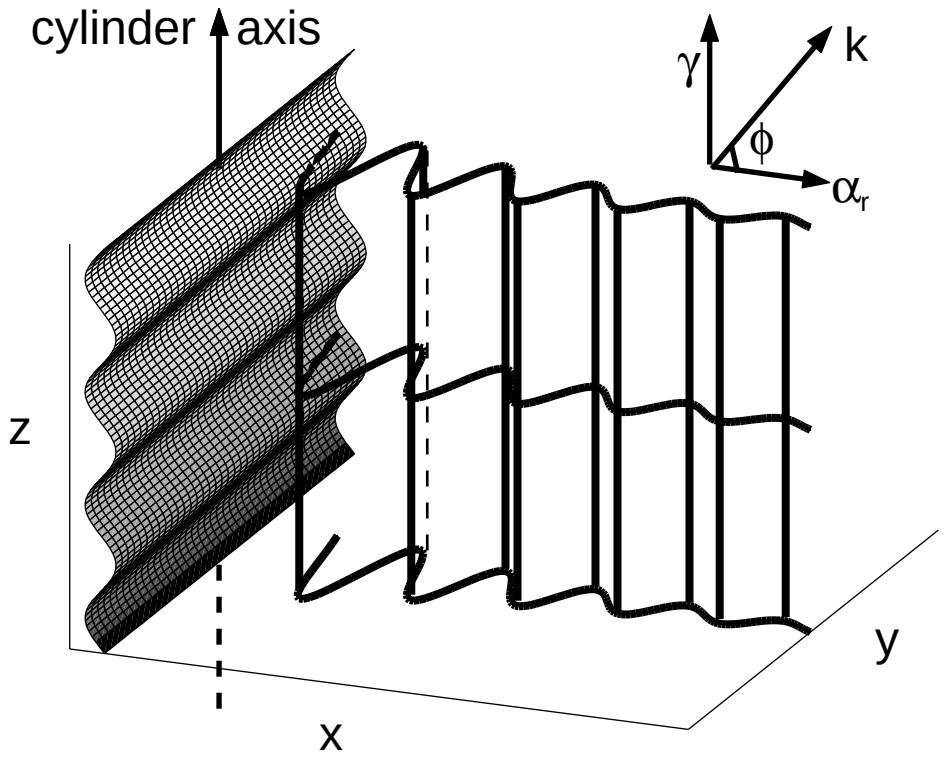

Figure 7.2. Perturbation geometry scheme.

The introduction, through the Laplace decomposition in x-direction, of a complex wavenumber α is an innovative feature, as it permits to carry out a combined spatio-temporal linear stability analysis that is a quite standard procedure for normal mode theory, but is not that common for initial-value problems. Both transient behaviour and asymptotic fate of the disturbances will be discussed in the following considering the resulting influence of this new characteristic.

7.2.3 Initial and boundary conditions

Governing equations (7.12), (7.13) and (7.14) need proper initial and boundary conditions to be solved. Among all solutions, those whose perturbation velocity field is zero in the free stream are sought. Periodic initial conditions for

$$\hat{\Gamma} = \frac{\partial^2 \hat{v}}{\partial y^2} - (k^2 - \alpha_i^2 + 2ikcos(\phi)\alpha_i)\hat{v} \tag{7.15}$$

can be shaped in terms of set of functions in the L^2 Hilbert space, as

$$\hat{v}(0,y) = e^{-(y-y_0)^2}\cos(n_0(y-y_0)), \qquad \text{case A}$$

and

$$\hat{v}(0,y) = e^{-(y-y_0)^2}\sin(n_0(y-y_0)), \qquad \text{case B}$$

for the symmetric and the asymmetric perturbations, respectively. Parameter n_0 is an oscillatory parameter for the shape function, while y_0 is a parameter which controls the distribution of the perturbation along y (by moving away or bringing nearer the perturbation maxima from the axis of the wake). In Fig. 7.3, the above initial conditions are shown, in terms of $\hat{v}(0,y)$, for different values of n_0.

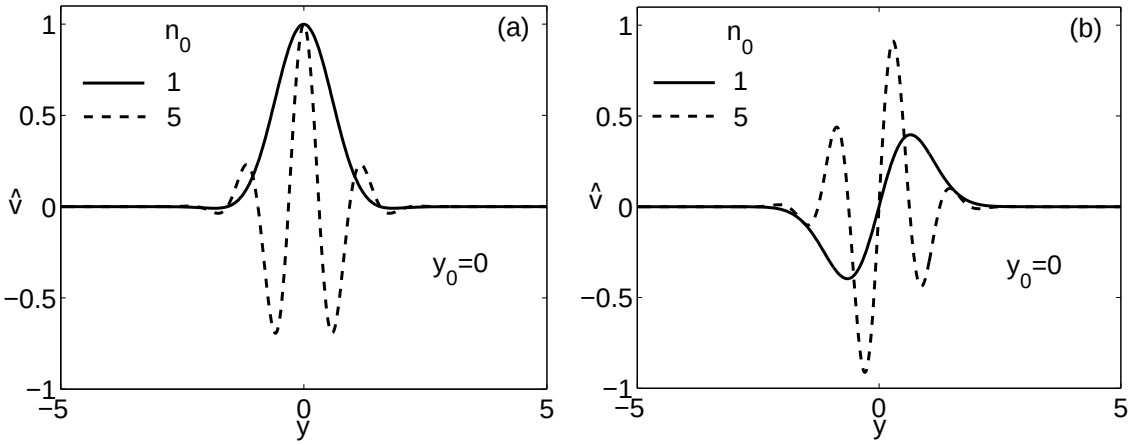

Figure 7.3. (a) Symmetric and (b) asymmetric initial conditions with $y_0 = 0$ and $n_0 = 1{,}5$.

The transversal vorticity $\hat{\omega}_y$ is chosen initially equal to zero throughout the y domain, to directly observe which is the net contribution of three-dimensionality on the transversal vorticity temporal evolution. Otherwise, non-zero initial conditions for the transversal vorticity

$$\hat{\omega}_y \;=\; i(\gamma\hat{u} - \alpha\hat{w}), \tag{7.16}$$

can be shaped in terms of set of functions in the L^2 Hilbert space, and one of the following conditions can be adopted

CASE I : $\hat{v}(0,y) = e^{-(y-y_0)^2} sin(n_0(y-y_0))$, $\hat{u}(0,y) = e^{-(y-y_0)^2} sin(n_0(y-y_0))$, $\hat{w}(0,y) = e^{-(y-y_0)^2} sin(n_0(y-y_0))$;

CASE II : $\hat{v}(0,y) = e^{-(y-y_0)^2} cos(n_0(y-y_0))$, $\hat{u}(0,y) = e^{-(y-y_0)^2} sin(n_0(y-y_0))$, $\hat{w}(0,y) = e^{-(y-y_0)^2} sin(n_0(y-y_0))$;

CASE III : $\hat{v}(0,y) = e^{-(y-y_0)^2} sin(n_0(y-y_0))$, $\hat{u}(0,y) = e^{-(y-y_0)^2} cos(n_0(y-y_0))$, $\hat{w}(0,y) = e^{-(y-y_0)^2} cos(n_0(y-y_0))$;

CASE IV : $\hat{v}(0,y) = e^{-(y-y_0)^2} cos(n_0(y-y_0))$, $\hat{u}(0,y) = e^{-(y-y_0)^2} cos(n_0(y-y_0))$, $\hat{w}(0,y) = e^{-(y-y_0)^2} cos(n_0(y-y_0))$;

Results will later show how the initial introduction of normal vorticity can influence the evolution of disturbances.
The trigonometrical system is a Schauder basis in each space $L^p[0,1]$, for $1 < p < \infty$. More specifically, the system $(1, sin(n_0 y), cos(n_0 y), \dots)$, where $n_0 = 1,2,\dots$, is a Schauder basis for the space of square-integrable periodic functions with period 2π. This means that any element of the space L^2, where the dependent variables are defined, can be written as an infinite linear combination of the elements of the basis.

Once initial and boundary conditions are properly set, the partial differential equations (7.12)-(7.14) are numerically solved by method of lines on a spatial finite domain $[-y_f, +y_f]$. The value y_f is chosen so that the numerical solutions are insensitive to further extensions of the computational domain size. Here, y_f is of the order of magnitude 10^1. The spatial derivatives are centre differenced and the resulting system is then integrated in time by an adaptative multi-step method (variable order Adams-Bashforth-Moulton PECE solver).

7.3 Transient dynamics of the perturbations

In general, one of the salient aspects of the initial-value problem is to observe the early transient evolution of various initial conditions. To this end, a measure of the perturbation growth can be defined in the phase space through the disturbance kinetic energy density

$$\begin{aligned} e(t;\alpha,\gamma) &= \frac{1}{2}\int_{-y_f}^{+y_f} (|\hat{u}|^2 + |\hat{v}|^2 + |\hat{w}|^2) dy \\ &= \frac{1}{2}\frac{1}{|\alpha^2+\gamma^2|}\int_{-y_f}^{+y_f} (|\frac{\partial \hat{v}}{\partial y}|^2 + |\alpha^2+\gamma^2||\hat{v}|^2 + |\hat{\omega}_y|^2) dy, \end{aligned} \tag{7.17}$$

The total kinetic energy can be obtained by integrating the energy density over all α and γ. The normalized amplification factor $G(t)$ can be introduced

$$G(t;\alpha,\gamma) = \frac{e(t;\alpha,\gamma)}{e(t=0;\alpha,\gamma)}. \tag{7.18}$$

This quantity can effectively measure the growth of a disturbance of wavenumbers (α,γ) at the time t, for a given initial condition at $t = 0$ (Criminale *et al.* 1997; Lasseigne *et al.* 1999). The temporal growth rate r is defined as

$$r(t;\alpha,\gamma) = \frac{log|e(t;\alpha,\gamma)|}{2t}, \quad t > 0 \tag{7.19}$$

and is introduced to evaluate both the early transient as well as the asymptotic behaviour of the perturbation. It can be noted that r is not defined for $t = 0$. This quantity has a precise physical meaning asymptotically in time.

In the following, a summary of significant transients for three-dimensional perturbations is presented. The results are all concerning the intermediate asymptotic region of the wake, which is where the spatial evolution is mainly taking place. This region can be considered of an extension equal to the distance from the body where the entrainment process is becoming negligibly small. For laminar steady 2D wakes this length turns out to be of the order of Re (see §5.3). In particular, the polar wavenumber k changes in a range of values reaching at maximum the order of magnitude $O(1)$, according to what suggested by recent modal analyses (Tordella, Scarsoglio & Belan, 2006; Belan & Tordella, 2006). The order of magnitude of the spatial damping rate α_i can vary around the polar wavenumber value.
First, a configuration with initial non-zero normal vorticity is considered. Figure 7.4 displays that initial vorticity $\hat{\omega}_y$ does not actually influence the perturbation evolution. Amplification factors in cases (II) and (IV) almost coincide with the one of the case with symmetric transversal velocity and zero initial vorticity (case A). A similar behaviour is shown by the amplification factors of cases (I) and (III), which are very close to the one of the case with asymmetric transversal velocity and zero initial vorticity (case B). Analogous agreements can be obtained with different values of parameters. This means that the contribution of the transversal vorticity to the global energy growth G is basically all due to the three-dimensionality of the imposed disturbance. This fact is true in the case where the disturbance is weakly inclined with respect to the base flow plane ($\phi = \pi/8$), and is even more evident for larger values of the obliquity angle. The transversal vorticity is immediately generated when $\phi \neq 0$, regardless the choice of the initial conditions. According to this result, normal vorticity will be initially taken equal to zero in the following.
Figure 7.5 yields differing examples of early transient periods and the corresponding temporal growth rates r when the obliquity angle ϕ is varied. A growing wave

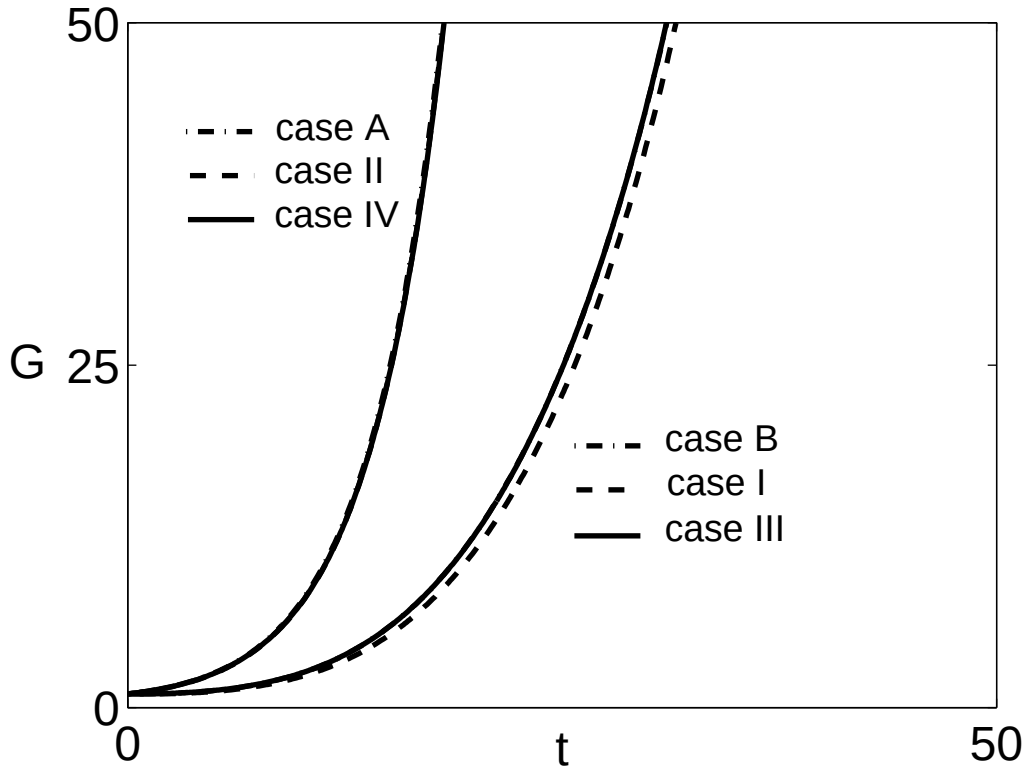

Figure 7.4. The amplification factor G as function of time. $Re = 100$, $k = 0.3$, $\alpha_i = 0.1$, $\beta_0 = 1$, $y_0 = 0$, $\phi = \pi/8$, $x_0 = 8.50$, differing initial conditions (cases A, B, I, II, III, IV).

becomes damped when the obliquity angle is larger than $3/8\pi$. For transversal waves with $\phi > 3/8\pi$, a low maximum of energy ($G \sim 7$) is reached before the perturbations are asymptotically damped.

Figure 7.6 shows that, for an unstable configuration occurring for a purely three-dimensional disturbance, the amplification is only delayed in time for higher values of n_0 (a logarithmic scale is used on the ordinate in Fig. 7.6a). This means that, in the temporal asymptotic limit, the effect of a perturbation oscillating many times across the basic flow is as destabilizing as the effect of a single spatially fluctuating wave. On the contrary, transients are actually affected by the spatial frequency of oscillations. By increasing n_0, the temporal trend of G is no more monotone but initial decreases of energy - lasting up to 15 time scales - are present before the asymptotic unstable states are reached.

Other examples of early transient periods and corresponding temporal growth rates

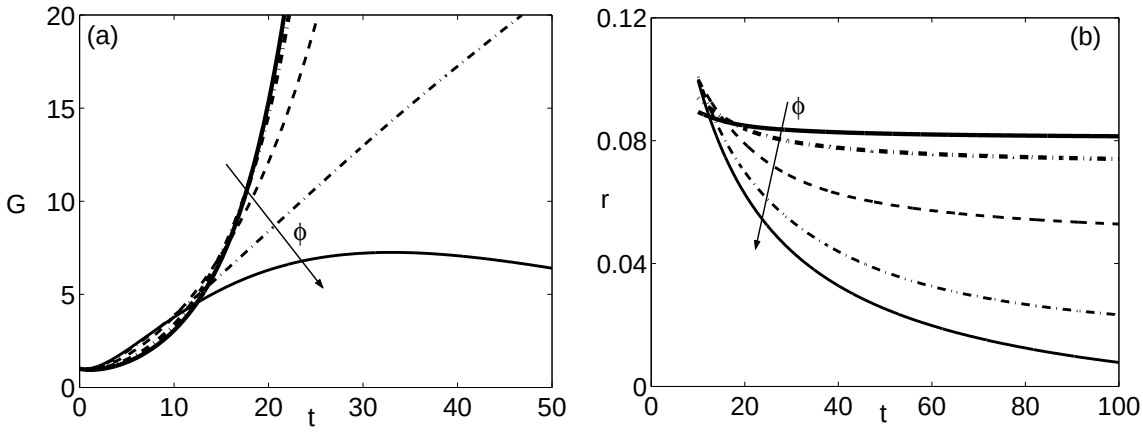

Figure 7.5. Effect of the obliquity angle (ϕ). (a) The amplification factor G and (b) the temporal growth rate r as function of time. $Re = 100$, $k = 1.5$, $\alpha_i = 0.01$, $n_0 = 1$, $y_0 = 0$, $x_0 = 14$, symmetric initial condition, $\phi = 0$,$\pi/8$,$\pi/4$,$(3/8)\pi$,$\pi/2$.

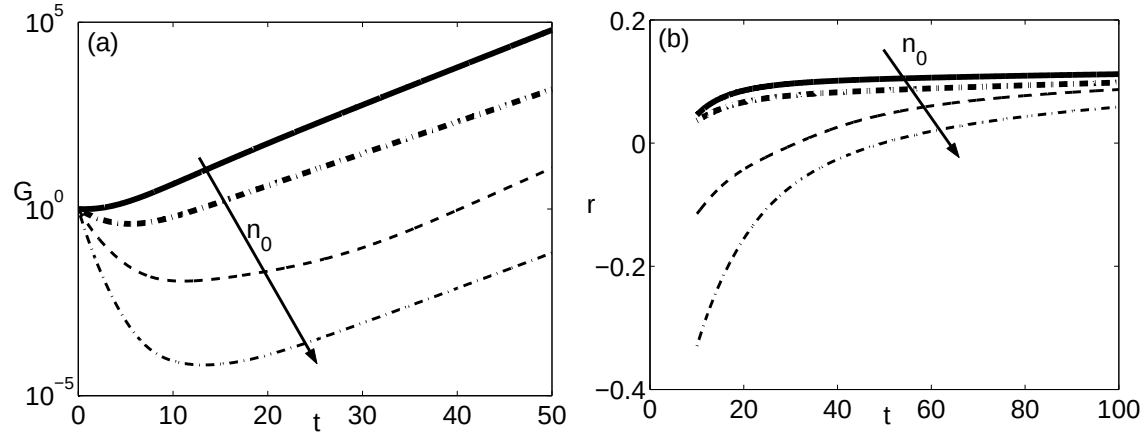

Figure 7.6. Effect of the shape function oscillatory parameter (n_0). (a) The amplification factor G and (b) the temporal growth rate r as function of time. $Re = 50$, $k = 0.9$, $\alpha_i = 0.15$, $\phi = \pi/2$, $y_0 = 0$, $x_0 = 14.00$, asymmetric initial condition, $n_0 = 1$,3,5,7.

r are shown in Figures 7.7 to 7.11. Fig. 7.7 displays that almost purely three-dimensional perturbations are all asymptotically stable when varying their wavenumbers k. But before the asymptotic states, they all show maxima of energy in the transients. Increasing k, the growth rate of the transient seems to tend to a limiting

value (see solid line in the figure 7.7a). The maximum growth is obtained for $k \sim 1$ and reaches a value $G \sim 6$.

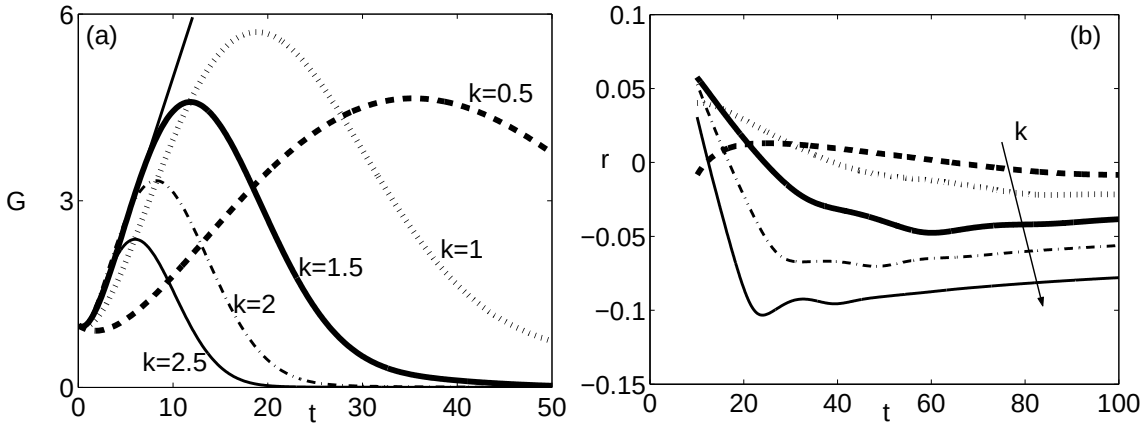

Figure 7.7. Effect of the wavenumber k. (a) The amplification factor G and (b) the temporal growth rate r as function of time. $Re = 100$, $\alpha_i = 0.01$, $n_0 = 1$, $\phi = 3/8\pi$, $y_0 = 0$, $x_0 = 6.50$, asymmetric initial condition, $k = 0.5$,1,1.5,2,2.5.

In Fig. 7.8 an interesting phenomenon is observed for a purely three-dimensional wave. It can be seen that, by increasing the order of magnitude of α_i, perturbations that are more rapidly damped in space lead to a faster growth in time (a logarithmic scale is used on the ordinate in Fig. 7.8a). Moreover, uniform ($\alpha_i = 0$) and slowly damped perturbations in streamwise direction are asymptotically damped in time, while for increasing values of the spatial damping rate the disturbances are deeply amplified in time.

In Figure 7.9, the influence of y_0 (the position where the concentration of the perturbation energy is maximum) on the perturbation evolution is considered. In asymptotically stable cases (a)–(b), the damping is more rapid and the maxima of energy disappear for larger y_0 values. In asymptotically unstable cases (c)–(d), an increase of y_0 leads to a delay of the perturbation amplification, and minima of energy are present before the asymptotic growths are reached (note that in part (c) of Fig. 7.9 a logarithmic scale was used on the ordinate). This means that if most of the perturbation energy is outside the base flow region, for an unstable configuration the growth is delayed in time, while for a stable configuration the decrease of energy is accelerated and the asymptotic state is reached earlier.

Figure 7.10 takes into account the influence, on the early time behaviour, of the perturbation symmetry and of the wake region considered in the analysis, which is

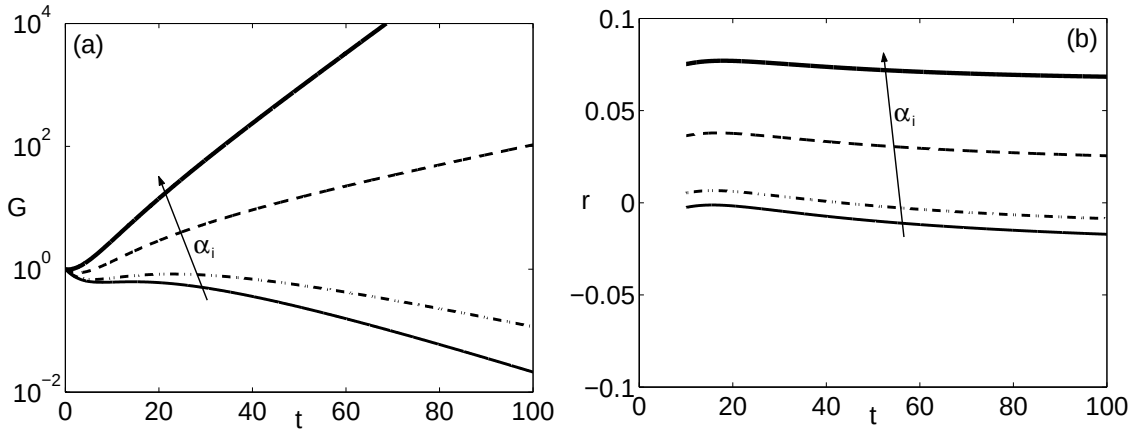

Figure 7.8. Effects linked to the presence of the imaginary part in the wavenumber α. (a) The amplification factor G and (b) the temporal growth rate r as function of time. $Re = 50$, $k = 1.2$, $n_0 = 1$, $\phi = \pi/2$, $y_0 = 0$, $x_0 = 14.50$, symmetric initial condition, $\alpha_i = 0{,}0.01{,}0.05{,}0.1$.

represented by the parameter x_0. All the configurations considered are asymptotically amplified, but the transients are different. The asymmetric cases (a) present, for both the intermediate position $x_0 = 10$ (solid curve) and the far field position $x_0 = 50$ (dashed curve), two temporal evolutions. For $x_0 = 10$ a local maximum, followed by a minimum, is visible in the energy density, then the perturbation is slowly amplifying and the transient can be considered extinguished only after hundreds of time scales. For $x_0 = 50$ these features are less marked. It can be noted that the far field configuration ($x_0 = 50$) has a faster growth than the intermediate field configuration ($x_0 = 10$) up to $t = 400$. However, in the asymptotic state the growth is comparable. In the symmetric cases (b) the growths become monotone after few time scales ($t = 20$) and the perturbations quickly reach their asymptotic states (around $t = 50$). The intermediate field configuration ($x_0 = 10$, solid curve) is always growing faster than the far field configuration ($x_0 = 50$, dashed curve). This particular case shows a behaviour that is generally observed in this analysis, that is, asymmetric conditions lead to transient evolutions that last longer than the corresponding symmetric ones, and demonstrates that the transient growth for a longitudinal station in the far wake can be faster than in the intermediate wake.

However, the more noticeable results presented in Fig. 7.10 are that the asymmetric growths in the early transient are much less rapid than the symmetric ones and that the function G, in the case of asymmetric perturbations only, clearly shows

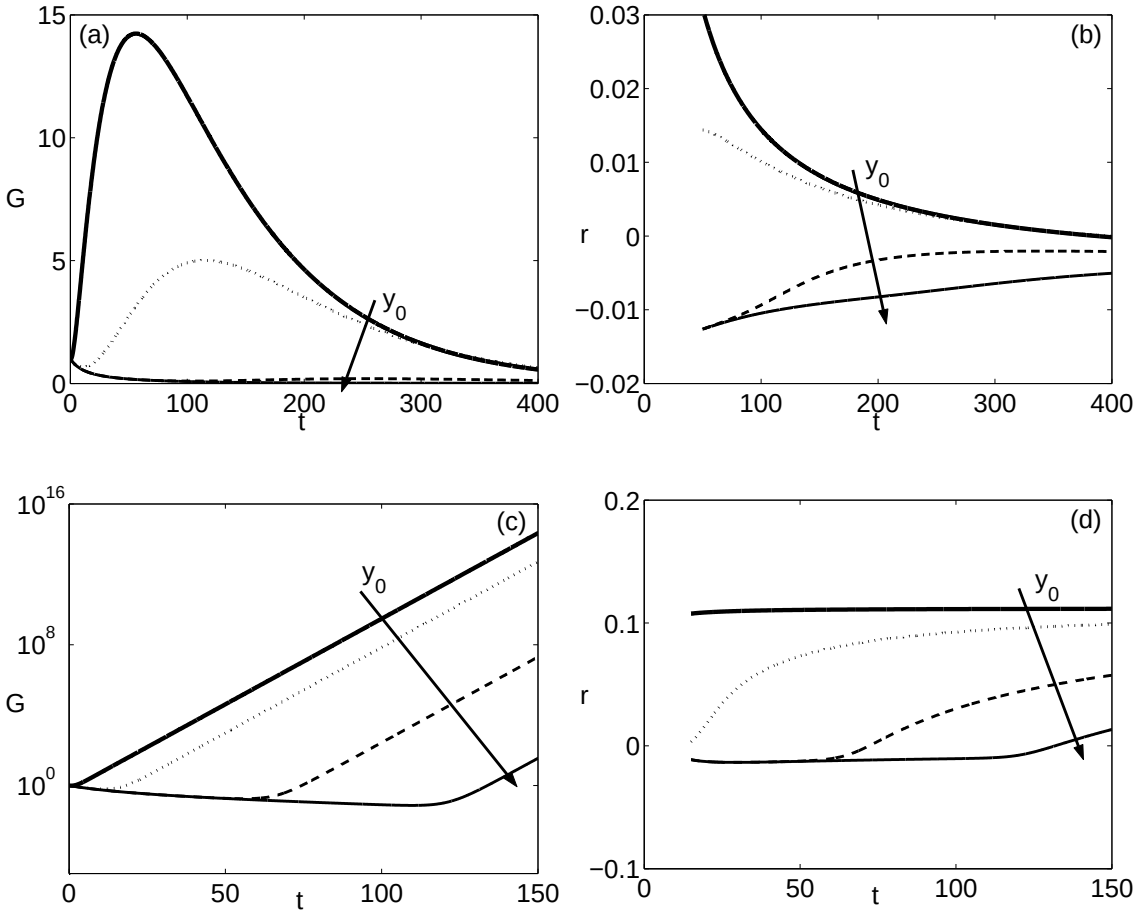

Figure 7.9. Effect of the shape function parameter y_0. (a)-(c) The amplification factor G and (b)-(d) the temporal growth rate r. $Re = 100$, $k = 1.2$, $\alpha_i = 0.01$, $n_0 = 1$, $x = 12$, symmetric initial condition, $y_0 = 0$,2,4,6. (a)-(b): $\phi = \pi/2$. (c)-(d): $\phi = 0$.

a modulation which is very evident in the first part of the transient, and which corresponds to a modulation in amplitude of the pulsation of the instability wave, see for example results for the asymmetric case in Fig. 7.13(b). In the early transient the angular frequency oscillates around a mean value with a regular period, which is the same visible on G, the square norm of the velocity oscillation, and an amplitude which is growing until this value jumps to a new value around which oscillates in a damped way. This second value is the asymptotic constant value. This behaviour is always observed in the case of asymmetric longitudinal or oblique instability waves.

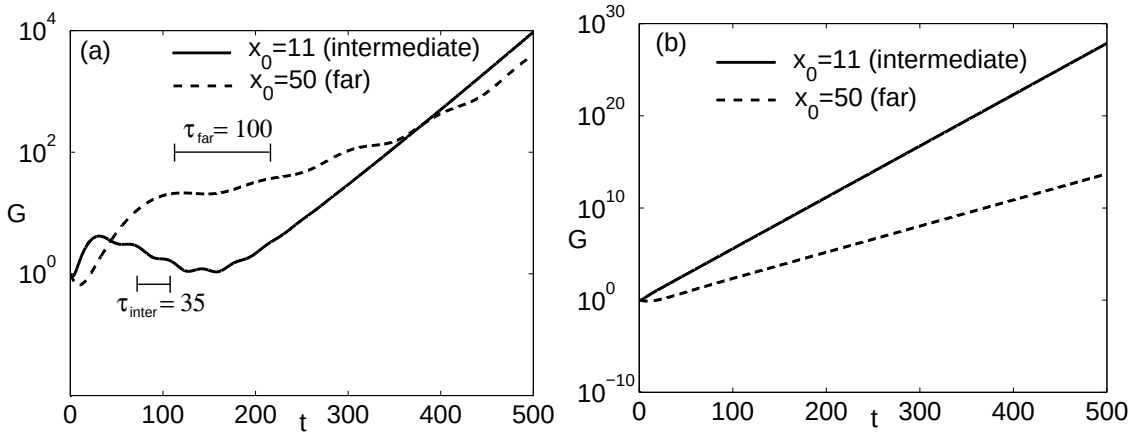

Figure 7.10. Effect of the symmetry of the perturbation. (a) - (b): The amplification factor G as function of time. (a) asymmetric initial condition, (b) symmetric initial condition. $Re = 100$, $k = 0.6$, $\alpha_i = 0.02$, $n_0 = 1$, $y_0 = 0$, $x_0 = 11$ and 50, $\phi = \pi/4$. Intermediate ($x_0 = 11$, solid curves) and far field ($x_0 = 50$, dashed curves) wake configurations. The periods τ_{inter},τ_{far} are those of the modulation visible on G, in the intermediate and far field, respectively.

Instead, it is not shown by transversal ($\phi = \pi/2$) waves or by symmetric waves where, on the one hand, the asymptotic value is rapidly reached after a short monotone growth and, on the other, the growth is many order of magnitude faster, and as a consequence, a modulation would not be easily observable. Thus, two time scales are observed in the transient and long term behaviour of longitudinal and oblique perturbations: namely, the periodicity associated to the average value of the pulsation in the early transient, clearly visible in the asymmetric case only, and the final asymptotic pulsation. The asymptotic value of the pulsation is usually higher than the initial one.

Figure 7.11 illustrates a very interesting comparison between two-dimensional and three-dimensional waves (a logarithmic scale on the ordinate is used in part (a) of Fig. 7.11). The purely two-dimensional wave (solid curve) is immediately reaching a low maximum of amplitude (at about $t = 15$), then the perturbation decreases while oscillating and reaches an absolute minimum around $t = 150$. Afterwards, the disturbance slowly grows up to about $t = 300$, where an inflection point of the amplification factor G occurs. Then, the growth becomes faster and the perturbation is strongly amplified in time. The purely three-dimensional perturbation (dashed curve) is instead immediately amplified following a monotone trend, and does not

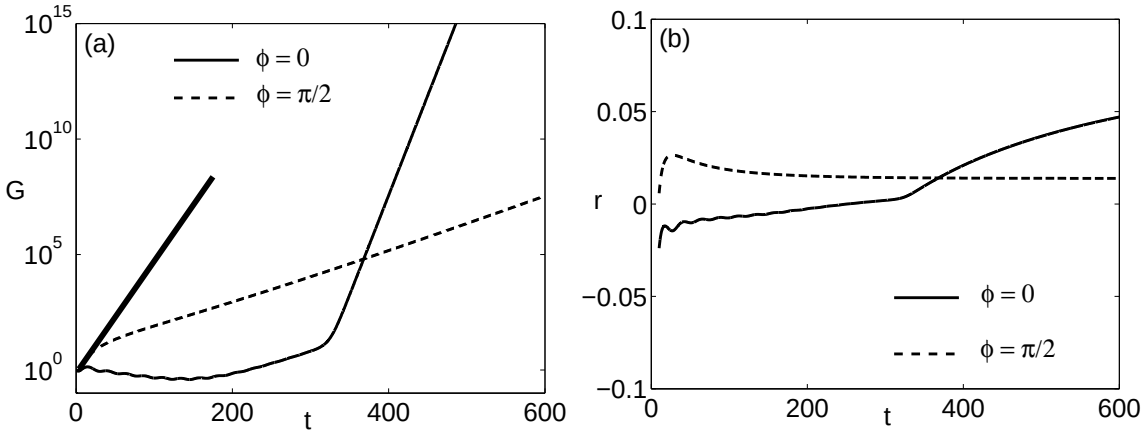

Figure 7.11. Effect of the angle of obliquity ϕ. (a) The amplification factor G and (b) the temporal growth rate r as function of time. $Re = 100$, $k = 0.7$, $n_0 = 1$, $\alpha_i = 0.02$, $y_0 = 0$, $x_0 = 11.50$, asymmetric initial condition, $\phi = 0$ (solid curves), $\phi = \pi/2$ (dashed curves).

present fluctuations in time. The initial growth is actually rapid and an inflection point of the amplification factor G can be found around $t = 50$. Beyond this point, the growth changes its velocity and becomes slower, but still destabilizing. Both cases have asymmetric initial conditions and are ultimately amplified. The two-dimensional case turns out to be more unstable than the three-dimensional one, as the 2D asymptotically established exponential growth is more rapid than the 3D one (see solid and dashed curves in Fig. 7.11(a) for $t > 400$). However, it should be noted that for a quite extended part of the transient (up to about $t = 380$), the three-dimensional perturbation presents a larger growth than the two-dimensional one. Moreover, both the transients are lasting hundred time scales, a fact that is in agreement with what previously stated for asymmetric inputs. This configuration presents a 3D rapid growth, a condition that could in principle lead to by-pass transition. However, in this case, the early 3D amplification is slower than the 2D asymptotic growth (compare thick line and solid curve beyond $t > 400$, in Fig. 7.11(a)), thus the lift-up mechanism cannot occur.

As a general comment, a long-term unstable behaviour (see Figures 7.6 and 7.11) as well as initial transient growth followed by asymptotic damping (see Fig. 7.9) is shown for viscous transversal waves ($\phi = \pi/2$). Unstable final behaviour for purely transversal waves was instead always observed in inviscid stability analysis carried out with the present initial-value problem formulation (see Blossey *et al.* 2007)

in the two-dimensional parallel jet and mixing layer. An initial transient growth, followed by a non permanent decay, is also displayed by two-dimensional waves (see Fig. 7.11). Longitudinal waves, however, have in general a monotone increasing or decrasing behaviour, and sometimes show a minimum of energy before an ultimate growth. A two-dimensional perturbation is usually reaching its (stable or unstable) asymptotic state faster than oblique waves, when the other parameters are fixed (see an example in figure 7.12, §7.4).

7.4 Asymptotic behaviour and comparison with normal mode analysis

Computations to evaluate the long time asymptotics are made by integrating the equations forward in time beyond the transient (Criminale *et al.* 1997; Lasseigne *et al.* 1999) until the temporal growth rate r, defined in relation (7.19), asymptotes to a constant value ($dr/dt < \epsilon$). The choice of the threshold ϵ can offer a quantitative support of when the transient can be considered extinguished. In Fig. 7.12, the temporal growth rates of three configurations with different angles of obliquity are shown. The open circles indicate when r can be approximated as a constant value, according to the above criterium ($\epsilon \sim 10^{-4}$). These results demonstrate that, as stated before, an increase of the angle of obliquity implies transients that last longer.

The angular frequency (pulsation) f of the perturbation can be defined considering the phase φ of the complex wave at a fixed transversal station (for example $y = 1$)

$$\varphi(t;\alpha,\gamma) = arg(\hat{v}(y=1,t;\alpha,\gamma)) = tan^{-1}(\frac{\hat{v}_i(y=1,t;\alpha,\gamma)}{\hat{v}_r(y=1,t;\alpha,\gamma)}) \tag{7.20}$$

and then computing the time derivative of the phase perturbation φ

$$f(t;\alpha,\gamma) = \frac{|d\varphi(t;\alpha,\gamma)|}{dt} \tag{7.21}$$

Although defined at any time t, the frequency f is here referred to as an asymptotic property of the perturbation. Since defined through the perturbation velocity field, it is reasonable expecting constant values of frequency, once the asymptotic state is reached. Moreover, it can be observed that the temporal scale over which the pulsation asymptotes to a constant value is, at maximum, as long as the scale of the extinguishing transient, according to the criterium $dr/dt < \epsilon$ (see for example Fig.

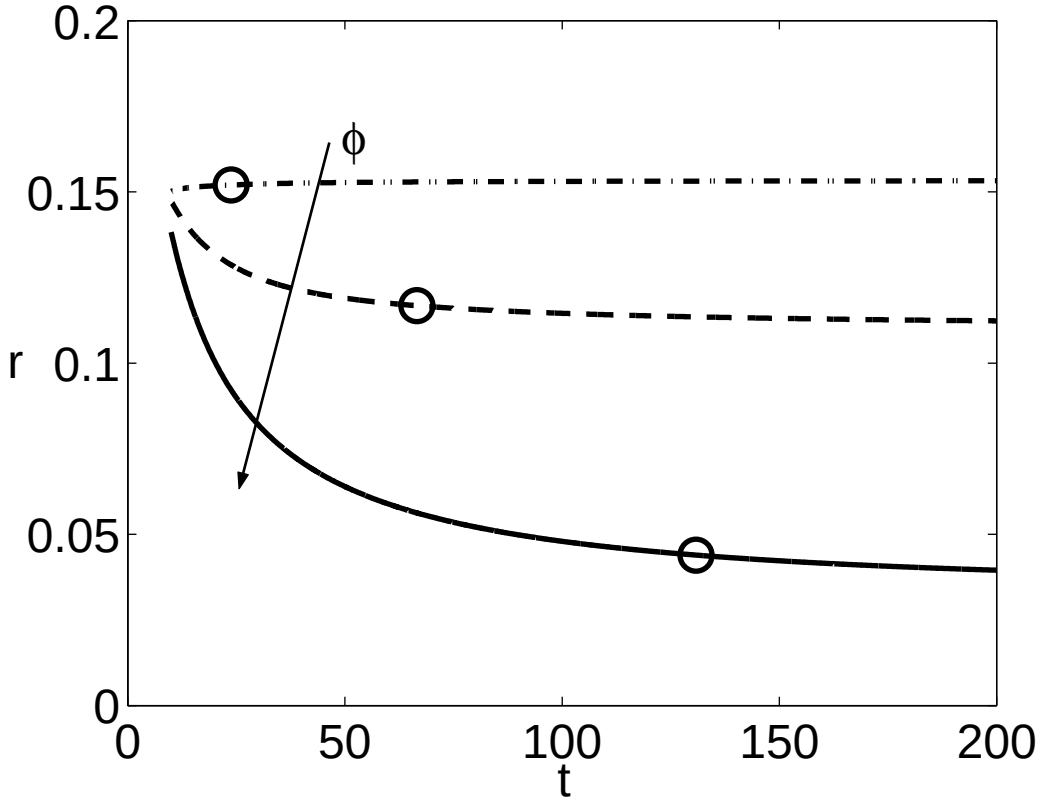

Figure 7.12. Temporal growth rate r as function of time (continuous curves) and temporal length of the transient (open circles) according to the criterium $dr/dt < \epsilon$, with $\epsilon \sim 10^{-4}$. $Re = 100$, $k = 1.2$, $\alpha_i = 0.05$, $n_0 = 1$, $y_0 = 0$, $x_0 = 10.50$, symmetric initial condition, $\phi = 0,\pi/4,\pi/2$.

7.13). This means that, beyond the time for which $dr/dt < \epsilon$ is becoming valid, both temporal growth rate and frequency are reaching their asymptotic values.

In Fig. 7.13, the complete evolution in time of the temporal growth rate and the frequency, for symmetric and asymmetric initial conditions, is shown for a particular configuration ($k = 0.5$, $\alpha_i = 0.02$, $x_0 = 10$, $\phi = 0$, $Re = 100$). These results verify that the transient is lasting longer for asymmetric inputs rather than for the symmetric ones (see Fig. 7.10), as can be seen by symbols indicating when the asymptotic state is reached. In this case, according to the criterium $dr/dt < \epsilon$ with $\epsilon \sim 10^{-4}$, the asymptotic state can be considered as reached beyond $t = 90$ for symmetric inputs, and beyond $t = 600$ for asymmetric inputs. In general, for asymmetric perturbations the transient is extinguished after a time scale $t \sim 10^2$,

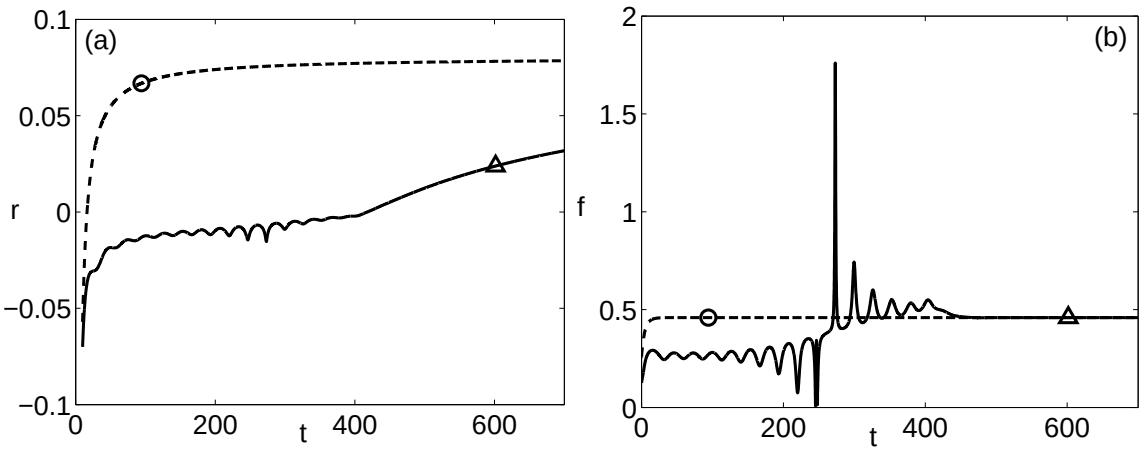

Figure 7.13. (a) Temporal growth rate and (b) angular frequency as function of time for symmetric (dashed curves) and asymmetric (solid curves) initial conditions, and temporal length of the transient (circles: symmetric perturbation, triangles: asymmetric perturbation) according to the criterium $dr/dt < \epsilon$. $Re = 100$, $x_0 = 10$, $k = 0.5$, $\alpha_i = 0.02$, $\phi = 0$, $y_0 = 0$, $n_0 = 1$, $\epsilon \sim 10^{-4}$.

while for symmetric disturbances the transient time scale is $t \sim 10$. Moreover, as previously said, the frequency asymptotes to a constant value after a time, at most, equal to the one of the extinguishing transient. Here, this fact is confirmed for both symmetric and asymmetric disturbances, as the frequency reaches its asymptotic value just before the transient can be thought of as concluded (see symbols in Fig. 7.13(b) indicating the length of the transient, according to the criterium $dr/dt < \epsilon$). It should be noted that, for the asymmetric case, frequency f and temporal growth rate r rapidly oscillate around a mean value in the transient up to $t = 500$ and then reach their asymptotic states, while in the symmetric case a monotone trend is observed for both frequency and temporal growth rate before the final states are reached.

Figure 7.14 presents a longitudinal comparison between the initial-value problem and the asymptotic theory results represented by the zero order Orr-Sommerfeld problem in terms of temporal growth rate r and pulsation f.
In fig. 7.14 the imaginary part α_i of the complex longitudinal wavenumber is fixed, and differing polar wavenumbers ($k = \alpha_r$) are considered. For both the symmetric and asymmetric arbitrary disturbances here considered, a good agreement with the stability characteristics given by the multiscale near-parallel Orr-Sommerfeld theory can be observed. However, it should be noted that the wavenumber corresponding

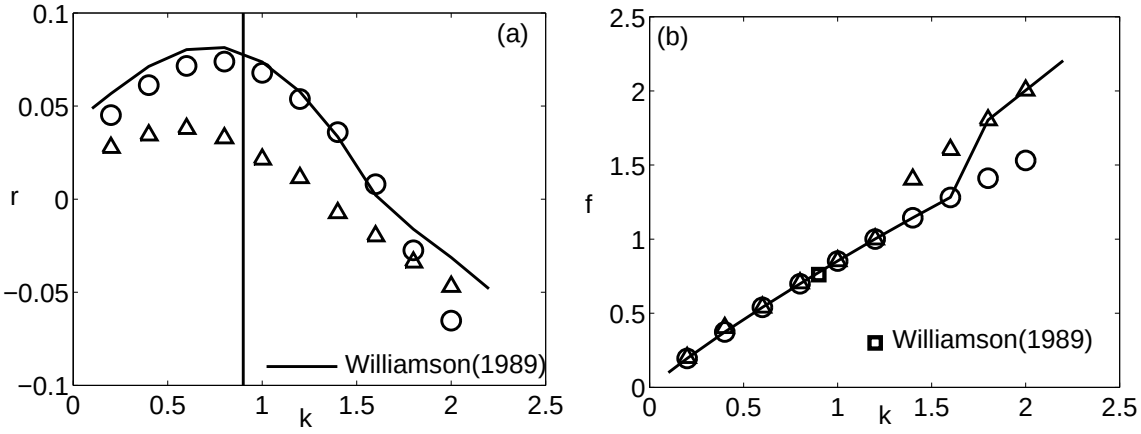

Figure 7.14. $n_0 = 1$, $y_0 = 0$, $\phi = 0$, $\epsilon \sim 10^{-4}$. **(a)** Temporal growth rate and **(b)** pulsation. Comparison among the asymptotic results obtained by the initial-value problem analysis (circles: symmetric perturbation; triangles: asymmetric perturbation), normal mode analysis (solid curves), and experimental data (Williamson 1989, thick line in (a) and square in (b)). $\alpha_i = 0.05$, $x_0 = 11$, $Re = 50$.

to the maximum growth factor in the case of asymmetric perturbations is about 15% lower than the one obtained in the case of symmetric perturbations and the one obtained by the normal mode analysis. When the perturbations are asymmetric, the transient is very long, of the order of hundreds time scales. This difference can be due either to the fact that the true asymptote is not yet reached, or to the fact that the extent of the numerical errors in the integration of the equations is higher than that obtained in the case of symmetric transients, which last only a few dozen time scales. Note that this satisfactory agreement is observed by using arbitrary initial conditions in terms of elements of the trigonometrical Schauder basis for the L^2 space, and not by considering as initial condition the most unstable waves given by the Orr-Sommerfeld dispersion relation. Moreover, a maximum of the perturbation energy (in terms of r) is found around $k = 0.8$ and confirmed by both the analyses.

As shown in Fig. 7.14, initial-value problem results are also contrasted with the laboratory experimental results obtained in 1989 by Williamson, who gave a quantitative determination of the Strouhal number and wavelength of the vortex shedding – oblique and parallel modes – of a circular cylinder at low Reynolds number. The comparison is quantitatively good, because it shows that a wavenumber close to the wavenumber that theoretically has the maximum growth rate at $Re = 50$ (see part (a) of Fig. 7.14) has a – theoretically deduced – frequency which is very close to

the frequency measured in the laboratory. At this point, also the laboratory experimental uncertainty, globally of the order of a $\pm 10\%$ in an accurate measurement set up, should be introduced. The uncertainty associated to the laboratory method and to the theoretical model (estimated through the difference between the position of the maximum growth rate showed by the two cases of asymmetric and symmetric perturbation) overlaps, which confirms the quality of this comparison. The same quantitative agreement is observed also at $Re = 100$.

7.5 Concluding remarks

The three-dimensional stability analysis of the intermediate asymptotics of the two-dimensional viscous growing wake has been considered as an initial-value problem. The vorticity formulation is analogous to the one first proposed by Criminale & Drazin (1990). The perturbative equations are Laplace-Fourier transformed in the plane normal to the base flow. Differently to what usually done, a complex wavenumber in the streamwise direction has been introduced, by means of a spatial Laplace transform in streamwise direction.

An important point is the kind of base flow used in the formulation. Since the longitudinal component of the Navier-Stokes matched asymptotic expansion is only considered, the initial-value problem becomes a near parallel analysis parameterized on the streamwise variable, which makes this study similar to a zero order multiscale near-parallel Orr-Sommerfeld analysis. The use of a parameterized base flow can be thought of as a first step to better describe the spatial evolution of the physical system. In this regard, the introduction of the imaginary part of the longitudinal wavenumber (the spatial damping rate) was done to explicitly include also in the structure of the perturbation, which otherwise would have been homogeneous in the x coordinate, a degree of freedom associated to the spatial evolution of the system.

Various transient scenarios have been observed in the region of the wake where the entrainment is present for Re 50,100. For example, initial damping followed by a fast growth for perturbations aligned with the basic flow, initial transient growths that smoothly level off and are followed either by an ultimate damping or by a slow amplification for oblique waves. As a general and summarizing comment, it can be concluded that the most important parameters affecting these configurations are the angle of obliquity, the symmetry of the perturbation and the spatial growth rate. While the symmetry of the disturbance is remarkably influencing the transient behaviour leaving inalterate the asymptotic fate, a variation of the obliquity and the

spatial growth rate can significantly change both the early trend and the final stability configuration. The number of oscillations and the distribution in y direction were also considered. However, their effect is only to extend or shorten the length of the transient, while the ultimate state is not different. More specifically, if the perturbation oscillates rapidly or lies mainly outside the shear region then, for a stable configuration, the final damping is accelerated while, for an unstable configuration, the asymptotic growth is delayed. The asymptotic fate of purely transversal viscous waves can show a long-term unstable behaviour as well as initial transient growth followed by asymptotic damping. On the contrary, a weak final growth is generally observed for inviscid transversal waves in 2D parallel jets and mixing layers studied with the same initial-value problem formulation.

For disturbances aligned with the flow, it has been demonstrated that the asymptotic behaviour is in good agreement with the zero order results of spatio-temporal multiscale modal analyses. It should be noted that this agreement is obtained not using as initial condition the most unstable wave given by the Orr-Sommerfeld dispersion relation at any section of the wake, but arbitrary initial conditions in terms of elements of the trigonometrical Schauder basis for the L^2 space.

Chapter 8

Multiple scales analysis for the stability of long waves in near-parallel flows

In this chapter, the three-dimensional stability analysis of long waves applied to the two-dimensional wake is studied as an initial-value problem by means of a multiple scales approach. Since different scales can be identified in the stability analysis of spatially developing flows, the polar wavenumber can be considered a small parameter for a perturbative analysis in the limit of long waves. Indeed, there are some flow configurations for which long waves are destabilizing (for example Blasius boundary layer and three-dimensional cross flow boundary layer). In such instances, wavenumber of the unstable wave is much less than $O(1)$.

The initial-value problem formulation is carried on in terms of velocity and vorticity, similarly to what first proposed by Criminale & Drazin (1990), but considering now a non-parallel base flow (see §8.1.1). The base flow is, in fact, approximated using both the longitudinal as well as the transversal components of the asymptotic Navier-Stokes expansions (see §2.3), so that non-parallelism is directly inserted in the stability analysis. A regular perturbation expansion for $k \to 0$ is defined in §8.1.2. The introduction of a complex wavenumber in streamwise direction, considered when the transformation to the phase space is performed, makes the equations solvable at any order. A combined Laplace-Fourier transform in the x and z directions is proposed in order to consider a perturbation characterized by real streamwise and spanwise wavenumbers, and a uniform or damped spatial longitudinal distribution. Growing streamwise distributions are not allowed, as the perturation kinetic energy has to remain finite. Perturbative equations are presented and discussed up to

order $O(k)$. Results concerning the perturbation temporal evolution are presented in §8.2. Comparisons between multiscaling $O(1)$ and full problem solutions in the early transient show a good agreement in differing physical configurations (see §8.2.1). An asymptotic comparison between multiscale data and full problem results can be made. It can be demonstrated that the agreement turns out to be very good. Conclusive comments are given in §8.3.

The recognition of some free shear flows as systems which slowly evolve with respect to small unsteady perturbations allows the use of asymptotic methods (see Bender & Orszag, 1978) to study their stability.
In literature, the WKBJ method has been usually adopted, defining as small parameter the inverse of the Reynolds number, $\varepsilon = 1/Re$ (see for example Bouthier, 1973; Belan & Tordella, 2006; Tordella, Scarsoglio & Belan, 2006). In this way, the perturbative method is based on the base flow parameter characterizing its streamwise evolution. However, it should be noted that an asymptotic perturbative expansion based on the inverse of the Reynolds number leads to a singular perturbation analysis, as in the Orr-Sommerfeld equation the highest order term is vanishing for ε values going to zero.
Here, instead, the definition of the polar wavenumber k as small parameter of the perturbation approach (see Lasseigne *et al.*, 1999; Blossey, Criminale & Fisher, 2007) leads to a regular perturbation scheme. The use of a perturbation Laplace decomposition in streamwise direction (Scarsoglio, Tordella & Criminale 2007) yields solvable equations at any order. The validity of the multiscale approach is here analyzed in the case of the two-dimensional wake.

8.1 The initial-value problem by means of multiscale approach

8.1.1 Formulation

The inner solution, that includes both the longitudinal and the transversal components of the asymptotic Navier-Stokes expansions up to $O(x^{-3/2})$ (see §2.3), is considered to approximate the wake profile. In this way, the transversal non-linear and diffusive dynamics of the base flow is directly introduced into the initial-value problem formulation. The base flow is not parameterized with respect to the longitudinal coordinate only (see §7.2.1 and Scarsoglio *et al.* 2007), but a further improvement concerning the base flow spatial evolution is made. In fact, the two

velocity components are both explicit functions of x and y. As a consequence, the non-parallelism is fully included and its influence on the perturbation evolution can be considered.

The continuity and Navier-Stokes equations for the perturbed system are linearized with respect to small three-dimensional oscillations

$$\frac{\partial \widetilde{u}}{\partial x} + \frac{\partial \widetilde{v}}{\partial y} + \frac{\partial \widetilde{w}}{\partial z} = 0 \tag{8.1}$$

$$\frac{\partial \widetilde{u}}{\partial t} + \widetilde{u}\frac{\partial U}{\partial x} + U\frac{\partial \widetilde{u}}{\partial x} + \widetilde{v}\frac{\partial U}{\partial y} + V\frac{\partial \widetilde{u}}{\partial y} + \frac{\partial \widetilde{p}}{\partial x} = \frac{1}{Re}\nabla^2\widetilde{u} \tag{8.2}$$

$$\frac{\partial \widetilde{v}}{\partial t} + \widetilde{u}\frac{\partial V}{\partial x} + U\frac{\partial \widetilde{v}}{\partial x} + \widetilde{v}\frac{\partial V}{\partial y} + V\frac{\partial \widetilde{v}}{\partial y} + \frac{\partial \widetilde{p}}{\partial y} = \frac{1}{Re}\nabla^2\widetilde{v} \tag{8.3}$$

$$\frac{\partial \widetilde{w}}{\partial t} + U\frac{\partial \widetilde{w}}{\partial x} + V\frac{\partial \widetilde{w}}{\partial y} + \frac{\partial \widetilde{p}}{\partial z} = \frac{1}{Re}\nabla^2\widetilde{w} \tag{8.4}$$

where ($\widetilde{u}(x,y,z,t)$, $\widetilde{v}(x,y,z,t)$, $\widetilde{w}(x,y,z,t)$) and $\widetilde{p}(x,y,z,t)$ are the perturbation velocity and pressure respectively. The independent spatial variables z and y are defined from $-\infty$ to $+\infty$, x from 0 to $+\infty$. All physical quantities are normalized with respect to the free stream velocity, the spatial scale of the flow D and the density. By combining momentum equations (8.2)-(8.4) to eliminate the pressure terms, the resulting governing equations become

$$\nabla^2\widetilde{v} = \widetilde{\Gamma}, \tag{8.5}$$

$$\begin{aligned}\frac{\partial \widetilde{\Gamma}}{\partial t} = &-[U\frac{\partial}{\partial x} + V\frac{\partial}{\partial y} - \frac{1}{Re}\nabla^2]\widetilde{\Gamma} - [\frac{\partial \Omega_z}{\partial x}\frac{\partial}{\partial x} + \frac{\partial^2 \Omega_z}{\partial x^2}]\widetilde{u} - [\frac{\partial \Omega_z}{\partial y}\frac{\partial}{\partial x} + \frac{\partial^2 \Omega_z}{\partial x \partial y}]\widetilde{v} + \\ &+\frac{\partial \Omega_z}{\partial x}\frac{\partial \widetilde{w}}{\partial z} + \frac{\partial V}{\partial y}\frac{\partial \widetilde{\omega}_x}{\partial z} - \frac{\partial V}{\partial x}\frac{\partial \widetilde{\omega}_y}{\partial z} - [\frac{\partial U}{\partial x}\frac{\partial}{\partial x} + \frac{\partial V}{\partial x}\frac{\partial}{\partial y}]\widetilde{\omega}_z,\end{aligned} \tag{8.6}$$

$$\frac{\partial \widetilde{\omega}_y}{\partial t} = -[U\frac{\partial}{\partial x} + V\frac{\partial}{\partial y} + \frac{\partial U}{\partial x} - \frac{1}{Re}\nabla^2]\widetilde{\omega}_y - \frac{\partial U}{\partial y}\frac{\partial \widetilde{v}}{\partial z} + \frac{\partial V}{\partial x}\frac{\partial \widetilde{w}}{\partial y}, \tag{8.7}$$

where the perturbation vorticity ($\widetilde{\omega}_x$,$\widetilde{\omega}_y$,$\widetilde{\omega}_z$), the mean vorticity in spanwise direction $\Omega_z = \dfrac{\partial V}{\partial x} - \dfrac{\partial U}{\partial y}$ and the kinematics relation $\widetilde{\Gamma} = \dfrac{\partial \widetilde{\omega}_z}{\partial x} - \dfrac{\partial \widetilde{\omega}_x}{\partial z}$ have already been included. Equations (8.6) and (8.7) are the Orr-Sommerfeld and Squire equations respectively, written in partial differential equation form and expressed through different dependent variables. Since 7 scalar unknown quantities ($\widetilde{u}$,$\widetilde{v}$,$\widetilde{w}$,$\widetilde{\omega}_x$,$\widetilde{\omega}_y$,$\widetilde{\omega}_x$,$\widetilde{\Gamma}$) are involved in the three scalar equations (8.5)-(8.7), four more scalar relations are needed. Thus, the perturbation vorticity definition and the continuity equation

$$\widetilde{\underline{\omega}} = \nabla \times \widetilde{\underline{u}}, \tag{8.8}$$

$$\nabla \cdot \widetilde{\underline{u}} = 0, \tag{8.9}$$

where $\widetilde{\underline{\omega}} = (\widetilde{\omega}_x,\widetilde{\omega}_y,\widetilde{\omega}_z)$ and $\widetilde{\underline{u}} = (\widetilde{u},\widetilde{v},\widetilde{w})$, formally close the perturbative system (8.5)-(8.7). From equations (8.5)-(8.7), it can be noted that perturbation vorticity vanishes in the free stream.
A combined spatial Laplace-Fourier decomposition in the x-z plane is now performed for every dependent variable. The transformed perturbation quantities $(\widetilde{\underline{u}},\widetilde{\underline{\omega}},\widetilde{\Gamma})$ are now called $(\hat{\underline{u}},\hat{\underline{\omega}},\hat{\Gamma})$. A general function

$$\hat{g}(y,t;\alpha,\gamma) = \int_{-\infty}^{+\infty}\int_{0}^{+\infty} \widetilde{g}(x,y,z,t)e^{-i\alpha x - i\gamma z}dxdz \tag{8.10}$$

indicates the Laplace-Fourier transform of a dependent variable in the $\alpha-\gamma$ phase space and in the remaining independent variables y and t. In general α is complex ($\alpha = \alpha_r + i\alpha_i$), while γ is real. In order to have a finite perturbation kinetic energy, the imaginary part α_i of the complex longitudinal wavenumber can only assume non-negative values. In so doing, perturbative waves are allowed to spatially decay ($\alpha_i > 0$) or remain constant in amplitude ($\alpha_i = 0$). The governing equations (8.5)-(8.7), joined by the scalar relations (8.8)- (8.9), can now be expressed as follows

$$\frac{\partial^2\hat{v}}{\partial y^2} - (k^2 - \alpha_i^2 + 2ikcos(\phi)\alpha_i)\hat{v} = \hat{\Gamma} \tag{8.11}$$

$$\frac{\partial\hat{\Gamma}}{\partial t} = G\hat{\Gamma} + H\hat{v} + K\hat{\omega}_y \tag{8.12}$$

$$\frac{\partial\hat{\omega}_y}{\partial t} = L\hat{\omega}_y + M\hat{v} \tag{8.13}$$

where the perturbation angle of obliquity $\phi = tan^{-1}(\gamma/\alpha_r)$ with respect to the x-y physical plane, the polar wavenumber $k = \sqrt{\alpha_r^2+\gamma^2}$, the wavenumbers $\alpha_r = kcos(\phi)$ and $\gamma = ksin(\phi)$ in the x and z directions respectively, and the spatial damping rate α_i in the streamwise direction have already been introduced. The terms G, H, K, L and M are ordinary differential operators, written in the form $G = G(y;k,\phi,\alpha_i,Re)$, and similarly for H, K, L and M, since they are function of y, and are parameterized through the polar wavenumber k, the angle of obliquity ϕ, the spatial growth rate α_i, the Reynolds number Re. With respect to equations (7.12)-(7.14), equations (8.11)-(8.13) have additional terms due to the transversal

component V of the base flow (and its longitudinal and transversal variations). A more accurate description of the mean vorticity leads, among other things, to the explicit presence in equation (8.12) of the transversal vorticity $\hat{\omega}_y$. This means that three-dimensional effects causing the perturbation transversal vorticity evolution can now directly influence the temporal behaviour of the other disturbance vorticity components. If $\phi = 0$ there is no production of transversal vorticity at any time, and transversal vorticity contribute in equation (8.12) vanishes. The explicit expressions for operators in equation (8.12) are

$$G = - i(kcos(\phi)+i\alpha_i)U - V\frac{\partial}{\partial y} + \frac{1}{Re}[\frac{\partial^2}{\partial y^2} - k^2 + \alpha_i^2 - 2ikcos(\phi)\alpha_i], \tag{8.14}$$

$$\begin{aligned} H = & - \frac{i(kcos(\phi)+i\alpha_i)}{k^2+2ikcos(\phi)\alpha_i-\alpha_i^2}\frac{\partial^2\Omega_z}{\partial x^2}\frac{\partial}{\partial y} - \frac{\partial^2\Omega_z}{\partial x\partial y} - i(kcos(\phi)+i\alpha_i)\frac{\partial\Omega_z}{\partial y} + \\ & + \frac{k^2cos^2(\phi)+2ikcos(\phi)\alpha_i-\alpha_i^2-k^2sin^2(\phi)}{k^2+2ikcos(\phi)\alpha_i-\alpha_i^2}\frac{\partial\Omega_z}{\partial x}\frac{\partial}{\partial y} + \\ & + (k^2cos^2(\phi)+2ikcos(\phi)\alpha_i-\alpha_i^2)\frac{\partial U}{\partial x} + k^2sin^2(\phi)\frac{\partial V}{\partial y} + \\ & - \frac{k^2cos^2(\phi)+2ikcos(\phi)\alpha_i-\alpha_i^2}{k^2+2ikcos(\phi)\alpha_i-\alpha_i^2}\frac{\partial U}{\partial x}\frac{\partial^2}{\partial y^2} - \frac{k^2sin^2(\phi)}{k^2+2ikcos(\phi)\alpha_i-\alpha_i^2}\frac{\partial V}{\partial y}\frac{\partial^2}{\partial y^2} + \\ & - i(kcos(\phi)+i\alpha_i)\frac{\partial V}{\partial x}\frac{\partial}{\partial y} + \frac{i(kcos(\phi)+i\alpha_i)}{k^2+2ikcos(\phi)\alpha_i-\alpha_i^2}\frac{\partial V}{\partial x}\frac{\partial^3}{\partial y^3}, \end{aligned} \tag{8.15}$$

$$\begin{aligned} K = & + \frac{ksin(\phi)}{k^2+2ikcos(\phi)\alpha_i-\alpha_i^2}\frac{\partial^2\Omega_z}{\partial x^2} - 2\frac{(kcos(\phi)+i\alpha_i)ksin(\phi)}{k^2+2ikcos(\phi)\alpha_i-\alpha_i^2}\frac{\partial\Omega_z}{\partial x} + \\ & + \frac{(kcos(\phi)+i\alpha_i)ksin(\phi)}{k^2+2ikcos(\phi)\alpha_i-\alpha_i^2}\frac{\partial U}{\partial x}\frac{\partial}{\partial y} - \frac{(kcos(\phi)+i\alpha_i)ksin(\phi)}{k^2+2ikcos(\phi)\alpha_i-\alpha_i^2}\frac{\partial V}{\partial y}\frac{\partial}{\partial y} + \\ & - iksin(\phi)\frac{\partial V}{\partial x} - i\frac{ksin(\phi)}{k^2+2ikcos(\phi)\alpha_i-\alpha_i^2}\frac{\partial V}{\partial x}\frac{\partial^2}{\partial y^2}, \end{aligned} \tag{8.16}$$

while for operators in equation (8.13) the following relations hold

$$\begin{aligned} L = & - i(kcos(\phi)+i\alpha_i)U - V\frac{\partial}{\partial y} + \frac{1}{Re}[\frac{\partial^2}{\partial y^2} - k^2 + \alpha_i^2 - 2ikcos(\phi)\alpha_i] + \\ & - \frac{\partial U}{\partial x} + \frac{i(kcos(\phi)+i\alpha_i)}{k^2+2ikcos(\phi)\alpha_i-\alpha_i^2}\frac{\partial V}{\partial x}\frac{\partial}{\partial y}, \end{aligned} \tag{8.17}$$

$$M = - iksin(\phi)\frac{\partial U}{\partial y} + \frac{iksin(\phi)}{k^2+2ikcos(\phi)\alpha_i-\alpha_i^2}\frac{\partial V}{\partial x}\frac{\partial^2}{\partial y^2}. \tag{8.18}$$

The full linear system (8.11)-(8.13) is to be solved subject to appropriate initial and boundary conditions. Among all solutions, those whose perturbation velocity field is zero in the free stream are sought. Periodic initial conditions for

$$\hat{\Gamma} = \frac{\partial^2 \hat{v}}{\partial y^2} - (k^2 - \alpha_i^2 + 2ikcos(\phi)\alpha_i)\hat{v} \tag{8.19}$$

can be shaped in terms of set of functions in the L^2 Hilbert space, as

$$\hat{v}(0,y) = e^{-(y-y_0)^2}\cos(n_0(y-y_0)) \quad \text{or} \quad \hat{v}(0,y) = e^{-(y-y_0)^2}\sin(n_0(y-y_0)), \tag{8.20}$$

for the symmetric and the asymmetric perturbations, respectively. Parameter n_0 is an oscillatory parameter for the shape function, while y_0 is a parameter which controls the distribution of the perturbation along y (by moving away or bringing nearer the perturbation maxima from the axis of the wake). It can be verified (see §7.3) that a possible introduction of an initial transversal vorticity $\hat{\omega}_y(0,y) \neq 0$ does not substantially modify the perturbation temporal behaviour, as the contribution of the transversal vorticity to the perturbation energy evolution is basically all due to the three-dimensionality of the disturbance, regardless the specific initial condition imposed. Thus, initial condition for $\hat{\omega}_y$ is chosen equal to zero.
The trigonometrical system $(1,sin(n_0y),cos(n_0y),\dots)$, where $n_0 = 1,2,\dots$, is a Schauder basis for the space of square-integrable periodic functions with period 2π. This means that any element of the space L^2, where the dependent variables are defined, can be written as an infinite linear combination of the elements of the basis.
Once initial and boundary conditions are included, the full linear system (8.11)-(8.13) is numerically solved by the method of lines on a spatial bounded domain $[-y_f, + y_f]$. The value of y_f is chosen so that the numerical solutions are not sensitive to further extensions of the computational domain size. Here, for the stability analysis of long waves, the numerical domain $2y_f$ can vary its order of magnitude between 10^1 and 10^2.

8.1.2 Multiple spatial and temporal scales

In the stability analysis of spatially developing flows, different scales can be identified. In general, long and slow scales - related to the slow base flow evolution - as well as short and fast scales - linked to the disturbance dynamics - can be defined. The WKBJ method has been usually carried on adopting as small parameter of

the perturbation expansion the inverse of the Reynolds number (see for instance Bouthier, 1973; Belan & Tordella, 2006; Tordella, Scarsoglio & Belan, 2006), which characterizes the non-parallelism of the base flow. Here, the choice of the small parameter is no more related to streamwise evolution of the base flow, but is based on the perturbation characteristics.

In some flow configurations, in fact, it is observed that long waves can be destabilizing. Examples of this behaviour are the two-dimensional Blasius boundary layer as well as the three-dimensional cross-flow boundary layer. Studies on 2D and 3D boundary layers (see, among others, Mack, 1976; Schlichting 1968; Reshotko, 1976; Reed & Saric, 1989; Saric, Reed & White, 2003) confirm this fact and show that the perturbation wavenumber k is much less than $O(1)$ when instability occurs. In general, large wavenumber values would imply short scales that can be easily damped. Moreover, an inspection of equations (8.11)-(8.13) reveals the presence of the wavenumber k at different orders of magnitude and suggests that multiple times as well as multiple scales can be identified through it.

Thus, the small parameter which allows for a regular perturbation scheme is the polar wavenumber k. Two spatial scales - a short one, y, and a long one, $Y = ky$ - are defined. For the temporal dynamics, three temporal scales - the fast one, t, and the slow ones, $\tau = kt$ and $T = k^2 t$ - can be determined. Note that the scale $T = k^2 t$ is related to the viscous terms and becomes unnecessary in the inviscid case. The perturbation quantities $(\hat{v},\hat{\Gamma},\hat{\omega}_y)$ are now function of y,Y,t,τ,T, thus can be expressed as $\hat{\Gamma} = \hat{\Gamma}(y,Y,t,\tau,T;k,\phi,\alpha_i)$, and similarly for $\hat{v}$ and $\hat{\omega}_y$. The respective operators in the equations become

$$\frac{\partial}{\partial t} = \frac{\partial}{\partial t} + k\frac{\partial}{\partial \tau} + k^2\frac{\partial}{\partial T} \tag{8.21}$$

$$\frac{\partial}{\partial y} = \frac{\partial}{\partial y} + k\frac{\partial}{\partial Y} \tag{8.22}$$

$$\frac{\partial^2}{\partial y^2} = \frac{\partial^2}{\partial y^2} + 2k\frac{\partial^2}{\partial y \partial Y} + k^2\frac{\partial^2}{\partial Y^2} \tag{8.23}$$

A regular perturbation expansion for the dependent variables $(\hat{v},\hat{\Gamma},\hat{\omega}_y)$ can be assumed and expressed as

$$\begin{aligned} \hat{v} &= \hat{v}_0 + k\hat{v}_1 + k^2\hat{v}_2 + \cdots, \\ \hat{\Gamma} &= \hat{\Gamma}_0 + k\hat{\Gamma}_1 + k^2\hat{\Gamma}_2 + \cdots, \\ \hat{\omega}_y &= \hat{\omega}_{y0} + k\hat{\omega}_{y1} + k^2\hat{\omega}_{y2} + \cdots, \end{aligned} \tag{8.24}$$

with the following initial conditions

$$\begin{aligned}
\hat{\Gamma}_0(y,Y,0,0,0;k,\phi,\alpha_i) &= \hat{\Gamma}(y,Y,0,0,0;k,\phi,\alpha_i), \\
\hat{\Gamma}_1(y,Y,0,0,0;k,\phi,\alpha_i) &= \hat{\Gamma}_2(y,Y,0,0,0;k,\phi,\alpha_i) = \cdots = 0, \qquad (8.25) \\
\hat{\omega}_{y0}(y,Y,0,0,0;k,\phi,\alpha_i) &= \hat{\omega}_y(y,Y,0,0,0;k,\phi,\alpha_i), \\
\hat{\omega}_{y1}(y,Y,0,0,0;k,\phi,\alpha_i) &= \hat{\omega}_{y2}(y,Y,0,0,0;k,\phi,\alpha_i) = \cdots = 0. \qquad (8.26)
\end{aligned}$$

Initial conditions at order $O(1)$ are defined as in the full linear problem, while at higher orders ($O(k)$,$O(k^2)$,...) are equal to zero. Boundary conditions remain as stated in the full linear problem. It is necessary that the series expansions begin as indicated, so that all variables are at the same order of magnitude. This point can be noted from the definition, in the phase space, for $\hat{\Gamma}$, $\hat{\omega}_y$, and the constraint of incompressibility that requires the velocity to be divergence free.

Substituting relations (8.24) - together with the transformations (8.21)-(8.23) - in the full linear system (8.11)-(8.13), the following ordered hierarchy of equations, expressed up to $O(k)$, results

Order O(1)

$$\begin{aligned}
\frac{\partial^2 \hat{v}_0}{\partial y^2} + \alpha_i^2 \hat{v}_0 &= \hat{\Gamma}_0 \qquad (8.27) \\
\frac{\partial \hat{\Gamma}_0}{\partial t} - G_h \hat{\Gamma}_0 - H_h \hat{v}_0 &= 0 \qquad (8.28) \\
\frac{\partial \hat{\omega}_{y0}}{\partial t} - L_h \hat{\omega}_{y0} &= 0 \qquad (8.29)
\end{aligned}$$

where the subscript h (h = highest) indicates that these operators, at any order of the multiscaling, are involving only terms at the highest order of the perturbation expansion (8.24). As the order is here $O(1)$ ($h = 0$), these operators are acting on quantities ($\hat{\Gamma}_0$,$\hat{v}_0$,$\hat{\omega}_{y0}$). Operators $G_h = G_h(y;\phi,\alpha_i,Re)$ as well as H_h and L_h are function of the only short scale y. Their explicit expressions are

$$G_h = \alpha_i U - V\frac{\partial}{\partial y} + \frac{1}{Re}(\frac{\partial^2}{\partial y^2} + \alpha_i^2), \tag{8.30}$$

$$H_h = \frac{\partial \Omega_z}{\partial x}\frac{\partial}{\partial y} - \frac{1}{\alpha_i}\frac{\partial^2 \Omega_z}{\partial x^2}\frac{\partial}{\partial y} + \alpha_i\frac{\partial \Omega_z}{\partial y} - \frac{\partial^2 \Omega_z}{\partial x \partial y} - \frac{\partial U}{\partial x}(\alpha_i^2 + \frac{\partial^2}{\partial y^2}) + $$
$$+ \frac{1}{\alpha_i}(\alpha_i^2\frac{\partial}{\partial y} + \frac{\partial^3}{\partial y^3}), \tag{8.31}$$

$$L_h = \alpha_i U - V\frac{\partial}{\partial y} + \frac{1}{Re}(\frac{\partial^2}{\partial y^2} + \alpha_i^2) - \frac{\partial U}{\partial x} + \frac{1}{\alpha_i}\frac{\partial V}{\partial x}\frac{\partial}{\partial y}. \tag{8.32}$$

Order O(k)

$$\frac{\partial^2 \hat{v}_1}{\partial y^2} + \alpha_i^2 \hat{v}_1 = -2\frac{\partial^2 \hat{v}_0}{\partial y \partial Y} + 2icos(\phi)\alpha_i \hat{v}_0 + \hat{\Gamma}_1 \tag{8.33}$$

$$\frac{\partial \hat{\Gamma}_1}{\partial t} - G_h\hat{\Gamma}_1 - H_h\hat{v}_1 = -\frac{\partial \hat{\Gamma}_0}{\partial \tau} + G_{h-1}\hat{\Gamma}_0 + H_{h-1}\hat{v}_0 + K_{h-1}\hat{\omega}_{y0} \tag{8.34}$$

$$\frac{\partial \hat{\omega}_{y1}}{\partial t} - L_h\hat{\omega}_{y1} = -\frac{\partial \hat{\omega}_{y0}}{\partial \tau} + L_{h-1}\hat{\omega}_{y0} + M_{h-1}\hat{v}_0 \tag{8.35}$$

where the subscript $h-1$ (h = highest) indicates that these operators, at any order of the multiscaling, are involving only terms at order $h-1$ of the perturbation expansion (8.24). As the order is here $O(k)$ ($h=1$), these operators are acting on quantities ($\hat{\Gamma}_0$,$\hat{v}_0$,$\hat{\omega}_{y0}$). Operators $G_{h-1} = G_{h-1}(y,Y;\phi,\alpha_i,Re)$ as well as H_{h-1}, K_{h-1}, L_{h-1} and M_{h-1} are function of both the short scale y as well as the long scale Y. The explicit expressions are

$$G_{h-1} = -icos(\phi)U - V\frac{\partial}{\partial Y} + \frac{1}{Re}[2\frac{\partial^2}{\partial y \partial Y} - 2icos(\phi)\alpha_i], \tag{8.36}$$

$$H_{h-1} = \frac{\partial \Omega_z}{\partial x}\frac{\partial}{\partial Y} - \frac{1}{\alpha_i}\frac{\partial^2 \Omega_z}{\partial x^2}\frac{\partial}{\partial Y} - \frac{i}{\alpha_i^2}cos(\phi)\frac{\partial^2 \Omega_z}{\partial x^2}\frac{\partial}{\partial y} - icos(\phi)\frac{\partial \Omega_z}{\partial y} +$$
$$- 2\frac{\partial^2}{\partial y \partial Y}\frac{\partial U}{\partial x} + 2i\alpha_i cos(\phi)\frac{\partial U}{\partial x} + \frac{3}{\alpha_i}\frac{\partial^3}{\partial y^2 \partial Y}\frac{\partial V}{\partial x} + \alpha_i\frac{\partial V}{\partial x}\frac{\partial}{\partial Y} +$$
$$+ \frac{i}{\alpha_i^2}cos(\phi)\frac{\partial V}{\partial x}\frac{\partial^3}{\partial y^3} - icos(\phi)\frac{\partial V}{\partial x}\frac{\partial}{\partial y}, \tag{8.37}$$

$$K_{h-1} = \frac{2}{\alpha_i}sin(\phi)\frac{\partial \Omega_z}{\partial x} - \frac{i}{\alpha_i^2}sin(\phi)\frac{\partial^2 \Omega_z}{\partial x^2} - isin(\phi)\frac{\partial V}{\partial x}(1 - \frac{1}{\alpha_i^2}\frac{\partial^2}{\partial y^2}), \tag{8.38}$$

and

$$L_{h-1} = -icos(\phi)U - V\frac{\partial}{\partial Y} + \frac{1}{Re}[2\frac{\partial^2}{\partial y \partial Y} - 2icos(\phi)\alpha_i] + \\ + \frac{1}{\alpha_i}\frac{\partial V}{\partial x}(\frac{\partial}{\partial Y} + \frac{i}{\alpha_i}cos(\phi)\frac{\partial}{\partial y}), \tag{8.39}$$

$$M_{h-1} = -isin(\phi)\frac{\partial U}{\partial y} - \frac{i}{\alpha_i^2}sin(\phi)\frac{\partial V}{\partial x}\frac{\partial^2}{\partial y^2}. \tag{8.40}$$

Some remarks are in order here. First, a comment concerning the role of α_i is needed. Equations above are derived under the hypothesis $\alpha_i \neq 0$. If $\alpha_i = 0$, there is no temporal evolution of perturbations. This means that disturbances initially imposed remain constant as time passes and reach, in the end, an asymptotic condition of marginal stability ($r = 0$). This fact is deduced considering equation (8.27). For $\alpha_i = 0$, the homogeneous solution assumes the expression $\hat{v}_{0h} = c_1 + c_2 y$. Since the velocity field has to be zero in the free stream, $c_1 = 0$ and $c_2 = 0$. Thus $\hat{v}_0$, and therefore $\hat{\Gamma}_0$, are identically zero. This means that, in equation (8.28), there is no temporal evolution for $\hat{\Gamma}_0$, and since transversal vorticity $\hat{\omega}_{y0}$ is initially zero, there is no temporal evolution for the transversal vorticity, too. For $\alpha_i = 0$, initial perturbations are always present, remaining unvaried at any time.

For $\alpha_i \neq 0$, all equations can be solved in a most general way. Solution of equations for the generic order $h > 0$ is obtained by preventing secular terms in the dynamics. This results in the resolution of evolutive equations, in terms of the slow scales τ and T, which involve lower order quantities. When the base flow is parallel ($\underline{U} = (U(y),0)$), equations at order h explicitly depend on solutions at order $h-1$ as well as $h-2$ (see Criminale *et al.*, 2003). Here, instead, it can be evinced that the introduction of both the longitudinal as well as the transversal mean flow components leads to equations at order h which explicitly depend on solutions at order $h-1$, $h-2$, $h-3$ and $h-4$.

Order $O(1)$ ($h = 0$) is the most important approximation of the perturbative analysis and its formal expression is simplified with respect to the full problem. Note that short and fast scale variables (y and t, respectively) only appear. Terms corresponding to operators K and M are missing. The absence, in equation (8.29) of an operator acting on the transversal velocity $\hat{v}$, means that $\hat{\omega}_y$ is always zero for any time and any angle of obliquity. Three-dimensional aspects are all related to the streamwise perturbation vorticity component $\hat{\omega}_x$. In the limit $k \to 0$, the transversal vorticity $\hat{\omega}_y$ is negligible for the full problem solution, too. This can be explained considering operator M in equation (8.18). For $k \to 0$, this operator is going as well

to zero. The production of perturbation transversal vorticity is all due to this term, thus $\hat{\omega}_y$ can be considered absent at any time. Moreover, a comparison of operators G with G_h, and H with H_h, shows that order O(1) is better approximating the full linear system when perturbations are purely transversal rather than longitudinal. At order $O(k)$ ($h = 1$), corrections related to the slow temporal evolution of $\hat{\Gamma}_0$ and $\hat{\omega}_{y0}$ are inserted. Terms corresponding to operators G, H, K, L and M are now all present, and acting on perturbation quantities at order $h - 1$. As in the full problem with $k \to 0$, contribute of operators K_{h-1} and M_{h-1} is formally present if $\phi \neq 0$, but is always negligible. Operators G_{h-1} and H_{h-1} contain terms which mainly correct solution at order $O(1)$ in the longitudinal case. Therefore, at this order, it is reasonable expecting a good approximation of the full problem for both longitudinal as well as transversal perturbations. Long and short scales (Y and y, respectively), as well as slow and fast scales (τ and t, respectively) show up.

8.2 Perturbation temporal dynamics

In the present work, attention is aimed to the resolution of multiscaling at order $O(1)$, and comparison with the full linear problem as $k \to 0$. A summary of the most significant transient behaviour and asymptotic fate of three-dimensional perturbations is presented. Results will be mainly focused on parameters such as the obliquity, the symmetry, and the spatial damping rate of the disturbance. In particular, the latter parameter α_i can vary its order of magnitude around the polar wavenumber value.

8.2.1 Transient period of perturbations

To measure the perturbation temporal growth, the concepts of kinetic energy density $e(t; k,\phi,\alpha_i)$

$$\begin{aligned} e(t; k,\phi,\alpha_i) &= \frac{1}{2}\int_{-y_f}^{+y_f}(|\hat{u}|^2 + |\hat{v}|^2 + |\hat{w}|^2)dy = \frac{1}{2}\frac{1}{|k^2 + 2ikcos(\phi)\alpha_i - \alpha_i^2|} \\ &\times \int_{-y_f}^{+y_f}(|\frac{\partial \hat{v}}{\partial y}|^2 + |k^2 + 2ikcos(\phi)\alpha_i - \alpha_i^2||\hat{v}|^2 + |\hat{\omega}_y|^2)dy, \end{aligned} \tag{8.41}$$

and normalized amplification factor $G(t; k,\phi,\alpha_i)$

$$G(t; k,\phi,\alpha_i) = \frac{e(t; k,\phi,\alpha_i)}{e(t = 0; k,\phi,\alpha_i)}. \tag{8.42}$$

are introduced (see §7.3) in the phase space for both multiscale $O(1)$ quantities $(\hat{v}_0,\hat{\Gamma}_0,\hat{\omega}_{y0})$ and full problem solutions $(\hat{v},\hat{\Gamma},\hat{\omega}_y)$. The total kinetic energy can be obtained by integrating the energy density over all k and ϕ.
Moreover, the temporal growth rate r is defined as

$$r(t;\alpha,\gamma) = \frac{log|e(t;\alpha,\gamma)|}{2t}, \quad t > 0 \tag{8.43}$$

to evaluate the perturbation temporal evolution of solutions obtained by multiscaling at order $O(1)$ and full problem. The temporal growth rate r is not defined for $t = 0$. This quantity, in fact, has a precise physical meaning asymptotically in time.

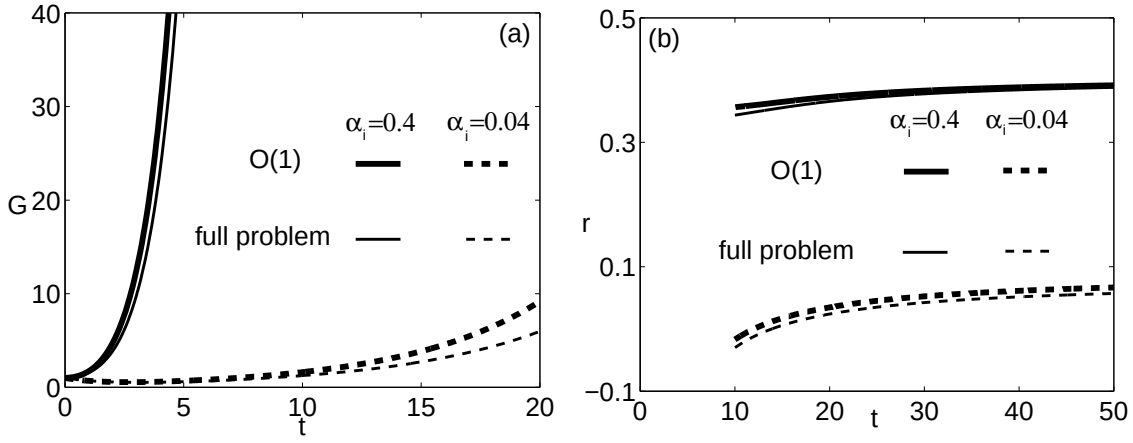

Figure 8.1. Effects of the spatial growth rate α_i. (a) The amplification factor G and (b) the temporal growth rate r as function of time. Comparison between multiscale $O(1)$ (thick curves) and full problem (thin curves). $Re = 50$, $k = 0.03$, $n_0 = 1$, $\phi = \pi/4$, $y_0 = 0$, $x_0 = 12$, asymmetric initial condition, $\alpha_i = 0.04$,0.4.

As previously mentioned, significant transients of three-dimensional perturbations are here presented to observe the agreement between solutions of multiscaling at order $O(1)$ and full problem. The results are all concerning the intermediate asymptotic region of the wake, which is where the spatial evolution is mainly taking place. The polar wavenumber k is around the order $O(10^{-2})$ or smaller.

In Fig. 8.1 an interesting phenomenon is observed, for a three-dimensional perturbation, by changing the value of α_i. Spatially damped waves are temporally amplified. The influence of the imaginary part of the longitudinal wavenumber is remarkable, as by changing its order of magnitude from 0.04 to 0.4 the perturbation is becoming more amplified in time. This confirms, as already observed in §7.3, that

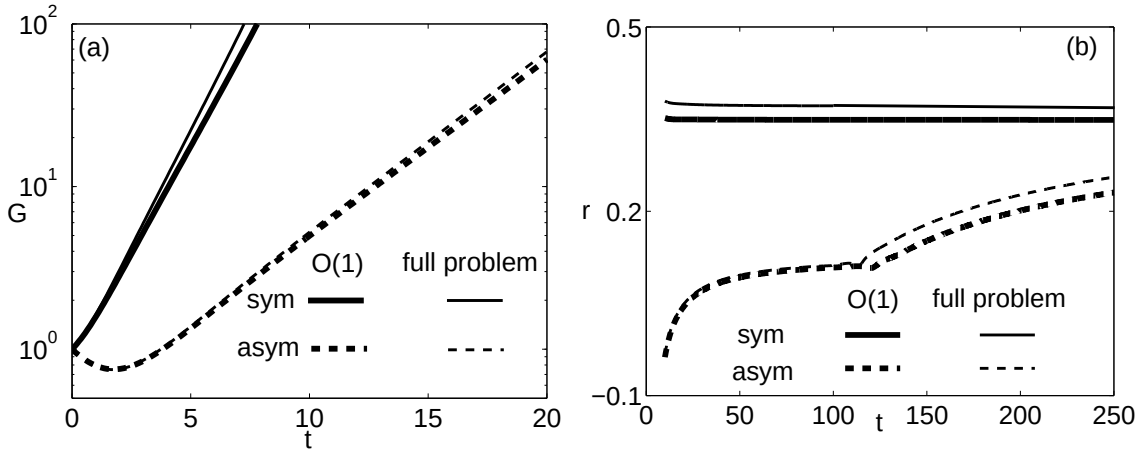

Figure 8.2. Comparison between multiscale $O(1)$ (thick curves) and full problem (thin curves). Effect of the symmetry of the perturbation. (a) The amplification factor G and (b) the temporal growth rate r as function of time. $Re = 100$, $k = 0.02$, $n_0 = 1$, $\phi = \pi/2$, $y_0 = 0$, $x_0 = 13.50$, $\alpha_i = 0.08$, symmetric and asymmetric initial conditions.

perturbations that are spatially confined are more amplified in time also in the limit $k \to 0$. The agreement between multiscale $O(1)$ (thick curves) and full problem (thin curves) is very good in the early transient as well as in the asymptotic state for both values of α_i considered.

Fig. 8.2 shows the influence of the perturbation symmetry on the early time behaviour (a logarithmic scale is used on the ordinate of part (a) of the figure). It can be noted that, as previously stated (see §7.3 and §7.4), the symmetric initial condition leads - in the transient behaviour - to a faster temporal growth than the asymmetric one, although both configurations are approaching the same asymptotic unstable state. Indeed, the transient in the asymmetric case is lasting longer ($t \sim 10^2$) than in the symmetric case ($t \sim 10^1$). The agreement between multiscale $O(1)$ and full problem turns out to be very good for asymmetric and symmetric conditions, for both the early transient and the ultimate fate.

Fig. 8.3 displays the effect of differing orders of magnitude for the polar wavenumber k. Three orders are considered, $k = 0.1$,0.01,0.001. As expected, for smaller values of the polar wavenumber the agreement between multiscale $O(1)$ and full problem is going better (multiscale $O(1)$ solution practically coincides with that of the full problem for $k = 0.001$). Order $O(10^{-2})$ or less, is the wavenumber value for which the multiscale approach can be considered consistent. In comparing the full

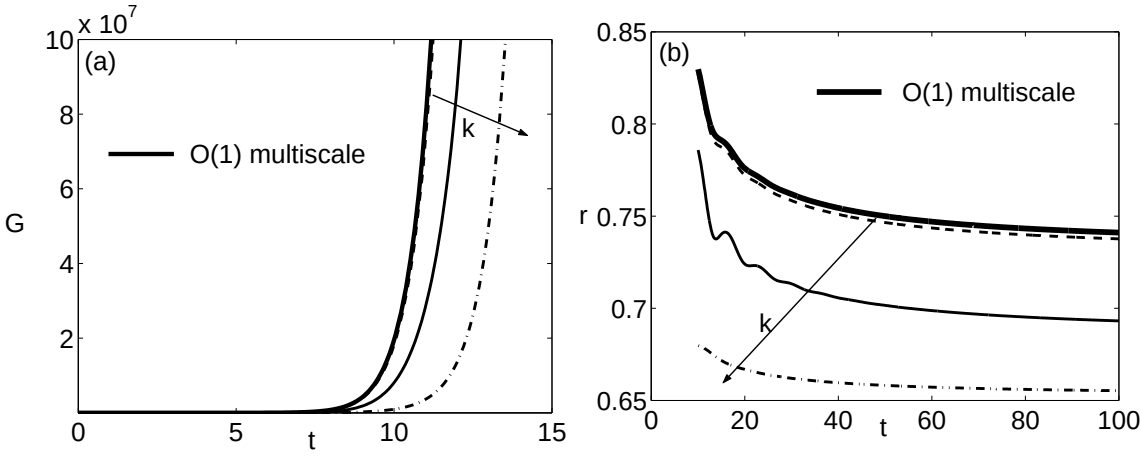

Figure 8.3. Effects of the polar wavenumber k. (a) The amplification factor G and (b) the temporal growth rate r as function of time. Comparison between multiscale $O(1)$ (thick curves) and full problem (thin curves). $Re = 100$, $n_0 = 1$, $\phi = 0$, $y_0 = 0$, $x_0 = 27$, $\alpha_i = 0.2$, symmetric initial condition, $k = 0.1$,0.01,0.001.

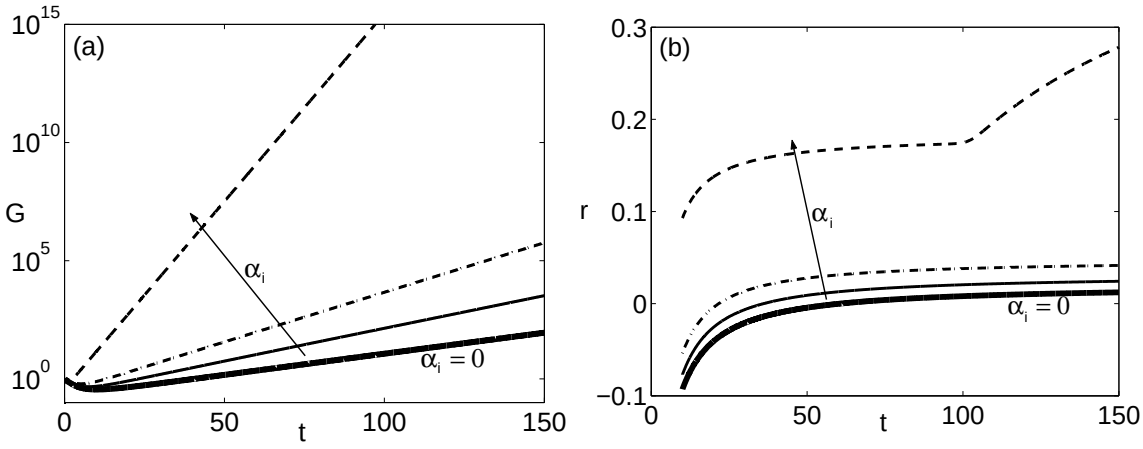

Figure 8.4. Comparison between multiscale $O(1)$ (thin curves) in the limit for $\alpha_i \to 0$, and full problem (thick curves) with $\alpha_i = 0$. (a) The amplification factor G and (b) the temporal growth rate r as function of time. $Re = 50$, $n_0 = 1$, $\phi = \pi/2$, $y_0 = 0$, $x_0 = 12$, asymmetric initial condition, $k = 0.04$, $\alpha_i = 0.005$,0.01,0.05 (multiscale $O(1)$), $\alpha_i = 0$ (full problem).

problem with $k = 0.01$ and the multiscale $O(1)$, it can be noted that the multiscale solution tends to overestimate the actual growth of the perturbation.

In Fig. 8.4, the limit for $\alpha_i \to 0$ is considered. Here, the thick curves represent the full problem solution with $\alpha_i = 0$, while the thin curves are the multiscale $O(1)$ results with α_i values going to zero. The right limit of multiscale $O(1)$ solution for $\alpha_i \to 0$ is finite, and is closely reaching the full problem solution with $\alpha_i = 0$. As can be observed, curves with smaller spatial growth rates are approaching the thick curve from above. This behaviour holds in the early transient as well as the asymptotic state (a logarithmic scale is used on the ordinate of part (a) of the figure).

8.2.2 Asymptotic comparison with the full linear problem

Computations to evaluate the long time asymptotics are made by integrating the equations forward in time beyond the transient (Criminale et al. 1997; Lasseigne et al. 1999) until the temporal growth rate r, defined in relation (8.43), asymptotes to a constant value ($dr = dt < \epsilon$). The choice of the threshold ϵ can offer a quantitative support of when the transient can be considered extinguished.

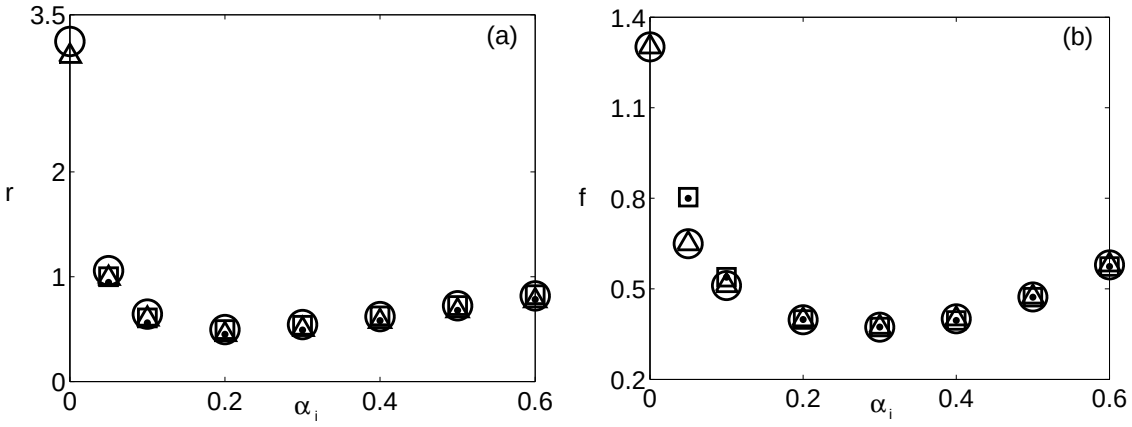

Figure 8.5. $n_0 = 1$, $y_0 = 0$, $\phi = \pi/4$, $\epsilon \sim 10^{-4}$. **(a)** Temporal growth rate and **(b)** angular frequency. Comparison between multiscale $O(1)$ (squares: symmetric inputs, dots: asymmetric inputs) and full linear problem (circles: symmetric inputs, triangles: asymmetric inputs). $k = 0.01$, $x_0 = 10$, $Re = 100$.

The angular frequency (pulsation) f of the perturbation can be defined, for both multiscale $O(1)$ as well as full problem solutions, as the temporal derivative of the phase φ of the complex wave, at a fixed transversal station

$$f(t;\alpha,\gamma) = \frac{|d\varphi(t;\alpha,\gamma)|}{dt} \tag{8.44}$$

where

$$\varphi(t;\alpha,\gamma) = arg(\hat{v}(y=1,t;\alpha,\gamma)) = tan^{-1}(\frac{\hat{v}_i(y=1,t;\alpha,\gamma)}{\hat{v}_r(y=1,t;\alpha,\gamma)}) \tag{8.45}$$

Since defined through the perturbation velocity field, it is reasonable expecting constant values of frequency, once the asymptotic state is reached. In §7.4, in fact, it was found that beyond the time for which $dr = dt < \epsilon$ is becoming valid, both temporal growth rate as well as frequency are reaching their asymptotic values.

Now, an asymptotic comparison between multiscale $O(1)$ and full problem can be made, see Fig. 8.5. The polar wavenumber k is fixed $k = 0.01$, while the imaginary part α_i of the complex longitudinal wavenumber is assuming differing values in the range [0,0.6]. Multiscale $O(1)$ results (squares and dots) are in excellent agreement, for symmetric and asymmetric initial inputs, with full problem data (circles and triangles). Note that the agrement improves for increasing values of α_i. A minimum of the perturbation energy (in terms of r) is found around $\alpha_i = 0.2 - 0.3$ and a similar behaviour is shown by the angular frequency f.

8.3 Concluding remarks

The three-dimensional stability analysis of long waves applied to the two-dimensional viscous wake has been considered by means of a multiple scales approach. The initial-value problem is based on the vorticity-velocity formulation first proposed by Criminale & Drazin (1990). The governing equations are Laplace-Fourier transformed in the plane normal to the base flow. A complex wavenumber in the streamwise direction has been introduced, by means of a spatial Laplace transform in streamwise direction. The two-dimensional wake is described by the asymptotic Navier-Stokes expansion solutions, which take into account the transversal nonlinear and diffusive dynamics of the physical system.

A regular perturbation scheme, where the polar wavenumber k is defined as small parameter, has been proposed. The introduction of a complex wavenumber in streamwise direction makes the equations solvable at any order in a general way, provided that $\alpha_i \neq 0$. However, the right limit of multiscale $O(1)$ solutions for $\alpha_i \to 0$ is finite, and approaches the full problem solution for $\alpha_i = 0$.

General properties of perturbative equations have been presented and discussed up to order O(k), while order $O(1)$ of the multiscaling is only solved. Different transient

configurations have been observed by changing the most important parameters - angle of obliquity, spatial damping rate and symmetry of the perturbation - affecting the temporal evolution. Unstable configurations in time have always been observed in the limit of long waves. In general, for k of the order of about $O(10^{-2})$, the comparison between multiscale approach and full problem formulation turns out to show a good agreement. Multiscale data have been compared with full problem results in the asymptotic temporal limit. As far as small wavenumbers are considered, the agreement turns out to be excellent for both symmetric as well as asymmetric initial conditions arbitrarily expressed in terms of elements of the trigonometrical Schauder basis for the L^2 space.
An extension to order $O(k)$ of the multiscale analysis can be made, in order to better describe the long term state of perturbations that are not purely transversal with respect to the base flow plane. The present multiscale approach, here validated in the case of the two-dimensional weakly non-parallel wake, can be applied to other near-parallel shear flows, for example the three-dimensional boundary layer.

Chapter 9

Conclusions

The hydrodynamic linear stability of the two-dimensional bluff-body wake has been studied by means of the normal mode analysis and the initial-value problem.
The common aspect of the two perturbative approaches is the steady non-parallel base flow, which is accurately described through asymptotic Navier-Stokes expansions. The physical domain is divided into two region, namely inner and outer flow regions. For both the regions, analytical asymptotic Navier-Stokes expansions are adopted. Matching criteria, based on the matching of differential physical quantities (pressure gradient and vorticity) involved in the system dynamics, have been discussed together with the structure of the expansions expressed in terms of inverse powers of the coordinates. According to the boundary layer model, the inner expansions for the 2D velocity field is used to approximate the wake profile. In so doing, the longitudinal as well as the transversal non-linear and diffusive dynamics are directly taken into account.

The modal analysis has been first considered. The stability analysis of the intermediate and far region of the near-parallel two-dimensional wake is studied by means of a multiscale approach. The disturbance is tuned to the local wavenumber along the wake, selected by the zero order theory, and is associated to a classical spatial and temporal WKBJ analysis. The multiscale approach, based on the introduction of a small parameter equal to the inverse of the Reynolds number, explicitly accounts for the non-parallel effects associated to the lateral momentum dynamics. The correction due to the transversal dynamics increases with Re and is larger for the pulsation and the temporal growth factor than for the spatial growth factor. It is negligible for the wavenumber. Such corrections allow absolute instability pockets to show up in the first part of the intermediate wake. These pockets are present when the Reynolds number Re is equal to 50 and 100, but are absent when Re is

as low as 35. This is in agreement with the general notion of a critical Reynolds number of about 47 for the onset of the first instability.
Moreover, for $Re = 50$ and $Re = 100$, angular frequency results in agreement with numerical and experimental global data in literature are found in the wake region where the temporal growth rates are close to zero. Convective instability is observable throughout the domain, and this configuration asymptotically sets on a condition of marginal stability. All instability characteristics tend to vanish in the far wake, a fact that is independently confirmed by the asymptotic analysis of the Orr-Sommerfeld equation.

Through the use of the Navier-Stokes expansion solutions for the inner field of the wake, an estimate of the entrainment streamwise distribution in the intermediate and far wake has been analytically determined in terms of asymptotic expansions. The entrainment has been defined as the longitudinal volume flow rate variation in the streamwise direction. It turns out to be intense downstream the separation region, where the two-symmetric standing eddies are situated. Here, the maximum of the distribution is reached and the dependence on the Reynolds number is clear. Then, the entrainment continuously decreases in the intermediate wake, and is almost vanished in the far field. In particular, the decrease can be considered almost concluded for all the Re here taken into account at an average distance from the body of 50 - 60 diameters, which is a value of the same order of magnitude as the control parameter Re. This result confirms the validity of the spatio-temporal multiscaling approach, based on the inverse of the Reynolds number, and often adopted in wake stability analysis. In fact, unitary values of the slow temporal and spatial scales - defined as $\xi = x/Re$ and $\tau = t/Re$, respectively - are reached in the downstream region where the entrainment process can be considered extinguished.

Then, the linear stability analysis of the two-dimensional laminar wake has been studied as an initial-value problem. The wake is first represented through the longitudinal component of the Navier-Stokes expansions only. Thus, base flow is parameterized with respect to the Reynolds number and the longitudinal coordinate, and is growing in thickness and flow rate along the streamwise coordinate.
The vorticity-velocity formulation is due to Criminale & Drazin (1990), who first proposed it. The perturbative equations are Laplace-Fourier transformed in the x and z directions, respectively. In this case, differently to what usually done, a complex longitudinal wavenumber has been introduced, by means of a spatial Laplace transform in the streamwise direction. The introduction of the imaginary part of the longitudinal wavenumber (the spatial damping rate) was done to explicitly include also in the structure of the perturbation a degree of freedom related to the spatial

evolution of the system.

Many parameters - such as the angle of obliquity, the symmetry, the length, the spatial damping rate, the number of oscillations of the distribution in the y direction of the perturbation - have been introduced, and their influence has been observed in different transient configurations. Counter-intuitive behaviours - like initial damping followed by a fast growth for perturbations aligned with the basic flow, initial transient growths that smoothly level off and are followed either by an ultimate damping or by a slow amplification for oblique waves - as well as more expected monotone trends have been found. The most important parameters affecting the temporal evolution are the angle of obliquity, the symmetry of the perturbation and the spatial damping rate. While the symmetry of the disturbance is remarkably influencing the transient behaviour leaving inalterate the asymptotic fate, a variation of the obliquity and the spatial damping rate can significantly change both the early trend as well as the final stability configuration. Instead, the effect of the number of oscillations and the distribution in y direction is only to extend or shorten the length of the transient, while the ultimate state is not different.

For disturbances aligned with the flow, the asymptotic behaviour turned out to be in good agreement with the zero order results of spatio-temporal multiscale modal analyses. The agreement is obtained not using as initial condition the most unstable wave given by the Orr-Sommerfeld dispersion relation at any section of the wake, but arbitrary initial conditions in terms of elements of the trigonometrical Schauder basis for the L^2 space.

The three-dimensional stability of the near-parallel two-dimensional wake has been then analyzed as an initial-value problem by means of a multiscale approach, based on the slow and long scales associated to small wavenumbers. The two-dimensional wake is now described with both the longitudinal and the transversal asymptotic Navier-Stokes expansions, which take into account the transversal nonlinear and diffusive dynamics of the physical system. The initial-value problem extends the formulation previously presented for the parameterized growing wake to the case of a weakly non-parallel base flow. Similarly to what assumed before, in the perturbation decomposition a complex wavenumber in the streamwise direction has been introduced.

A regular perturbation scheme, where the polar wavenumber k is defined as the small parameter, has been considered. The stability analysis in the limit $k \to 0$ is studied because in some flow configurations (for example Blasius boundary layer and three-dimensional boundary layer) long waves turned out to be destabilizing. In these cases, instability occurs for wavenumbers that are much less than $O(1)$.

The introduction of a complex wavenumber in the streamwise direction made the equations solvable at any order in a general way, for $\alpha_i \neq 0$. Moreover, it has been observed that the right limit of multiscale $O(1)$ solutions for $\alpha_i \to 0$ is finite, and tends to the full problem solution with $\alpha_i = 0$.
Solutions up to order $O(1)$ have only been considered, and different transient configurations have been observed to validate the multiscaling. The parameters that mostly affect the transient - the angle of obliquity, the symmetry and the spatial damping rate of disturbance - have been changed. Interesting early growths have been shown. Amplified configurations in time have always been observed in the limit of long waves.
In general, for small polar wavenumber k of the order of about $O(10^{-2})$, the comparison between the multiscale approach and the full problem formulation showed a good agreement. Multiscale data have been compared with full problem results in the asymptotic temporal limit. As far as small wavenumbers are considered, the agreement is excellent for both symmetric as well as asymmetric initial conditions arbitrarily expressed in terms of elements of the trigonometrical Schauder basis for the L^2 space. This result confirms the validity of multiscale approach for long waves, even at the lowest order of expansion.

Some concluding comments are in order here, while comparing the two stability approaches. In general, for three-dimensional perturbations, both the methods use a combined Laplace-Fourier decomposition for the independent variables x and z, respectively. Then, two different strategies are used to solve the resulting partial differential equations in y and t.
In terms of the underlying mathematical complexities, the normal mode hypothesis strongly simplifies the linearized system, that is transformed into an eigenvalue problem. Indeed, the temporal dependence is specified through an exponential asymptotic behaviour, and the perturbative equations become ordinary differential equations in y. Moreover, in the combined spatio-temporal modal analysis applied to a near-parallel flow a few parameters are present - namely the Reynolds number and the longitudinal coordinate - and can be easily handled. Here, the perturbative hypothesis based on the sequence of saddle points is proposed. This approach is original and synthetic since the most destabilizing wavenumber is considered at every longitudinal station. Thus, the only parameter remaining is the Reynolds number.
In the initial-value problem, instead, no temporal evolution is prescribed for the perturbations. In this way, partial differential equations - in y and t - are to be solved. Since perturbations are arbitrarily chosen in terms of elements of the trigonometrical

Schauder basis for the L^2 space and do not have a prescribed temporal evolution, many more parameters have to be dealt with, for example the angle of obliquity, the symmetry, the length, the spatial damping rate and the number of oscillations of the distribution in the y direction of the perturbation. The initial-value problem turns out to be less concise than the modal analysis because of the increased number of parameters. Some of these are arbitrarily changed according to what suggested by results found in the modal analysis. This procedure, however, is not so easy and can be improved, since it does not completely exploit all the potential information offered by the initial-value problem. In fact, modal results cannot give information on significant early growth, as they only consider the ultimate state of perturbations. On the contrary, initial-value problem results often showed rapid transient amplifications. Moreover, phenomenons like lift-up and by-pass transition can, in principle, be captured within this framework. To better address the effort of describing the transient behaviour, an optimization scheme can be adopted. Optimal initial conditions are those for which the maximum energy growth occurs at a certain time t. Note that variational methods are not necessary for the optimization procedure, but the use of Lagrange multipliers is sufficient to maximize the energy, because the present formulation considers the temporal evolution of vorticity and velocity without using eigenfunction expansions.

The initial-value problem can be applied to the stability analysis of other mean shear flows. In particular, the linear stability of the near-parallel three-dimensional boundary layer can be studied by means of the multiscale approach based on small wavenumbers. For this physical problem, indeed, results in literature confirm that perturbative waves are long when instability occurs. The optimization scheme briefly described above can be adopted to observe which disturbance configurations are the most dangerous in terms of transient growth. The complete temporal evolution of optimal initial conditions could be helpful in predicting the breakdown of the laminar regime for flow configurations in presence of swept wings, rotating disks or axisymmetric bodies, since it is widely recognized that in low disturbance fields such as flight, boundary layer transition to turbulence generally occurs through the uninterrupted growth of linear instabilities.

Moreover, the present formulation applied to a free shear flow can be extended to include the non linear non-modal interaction between disturbances initially imposed. In turbulent mixings, if the mixing scales differ, and the largest scale also has the highest energy content, then the energy exchange is deeper than that which would occur if the scales were equal. If, instead, the largest scale has the lowest energy, the energy exchange is reduced and delayed with respect to the configuration with equal

scales. Here, the non-linear interaction between initial disturbances with different amplitude, length and obliquity can be considered to verify the analogy between unsteady dynamics and turbulent dynamics. If the analogy is correct, the reciprocal influence between a long wave with low energy and a short wave with high energy should lead to a lower early energy growth and a transient lasting longer than if two initial waves with the same scales were considered.

Bibliography

[1] Baird, M. H. I., Wairegi, T. & Loo, H. J. (1977). *Velocity and momentum of vortex rings in relation to formation parameters.* Can. J. Chem. Engng., **55**, 19–26.

[2] Belan, M. & Tordella, D. (2002). *Asymptotic expansions for two-dimensional symmetrical laminar wakes.* ZAMM, **82** (4), 219–234.

[3] Belan, M. & Tordella, D. (2006). *Convective instability in wake intermediate asymptotics.* J. Fluid Mech., **552**, 127–136.

[4] Bender, C. M. & Orszag, S. A. (1978). *Advanced mathematical methods for scientists and engineers.* New York, McGraw-Hill.

[5] Benney, D. J. & Gustavsson, L. H. (1981). *A new mechanism for linear and non-linear hydrodynamic instability.* Stud. in Applied Math., **64** (3), 185–209.

[6] Bergstrom, L. (1993). *Evolution of laminar disturbances in pipe Poiseuille flow.* Eur. J. Mech. B/Fluids, **12** (6), 749–768.

[7] Betchov, R. & Criminale, W. O. (1966). *Stability instability of the inviscid jet and wake.* Phys. Fluids, **9**, 359–362.

[8] Betchov, R. & Criminale, W. O. (1967). *Stability of parallel flows.* New York, Academic Press.

[9] Blossey, P. N., Criminale, W. O. & Fisher, L. S. (2007). *Initial-value Problems in Free Shear Flows.* Submitted to J. Fluid Mech.

[10] Bouthier, M. (1972). *Stabilité linéare des écoulements presque parallèles.* J. Mec., **11** (4), 599-621.

[11] Briggs, R. J. (1964). *Electron-stream interaction with plasmas.* Cambridge, MA: MIT Press, Research Monographe, **29**.

[12] Bun, Y. & Criminale, W. O. (1994). *Early-period dynamics of an incompressible mixing layer.* J. Fluid Mech., **273**, 31–82.

[13] Butler, K. M. & Farrell, B. F. (1992). *Three-dimensional optimal perturbations in viscous shear flow.* Phys. Fluids A, **4** (8), 1637–1650.

[14] Case, K. M. (1960). *Stability of inviscid plane couette flow.* Phys. Fluids, **3** (2),

143–148.

[15] Case, K. M. (1961). *Hydrodynamic stability and the inviscid limit.* J. Fluid Mech., **10** (3), 420–429.

[16] Chang, I. (1961). *Navier–Stokes solutions at large distances from a finite body.* J. Math. Mech., **10**, 811.

[17] Chomaz, J. M., Huerre, P. & Redekopp, L. G. (1988). *Bifurcations to Local and Global Modes in Spatially Developing Flows.* Phys. Rev. Lett., **60** (1), 25–28.

[18] Chomaz, J. M., Huerre, P. & Redekopp, L. G. (1991). *A frequency selection criterion in spatially developing flows.* Stud. in Applied Math., **84** (2), 119–144.

[19] Chomaz, J. M. (2005). *Global instabilities in spatially developing flows: non-normality and non-linearity.* Annu. Rev. Fluid Mech., **37**, 357–392.

[20] Craik, A. D. D. & Criminale, W. O. (1986). *Evolution of Wavelike Disturbances in Shear Flows: A Class of Exact Solutions of the Navier-Stokes Equations.* Proc. Roy. Soc. Lond. A, **406**, 13–26.

[21] Criminale, W. O. & Drazin, P. G. (1990). *The evolution of linearized perturbations of parallel shear flows.* Stud. in Applied Math., **83** (2), 123–157.

[22] Criminale, W. O., Long, B. & Zhu, M. (1991). *General three-dimensional disturbances to inviscid Couette flow.* Stud. in Applied Math., **85** (3), 249–267.

[23] Criminale, W. O., Jackson, T. L. & Lasseigne, D. G. (1995). *Towards enhancing and delaying disturbances in free shear flows.* J. Fluid Mech., **294**, 283–300.

[24] Criminale, W. O., Jackson, T. L., Lasseigne, D. G. & Joslin, R.D. (1997). *Perturbation dynamics in viscous channel flows.* J. Fluid Mech., **339**, 55–75.

[25] Criminale, W. O. & Drazin, P. G. (2000). *The initial-value problem for a modeled boundary layer.* Phys. Fluids, **12** (2), 366–374.

[26] Criminale, W. O., Jackson, T. L. & Joslin, R. D. (2003). *Theory and Computation in Hydrodynamic Stability.* Cambridge, Cambridge University Press.

[27] Dabiri, J. O. & Gharib, M. (2004). *Fluid entrainment by isolated vortex rings.* J. Fluid Mech., **511**, 311–331.

[28] DiPrima, R. C. & Habetler, G. J. (1969). *A completeness theorem for non-selfadjoint eigenvalue problems in hydrodynamic stability.* Archive for Rational Mechanics and Analysis, **34** (3), 218–227.

[29] Drazin, P. G. & Reid, W. H. (1984). *Hydrodynamic stability.* Cambridge, Cambridge University Press.

[30] Drazin, P. G. (2002). *Introduction to hydrodynamic stability.* Cambridge, Cambridge University Press.

[31] Goldstein, S. (1933). *On the Two-Dimensional Steady Flow of a Viscous Fluid behind a Solid Body. I.* Proc. Roy. Soc. London A, **142**, 545–562.

[32] Grinstein, F. F. (2001). *Vortex dynamics and entrainment in rectangular free jets.* J. Fluid Mech., **437**, 69–101.

[33] Grosch, C. E. & Salwen, H. (1978). *The continuous spectrum of the Orr-Sommerfeld equation. Part 1. The spectrum and the eigenfunctions.* J. Fluid Mech., **87**, 33–54.

[34] Gustavsson, L.H. (1979). *Initial-value problem for boundary layer flows.* Phys. Fluids, **22** (9), 1602–1605.

[35] Gustavsson, L.H. & Hultgren, L.S. (1980). *A resonance mechanism in plane Couette flow.* J. Fluid Mech., **98**, 149–159.

[36] Gustavsson, L.H. (1981). *Resonant growth of three-dimensional disturbances in plane Poiseuille flow.* J. Fluid Mech., **112**, 253–264.

[37] Gustavsson, L. H. (1991). *Energy growth of three-dimensional disturbances in plane Poiseuille flow.* J. Fluid Mech., **224**, 241–260.

[38] Hannemann, K. & Oertel, H. (1989). *Numerical simulation of the absolutely and convectively unstable wake.* J. Fluid Mech., **199**, 55–88.

[39] Helmholtz, H. (1868). *Über discontinuirliche Flüssigkeits-Bewegungen.* Akad. Wiss., Berlin, Monatsber., **23**, 215–228. Translated by F. Guthrie, *On discontinuous movements of fluids.* Phil. Mag., **36** (4), 337–346, 1868.

[40] Huerre, P. & Monkewitz, P. A. (1990). *Local and global instabilities in spatially developing flows.* Ann. Rev. Fluid Mech., **22**, 473–537.

[41] Hultgren, L. S. & Gustavsson, L. H. (1981). *Algebraic growth of disturbances in a laminar boundary layer.* Phys. Fluids, **24** (6), 1000–1004.

[42] Hultgren, L. S. & Aggarwal, A. K. (1987). *Absolute instability of the Gaussian wake profile.* Phys. Fluids, **30** (11), 3383–3387.

[43] Imai, I. (1951). *On the asymptotic behaviour of viscous fluid flow at a great distance from a cylindrical body, with special reference to Filon's paradox.* Proc. Roy. Soc. London A, **208**, 487–516.

[44] Kelvin, Lord (1887 a). *Rectilinear motion of viscous fluid between two parallel plates.* Mathematical and Physical Papers, **4**, 321–330, 1910.

[45] Kelvin, Lord (1887 b). *Broad river flowing down an inclined plane bed.* Mathematical and Physical Papers, **4**, 330–337, 1910.

[46] Kida T. (1984). *A new perturbation approach to the laminar fluid flow behind a two-dimensional solid body.* SIAM J. Appl. Math., **44** (5), 929–951.

[47] Kovásznay, L. S. G. (1948). *Hot-wire investigation of the wake behind cylinders at low Reynolds numbers.* Proc. Re. Soc. London S. A, **198**, 174–190.

[48] Kopp, G. A., Giralt, F. & Keffer, J. F. (2002). *Entrainment vortices and interfacial intermittent turbulent bulges in a plane turbulent wake.* J. Fluid Mech.,

469, 49–70.

[49] Lasseigne, D. G., Joslin, R. D., Jackson, T. L. & Criminale, W. O. (1999). *The transient period for boundary layer disturbances.* J. Fluid Mech., **381**, 89–119.

[50] Landahl, M. T. (1980). *A note on an algebraic instability of inviscid parallel shear flows.* J. Fluid Mech., **98**, 243–251.

[51] Mack, L. M. (1976). *A numerical study of the temporal eigenvalue spectrum of the Blasius boundary layer.* J. Fluid Mech., **73**, 497–520.

[52] Mattingly, G. E. & Criminale, W. O. (1972). *The stability of an incompressible two-dimensional wake.* J. Fluid Mech., **51**, 233–272.

[53] Maxworthy, T. (1972). *The structure and stability of vortex rings.* J. Fluid Mech., **51**, 15–32.

[54] Messiah, A. (1960). *Mecanique quantique.* Dunod, Paris.

[55] Miklavčič, M. & Williams, M. (1982). *Stability of mean flows over an infinite flat plate.* Arch. Rational Mech. Anal., **80**, 57–69.

[56] Miklavčič, M. (1983). *Eigenvalues of the Orr-Sommerfeld equation in an unbounded domain.* Arch. Rational Mech. Anal., **83**, 221–228.

[57] Monkewitz, P.A. & Nguyen, L. N. (1987). *Absolute instability in the near-wake of two-dimensional bluff bodies.* J. Fluids Struct., **1**, 165–184.

[58] Monkewitz, P.A. (1988). *The absolute and convective nature of instability in two-dimensional wakes at low Reynolds numbers.* Phys. Fluids, **31** (5), 999–1006.

[59] Monkewitz, P.A., Huerre, P. & Chomaz, J.M. (1993). *Global linear-stability analysis of weakly nonparallel shear flows.* J. Fluid Mech., **251**, 1–20.

[60] Müller, E. A. & Didden, N. (1980). *Zur erzeugung der zirkulation bei der bildung eines ringwirbels an einer dusenmundung.* Stroj. Casop., **31**, 363–372.

[61] Nayfeh, A. H. (1973). *Perturbation methods.* New York, Wiley.

[62] Oertel, H. (1990). *Wakes Behind Blunt Bodies.* Ann. Rev. Fluid Mech., **22**, 539–564.

[63] Orr, W. M'F. (1907 a). *The stability or instability of the steady motions of a perfect liquid and a viscous liquid. Part I.* Proc. R. Irish. Acad., **27**, 9–68.

[64] Orr, W. M'F. (1907 b). *The stability or instability of the steady motions of a perfect liquid and a viscous liquid. Part II.* Proc. R. Irish. Acad., **27**, 69–138.

[65] Pier, B. (2002). *On the frequency selection of finite-amplitude vortex shedding in the cylinder wake.* J. Fluid Mech., **458**, 407–417.

[66] Rayleigh, Lord (1880). *On the stability or instability of certain fluid motions.* Proc. London Math. Soc., **11**, 57–70. Also, Scientific Papers, **1**, 474–487, 1899.

[67] Rayleigh, Lord (1887). *On the stability or instability of certain fluid motions. Part II.* Scientific Papers, **3**, 17–23.

[68] Rayleigh, Lord (1892). *On the question of the stability of the flow of fluids.* Phil. Mag., **34**, 59–70. Also, Scientific Papers, **3**, 575–584, 1902.

[69] Rayleigh, Lord (1895). *On the stability or instability of certain fluid motions. III.* Scientific Papers, **4**, 203–209, 1899.

[70] Rayleigh, Lord (1913). *On the stability of the laminar motion of an inviscid fluid.* Scientific Papers, **6**, 197–204.

[71] Rayleigh, Lord (1915). *On the stability of the simple shearing motion of a viscous incompressible fluid.* Scientific Papers, **6**, 341–349.

[72] Reed, H. L. & Saric, W. S. (1989). *Stability of Three-Dimensional Boundary Layers.* Ann. Rev. Fluid Mech., **21**, 235–284.

[73] Reshotko, E. (1976). *Boundary-Layer Stability and Transition.* Ann. Rev. Fluid Mech., **8**, 311–349.

[74] Salwen, H. & Grosch, C.E. (1981). *The continuous spectrum of the Orr-Sommerfeld equation. Part 2. Eigenfunction expansions.* J. Fluid Mech., **104**, 445–465.

[75] Saric, W. S. & Nayfeh, A. H. (1975). *Nonparallel stability of boundary-layer flows.* Phys. Fluids, **18** (8), 945–950.

[76] Saric, W. S., Reed, H. L. & White, E. B. (2003). *Stability and Transition of Three-Dimensional Boundary Layers.* Ann. Rev. Fluid Mech., **35**, 413–440.

[77] Scarsoglio, S., Tordella, D. & Belan, M. (2005). *Analysis of the convective instability of the two-dimensional wake.* 22nd IFIP TC 7 Conference on System Modeling and Optimization. July 18-22, 2005, Torino, Italy.

[78] Scarsoglio, S., Tordella, D. & Criminale, W. O. (2006). *Initial-value problem for the two-dimensional growing wake.* 59th Annual Meeting Division of Fluid Dynamics (APS-DFD). November 19-21, 2006, Tampa Bay, Florida. Abstract in Bull. Am. Phys. Soc., **51** (9), November 2006.

[79] Scarsoglio, S., Tordella, D. & Criminale, W. O. (2007). *Temporal dynamics of small perturbations for a 2D growing wake.* Advances in turbulence XI. Proceedings of the 11th Euromech European Turbulence Conference (ETC11). June 25-28, 2007, Porto, Portugal, 221–223. Springer 2007.

[80] Scarsoglio, S., Tordella, D. & Criminale, W. O. (2007). *A multiscale approach to study the stability of long waves in near-parallel flows.* 60th Annual Meeting Division of Fluid Dynamics (APS-DFD). November 18-20, 2007, Salt Lake City, Utah. Abstract in Bull. Am. Phys. Soc., **52** (17), November 2007.

[81] Schlichting, H. (1968). *Boundary layer theory.* New York, McGraw-Hill.

[82] Schmid, P. J. & Henningson, D. S. (1994). *Optimal energy density growth in Hagen-Poiseuille flow.* J. Fluid Mech., **277**, 197–225.

[83] Schmid, P. J. & Henningson, D. S. (2001). *Stability and Transition in Shear Flows.* Springer.

[84] Schmid, P. J. (2007). *Nonmodal Stability Theory.* Ann. Rev. Fluid Mech., **39**, 129–162.

[85] Sommerfeld, A. (1908). *Ein beitraz zur hydrodynamischen erklaerung der turbulenten fluessigkeitsbewegungen.* Proc. Fourth Inter. Congr. Matematicians, Rome, 116–124.

[86] Sommerfeld, A. (1949). *Partial Differential Equations in Physics.* Lectures in Theoretical Physics, Vol. **6**, Academic Press.

[87] Squire, H. B. (1933). *On the stability for three-dimensional disturbances of viscous fluid flow between parallel walls.* Proc. Roy. Soc., Series A. Mathematical and Physical Sciences, **142**, 621–628.

[88] Stewartson, K. (1957). *On asymptotic expansions in the theory of boundary-layers.* J. Math. Phys., **36**, 173.

[89] Tordella, D. & Belan, M. (2003) *A new matched asymptotic expansion for the intermediate and far flow behind a finite body.* Phys. Fluids, **15** (7), 1897–1906.

[90] Tordella, D. & Belan, M. (2005) *On the domain of validity of the near-parallel combined stability analysis for the 2D intermediate and far bluff body wake.* ZAMM, **85** (1), 51–65.

[91] Tordella, D., Scarsoglio, S. & Belan, M. (2006). *A synthetic perturbative hypothesis for multiscale analysis of convective wake instability.* Phys. Fluids, **18** (5), 054105 (2006) (10 pages).

[92] Tordella, D., Scarsoglio, S. & Belan, M. (2006). *A synthetic perturbative hypothesis for multiscale analysis of bluff-body wake instability.* 6th Euromech Fluid Mechanics Conference (EFMC6). June 26-30, 2006, Stockholm, Sweden. Abstract in EFMC6 KTH Electronic version, Abstracts Volume 2.

[93] Tordella, D., Scarsoglio, S. & Belan, M. 2008. *Hydrodynamics linear stability theory. A comparison between Orr-Sommerfeld modal and initial value problem analyses.* Acc. Sc. Torino–Memorie Sc. Fis., Vol. **141** (to appear 2008).

[94] Triantafyllou, G. S., Triantafyllou, M. S. & Chryssostomidis, C. (1986). *On the formation of vortex street behind stationary cylinders.* J. Fluid Mech., **170**, 461–477.

[95] Tritton, D. J. (1988). *Physical fluid dynamics.* Oxford, Clarendon Press.

[96] Watson, J. (1960). *On the non-linear mechanics of wave disturbances in stable and unstable parallel flows. Part 2. The development of a solution for plane Poiseuille flow and for plane Couette flow.* J. Fluid Mech., **9**, 371–389.

[97] Whitham, G. B. (1974). *Linear and nonlinear waves.* New York, Wiley.

[98] Williamson, C. H. K. (1988). *Defining a universal and continuous Strouhal-Reynolds number relationship for the laminar vortex shedding of a circular cylinder.* Phys. Fluids, **31** (10), 2742–2744.

[99] Williamson, C. H. K. (1989). *Oblique and parallel modes of vortex shedding in the wake of a circular cylinder at low Reynolds numbers.* J. Fluid Mech, **206**, 579–627.

[100] Yang, X. & Zebib, A. (1989). *Absolute and convective instability of a cylinder wake.* Phys. Fluids A, **1**(4), 689–696.

[101] Zebib, A. (1987). *Stability of viscous flow past a circular cylinder.* J. Eng. Math., **21**, 155–165.